Improved mono-synaptic tracing tools for mapping, monitoring, and manipulation of neural circuits

Thomas R. Reardon

Submitted in partial fulfillment of the

requirements for the degree

of Doctor of Philosophy

under the Executive Committee

of the Graduate School of Arts and Sciences

COLUMBIA UNIVERSITY

2016

© 2016

Thomas R. Reardon

All rights reserved

Abstract

Improved mono-synaptic tracing tools for mapping, monitoring,
and manipulation of neural circuits

Thomas R. Reardon

This work concerns the use of engineered genetic tools to build maps of the mammalian nervous system. Within the practice of circuit neuroscience, one of the most effective tools to emerge in recent years are the neurotropic viruses. Among these are modified strains of rabies virus which are made safe for laboratory use. We introduce here a novel form of engineered rabies virus with substantially improved utility for exploring the structure and function of neural circuits. Additionally, using this new tool, an investigation of an important motor circuit, the cortico-striatal circuit, is presented.

Table of Contents

Acknowledgements

Science is best performed collaboratively and socially. Training in science, especially graduate school, is done in overwhelming isolation and with a preference for impersonal description. I write these acknowledgements with the hope that a transformation in scientific training will occur, a shift that would favor rewards and accolades for significant collaborations rather than the solitary efforts. It may be that impersonal accounts bring clear-headedness to the scientific narrative, but it is just as likely that such accounts allow for the concealment of otherwise social and personal agendas.

In that light, the reader will note that this monograph makes liberal use of the pronoun "we", which is both first-person and collaborative.

The "we" I hoped to capture and honor includes the following: Andrew Murray, with whom the majority of this work was conceived and performed; Gergely Turi, a meticulous physiologist; Christoph Wirblich and Matthias Schnell, Katherine Croce, and most importantly, my mentors and scolds, Tom Jessell and Attila Losonczy. I cannot imagine two scientists—two humans—more different than Tom and Attila, yet each has an incomprehensible love and passion for neuroscience. Attila is a cipher and a genius and has the sense of loyalty one can only dream of in a mentor. Though a physiologist, he invented the trick of virology at the heart of this paper! Tom shows all of us that there is no such thing as great science that is communicated poorly. He descends from the line that gave us Einstein and Watson, thinkers of such facility and simplicity of expression that we wonder why we were ever confused before. Great science is always easy to understand. Tom makes it so, and refuses to allow anyone to escape the rigor and honor of contributing to our canon.

A brief mention of a number of people who have impacted me and this work over the last several years. Ian Wickersham, brilliantly creative and the source of the tools we use here, and an encouraging and collaborative presence since our first emails five years ago. My colleagues in Attila's lab: Patrick Kaifosh, Matthew Lovett-Barron, Alexandra Kaufman, Nathan Danielson, Jeff Zaremba. My colleagues in Tom's lab: Samaher Fageiry, David Ng, Niccolo Zampieri, Ira Schieren. Of these, I want to particularly mention the selfless enthusiasm of Samaher and David, one who never grumbled as I made a mess of her work, and the other who never grumbled when I asked for cloning help for the hundredth time. In the lab of Charles Zuker, Lindsey MacPherson in particular, and Hao Jin, Mingyu Ye, have all been important advisors and selfless collaborators.

Steve Siegelbaum is the smartest scientist I have ever met, or heard, or watched. I pursued academic neuroscience because of him. Charles Zuker is larger than life and uses his position in the best possible way, to challenge young scientists to think bigger and yet to think more simply. Christoph Kellendonk is my ideal scientist, someone who wants to find the truth, wants to help people get there with him, and, along with Joshua Dudman, thinks the rest of neuroscience profoundly underappreciates the striatum.

My greatest collaborator is Xan Young. Our ongoing experiment is Roman Reardon. He deserves her, I do not. My only goal now is to repay the debt in love and gratitude before the interest comes due.

To all: Good job, us!

Part 1

Preface

This work concerns the use of engineered genetic tools to build maps of the mammalian nervous system. To a working neuroscientist, this is a straightforward response to an obvious problem: what is connected to what? But the question has some deeper philosophical tensions that we first examine before turning our attention to the neural circuit and behavior we care most about, motor cortex and the rise of volitional skilled movement.

What does it mean to map a neural circuit?

A unifying if dogmatic belief in contemporary neuroscience holds that animal behavior is anchored in the variable connections amongst neurons. No behavior exists, no memory trained or recalled, which is not somehow enabled by the activity of neurons over a defined set of connections. This has led to a somewhat controversial consensus that a fully detailed map of the nervous system could account for the myriad complexity of even human behavior. Since the acceptance of the Neuron Doctrine over a century ago (Shepherd, 1991), each generation of neurobiologists has attempted to find ever finer maps of these connections.

Arguments about neural maps quickly degenerate into dogma, pitting reductionists against phenomenologists (Alivisatos et al., 2012; Seung, 2011; Markram, 2006; Tononi & Koch, 2008; Watts & Swanson, 2002). But the larger question here is whether we can build practical but detailed maps of the neural connections which help not only elucidate but predict behavior (Lichtman & Denk, 2011). At root, we are always seeking to understand the response of the nervous system given some input, to understand the transformation of information from

sensory input to motor output. We wish to understand whether some basic truths exist which can simplify our understanding, patterns which appear again and again in the connections of neurons performing similar roles in different animals, or performing similar roles within the same animal, but in widely different behaviors. Thus, we seek patterns that might serve as elements of brains that range from milligrams to kilograms (Swanson, 2012). Where the structure within the structures (cortex, basal ganglia, etc.) is also conserved, and is the granularity at which genetically-identified circuit mapping works.

It is important to note early that neural communication can span more than the synaptic contacts contemplated here. There is non-synaptic communication, for example ephaptic and electrical coupling via gap junctions, as well as extra-synaptic communication from one neuron acting potentially on many responder neurons by means of neurotransmitter diffusion. There are even forms of non-synaptic communication such as gaseous neurotransmission. But as used in this work, neural circuit is meant to capture chemical neurotransmission and its dominance in the function of the nervous system.

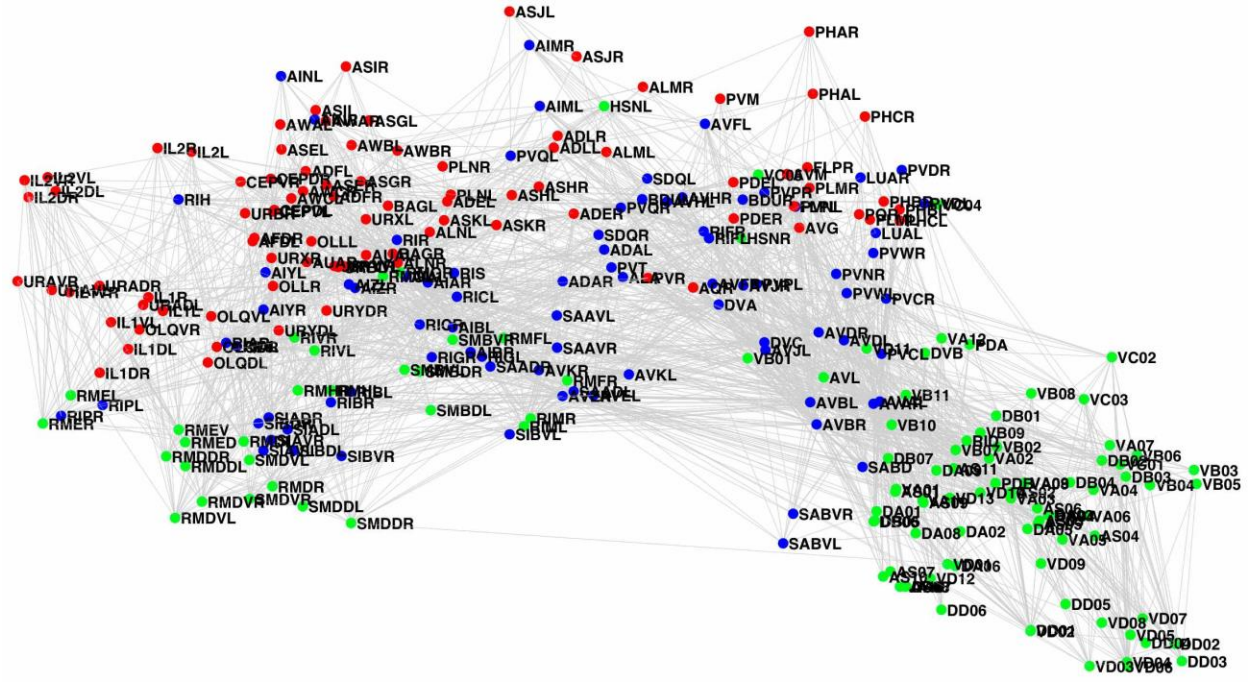

Figure 1.1: A 'complete map' of the nervous system of *Caenorhabditis elegans* (adapted from WORMATLAS)

From mapping in invertebrates to mapping by neural class

For some primitive animals such as *Caenorhabditis elegans*, a complete map exists of every connection amongst the 302 neurons (Figure 1.1) of its nervous system (White et al., 1986), leading to the possibility of computer models which might faithfully recapitulate the entirety of nematode behavior. At the other extreme lies *homo sapiens*, with a densely wired brain and dynamic connections numbering in the trillions. Notably, no other tissue, organ or system within the mammalian biome approaches the classification complexity of the nervous system (NIH Blueprint 2016). To start to understand the neural underpinnings of behavior in animals this complex, we require simplifications that group thousands to hundreds of thousands of neurons together in neural classes. The first classification is of course anatomical, where the region (e.g. cortex) and sub-region (e.g. cortical lamina) define the class. In the last two decades, the dominant theme of this simplification is the belief that, in addition to regional location,

neurons can and should be classed according to a few basic properties: developmental provenance, primary neurotransmitter, complement of receptors, physiological excitability, and relative location within their anatomical residence (among others, see Swanson et al., 1996; see Ascoli et al., 2008 for a comprehensive taxonomy).

Genetic identification of neural classes

Within the mammalian nervous system, this has led to the description and qualification of ever increasing classes of neurons. On the order of 150 classes account for most experimental usage today (NIH Blueprint for Neuroscience; NIH/GENSAT 2016), many of which are identified by the expression of a handful of specific genes related to either primary neurotransmitter or receptor complement. For instance, lower motor neurons, which manage the final output of all of the brains myriad calculations, are recognized universally by the expression of choline-acetyltransferase (ChAT), an enzyme crucial to the synthesis of the neurotransmitter released by motor neurons (Nachmansohn & Machado, 1943). Of course, the expression of all of these genes is driven by a cascade of transcription factors, which ought to be the means by which any one class of cell is identified, but the first-order classification of neural classes is dominated by the two factors (neurotransmitter and receptor) mentioned. It may be that any classification system for neurons produces false taxonomies, where in reality subtle differences amongst, say, interneurons within a cortical lamina, could ultimately produce a number of classes on the order of the number of neurons. The reason we want to explore the circuitry of classes is not to make a claim that the classes were correctly identified, but instead to leverage simplifications which might pragmatically assist us in understanding animal behavior without accounting for all the unique neural snowflakes of *Caenorhabditis elegans.*

Underlying all of this classification is an unstated faith that neurons within a class work together, under similar operating parameters, to transform synaptic inputs to axonal outputs, and enact behavior. The belief ultimately holds that the complete one-to-one mapping of all neurons is unnecessary because the complete mapping of classes is sufficient to explain behavior. As one might conclude in the object-oriented paradigm of computer science, the class owns the instance.

While the tools of genetic engineering opened up the possibility of classifying neurons by genetic properties, it was only with the introduction of conditional recombination that experiments could reliably leverage genetic identity (Sauer, 1987; Golic & Lindquist 1989). In particular, the ability to deliver DNA plasmids and viruses which were "turned on" in only neurons of the appropriate genetic background has allowed for tracing amongst genetically identified neurons where previously only bulk anatomical tracing was available.

Need and challenges to understanding behavior in terms of connections among genetically identified neurons

Studies of behavior in Mammalia rarely concern themselves with the effect on behavior from single neurons, but rather with the reproducible activity patterns of distinct sets of functionally coupled neurons, termed neural ensembles. Neurons grouped at this scale form the critical link between single-neuron computation and behavioral or cognitive functions. At a general level, ensembles fulfill the criteria of the neural classes described above, genetically identified and anatomically isolated within a local network. However, ensemble activity is sparse and only transiently stable within the local network, and complex behaviors usually invoke activity over multiple brain areas, which together with the sheer numbers of neurons and synapses in Mammalia restrict us from simple descriptive analysis of neural cause and

behavioral outcome, just as we learn very little of the properties of water from studying the electrostatic and steric properties of individual molecules of H_2O. Instead, we rely on statistical models and the intuitions they afford to make predictions about water. Similarly, only combined approaches from cellular and network analyses that define neural classes together with approaches from behavioral and theoretical neuroscience have potential to uncover organizing principles of behaviorally relevant ensemble activity.

To ask how neurons implement behavior is to ask what is learning. Motor learning is the most direct form of learning we undertake. We know that motor learning requires cortex and the basal ganglia working in concert. We concern ourselves here first with an investigation into the earliest signals of motor output. We imagine the nervous system as a grand input-output device with cortex at its pinnacle, seesawing back and forth between the processing of sensory inputs and the generation of motor plans that direct final motor output. This is of course a gross simplification, as the nervous system has an endless amount of short-circuits and reflex loops, but here we start from a modest assertion that volitional motor output begins in cortex, and that cortex both can generate new motor output as well as modulate output in progress.

To begin to understand the rules cortex follows in implementing its instructions to lower structures in the nervous system, we first leverage the abstraction of neural classes. To exploit classes previously identified, we use tracing tools which find connections among genetically-identified classes of neurons. The tracing we implement and enhance here is born from the belief that ensembles of neurons form repeated units that "gang up" to implement behavior. According to the statistical approach, albeit with limitations, this would seem the best way of attempt to dissect the function of neural ensembles.

Historical perspective on connectivity mapping

A reasonable claim could be made that the history of neuroscience is coincident with the history of neuroanatomical methods for analyzing the structure of neural networks. With the proposition in 1897 by Sherrington that synapses are the site of information transfer, tracing of these connections was the underlying framework for arguably all neuroscience that followed. The twin towers of neuroanatomy—Golgi and Ramón y Cajal—followed with the first proper visual exploration of individual neurons. This era of randomly labeled cells dominated the field for decades. While these approaches have been invaluable in for determining the architecture of local (intraregional) connectivity, the drawbacks were also significant: myelination obscured or excluded axons from impregnation with reagents, forcing scientists like Ramón y Cajal to focus their efforts on neonatal animals. Neurons were filled with dye randomly and completely, without regard to neuronal polarity. And of course *in vivo* application was untenable.

In the decades which followed, most of the progress in mapping neural circuits was done using synthetic dyes, or similar substrates which impregnated and darkly stained sparse populations of neurons to reveal the fine geometry of connectivity. Even prior to this, the crude technique of lesions leading to Wallerian degeneration of axons had illustrated the longest-range projections of the nervous system—remarkably, as recently as the 1960s, such lesion studies were still providing the bulk of advances in knowledge of neural paths, as with the first comprehensive studies of cortico-striatal projections (Webster, 1961), which provides the necessary background for Part 2 in this monograph (Figure 1.2). Cell-filling dyes such as Procion yellow allowed for staining the full extent of single neurons after direct injection into the cell body (Stretton & Kravitz, 1968), and later helped to join physiology with anatomy by allowing the diffusion of dye through a patch pipette. After 1970, a shift in techniques arose which relied

on the underlying biological processes of neurons to achieve their effect. The most important result was the establishment of tracers which took advantage of neuronal polarization, yielding tracers of either anterograde or retrograde action (Kristensson et al., 1971). From that point forward, the selectivity of neuronal labeling became a key feature in circuit mapping studies. A common property of these selective tracers is their biological, rather than purely synthetic, origin.

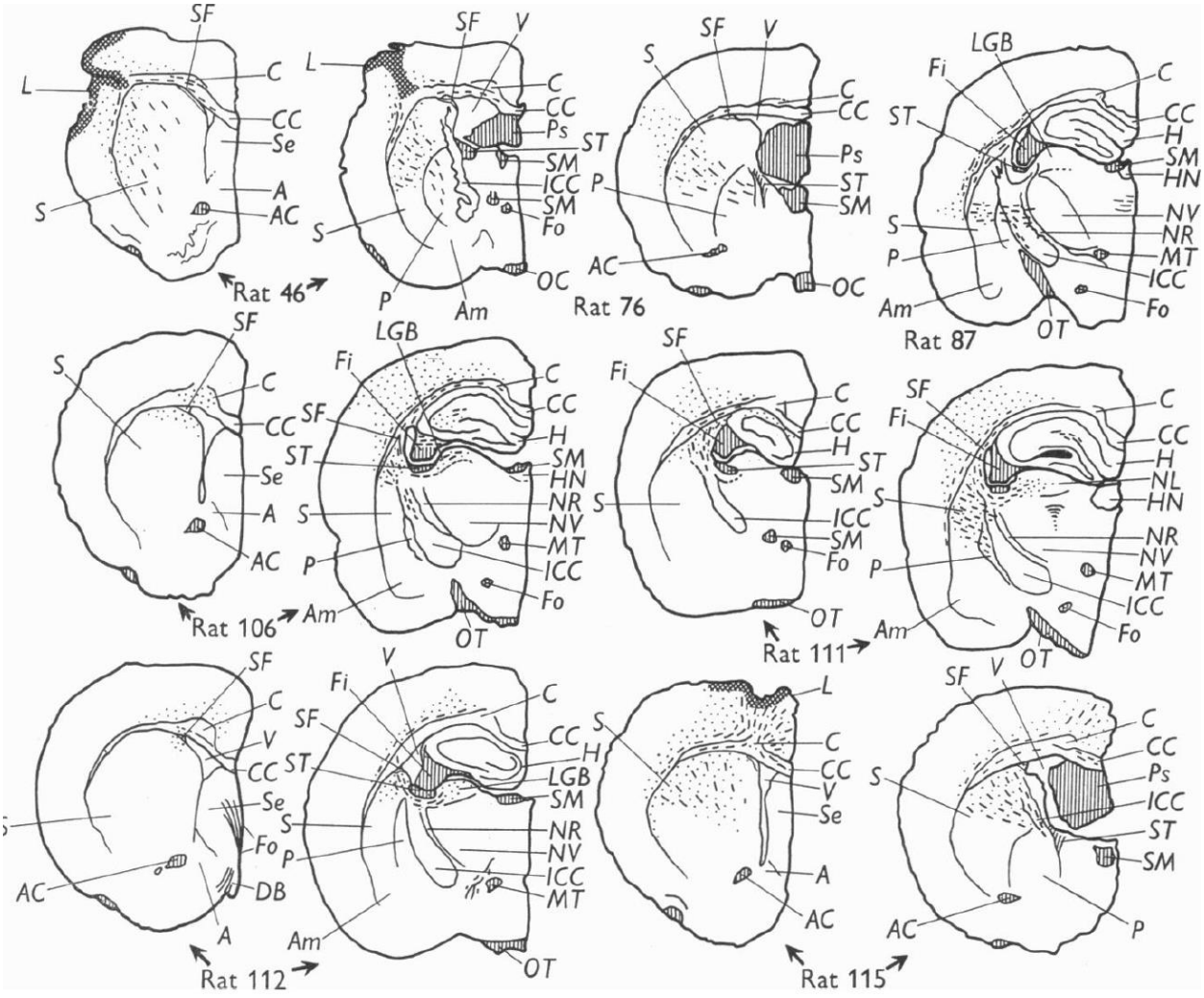

Figure 1.2: the first systematic attempt to map cortical projections to the striatum; lesions of cortex caused Wallerian degeneration of cortical axons in striatum, which are then impregnated with silver stain for visualization (adapted from Webster, 1961)

Continued refinement of tools led to the introduction of biological-synthetic hybrids, such as conjugated forms of cholera toxin subunit B (CTB) or wheat germ agglutinin (WGA). The greatest benefit obtained was perhaps the ability to introduce them *in vivo* in a circuit of inquiry. Collectively, these macromolecular tools, including dextran amines (Glover et al., 1986), latex beads (Katz et al., 1984), and DiI (Honig & Hume, 1986, in culture), all suffered from one key deficit: they could not amplify themselves once introduced into the cell. While many of the proteins such as horseradish peroxidase (HRP) engaged cellular machinery to obtain retrograde or anterograde specificity, they were not easily adopted by the emerging tools of molecular biology due to issues of ectopic expression (HRP is a plant protein which does not functionally express in mammalian cells). The amplification problems were thus not easily solvable by genetic means, since it was difficult or impossible to enable neurons to make tracer proteins autonomously.

Viral pathway and connectivity tracing techniques were introduced first to address the issue of signal amplification but ultimately proved to be even more useful for the ability to engineer them as agents which would label neurons based on genetic-identity (Enquist, 1994). These are discussed further below.

Static and dynamic mapping: marker proteins and functional proteins

Neuroanatomical mapping traditionally attempts to construct "labeled lines" of the nervous system. These are static maps, charting the possible flow of information from sensory input to behavioral output. They are invaluable in our quest for boundary anatomical constraints on information processing and coding, but these static maps can only give us part of the picture as they capture every potential channel for nervous signaling without describing how those signals are processed at their destination. Dynamic mapping is the refinement of static maps such

that certain connections are re-described in terms of their activity and response. In a dynamic map, one neuron may output the exact same signal to three different regions of the brain, but the neurons at the receiving end may have significantly different responses. This could be as subtle as differences in synaptic strength, causing one neuron to respond more strongly to the same input that another like neuron receives. It could be more dramatic, such as the change in valence from excitatory to inhibitory.

Using viral genetic tools, we are able to both build static maps of inputs to a particular neuron using fluorescent proteins as payloads in the viruses, as well as deploy functional proteins that allow us to monitor and manipulate activity of individual neurons and thus build dynamic maps. (Kaifosh et al., 2013; Petreanu et al., 2007).

The modern era: using deletion-mutant rabies virus to create static and dynamic maps

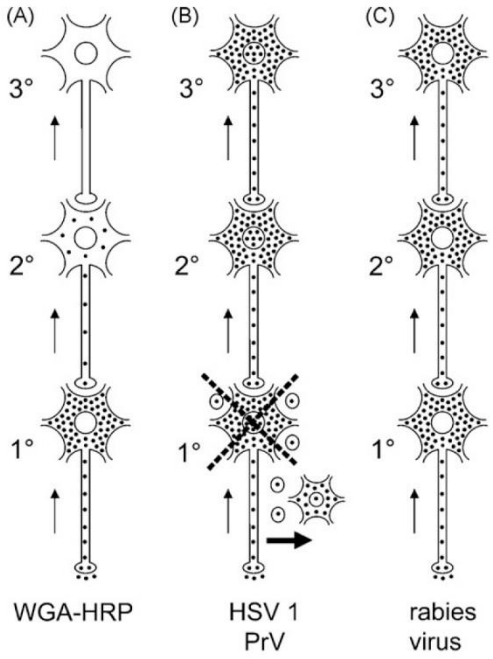

Figure 1.3: retrograde tracers, adapted from Ugolini 2010: WGA-HRP, a tracer based on the proteins wheat-germ-agglutinin and horseradish peroxidase; HSV-1, herpes simplex virus, PrV pseudorabies virus)

Tracing tools which rely on genetic encoding and expression have two major advantages over traditional synthetic tracers, namely the ability to target specific types of cells and the potential to amplify signals or other proteins of interest. The explosion of recombinant-engineering tools allowed for the exploration of a variety of protein-based and viral-based mechanisms to tracing. Some of the earliest tools used, such as a complex of wheat germ agglutinin and horseradish peroxidase (WGA-HRP) relied on the uptake of proteinaceous material by axons and the transport of that material in either a preferentially retrograde or anterograde fashion (Figure 1.3). These tools leverage the transport properties of one protein (the lectin WGA) with the reporter properties of another (stainable HRP). However, they suffer

from two major drawbacks: it is not proven that the transport of proteins is truly trans-synaptic, and more importantly, the amount of "signal", or expression, from the reporter gene was dependent on the amount of initial uptake.

Viral tools in contrast solve the problem of signal weakness because they can amplify in situ (note that viruses can be replication-incompetent yet still amplify genomically within a cell). Even a small amount of virus, perhaps a single virion, can amplify within a cell and produce both strong visual signals as well as targeted functional effectors. The two best known virus families for trans-synaptic tracing are the herpes simplex viruses (HSVs) and rabies viruses (RABVs) (Figure 1.3, 1.4)

Herpes simplex HSV-1 and related strains such as pseudorabies PrV (not to be confused with pseudotyped rabies) have enjoyed wide usage (Ugolini 2010; Enquist et al., 1998). The alpha-herpesvirus family consists of large, double-stranded DNA viruses. They express as many as 100 different genes from more than 150,000 base pairs. As such, it is a challenge to engineer it to make specific proteins of interest, or more importantly to remove native genes which are otherwise deleterious. This exposes the most significant drawback to HSV, which is cytotoxicity. The virus spreads rapidly and expresses strongly, and neurons rapidly disintegrate during storms of apoptosis (Thompson et al., 1983). Work has progressed toward taming the virus for usage in experimental neuroscience (Zeier, et al, 2009), but that work lags behind similar work on rabies viruses, a radically simpler RNA virus.

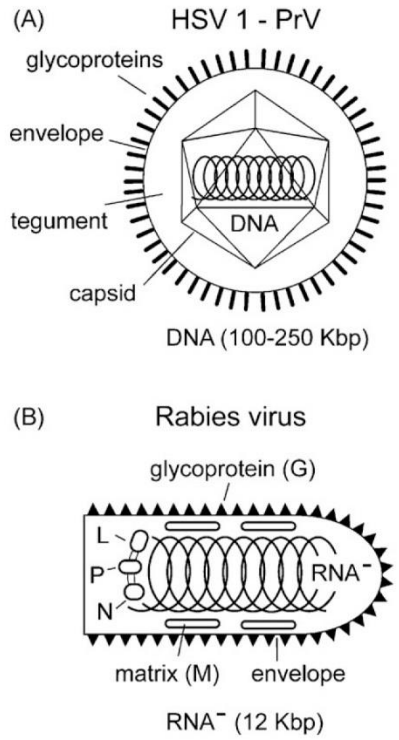

Figure 1.4: A: the alpha-herpesvirus HSV-1, or pseudorabies, showing both capsid and envelope; B: rabies virus, a much simpler RNA virus, has only 5 genes on one continuous segment, lacks a capsid and displays only a single glycoprotein along its surface

The first appearance of rabies as a systematic tracer of neural connections appears with the work of Ugolini in 1995. Coincidentally, another breakthrough that year was the cloning and rescue from DNA of rabies virus. Using a laboratory strain of rabies virus, CVS-11, Ugolini was able to demonstrate that the spread of virus occurs along well-known nerve paths, that virus is taken up at axon terminals and transported in an exclusively retrograde fashion (a view since overturned in the context of primary sensory neurons by Zampieri et al, 2014), and that axons of passage were not infected. Whether the virus transports exclusively trans-synaptically was not definitely showed but suggested.

Kelly & Strick (2000) exploited CVS-11 rabies as a poly-synaptic tracer in rodents and primates (Figure 1.5). The virus is lethal in its fully constituted form, but because it is “fixed”, it

has well understood transmission kinetics. By timing the course of the spread of infection through different nuclei and regions of the CNS, they were able to establish loops of connectivity from cortex to striatum to basal ganglia output and thalamus, and around again.

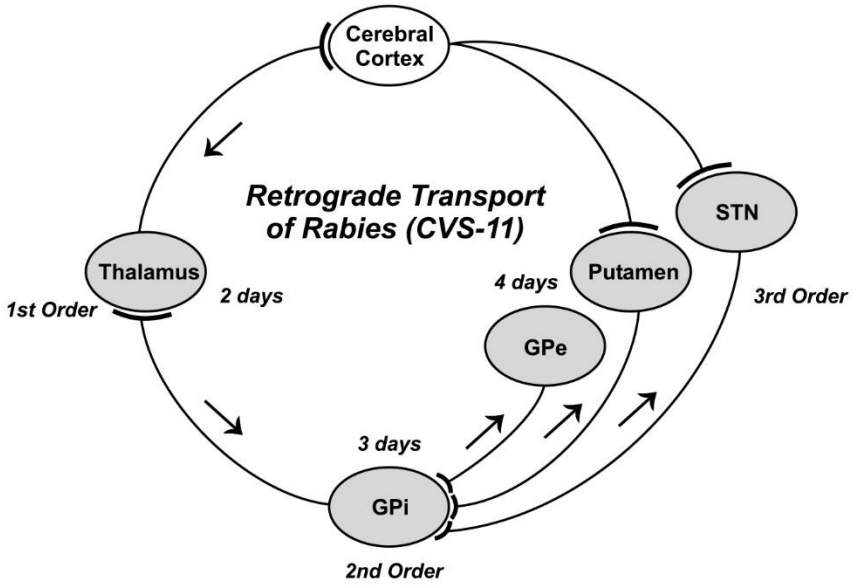

Figure 1.5: poly-synaptic spread of rabies virus in the cortico-basal-ganglia-thalamic loop (adapted from Kelly & Strick 2000)

The current era of genetically-identified circuit tracing began with Wickersham, et al (2006), when they succeeded in engineering rabies virus such that the singular gene required for cellular uptake and egress was deleted and reintroduced in trans (Figure 1.6). This deletion restricts the spread of virus to one synaptic jump. When combined with pseudotyping—the use of ectopic surface glycoproteins to alter the tropism of enveloped viruses--genetically identified neurons can be targeted, from ensembles down to single cells, and the virus offers the potential to identify all of the inputs to a targeted cell.

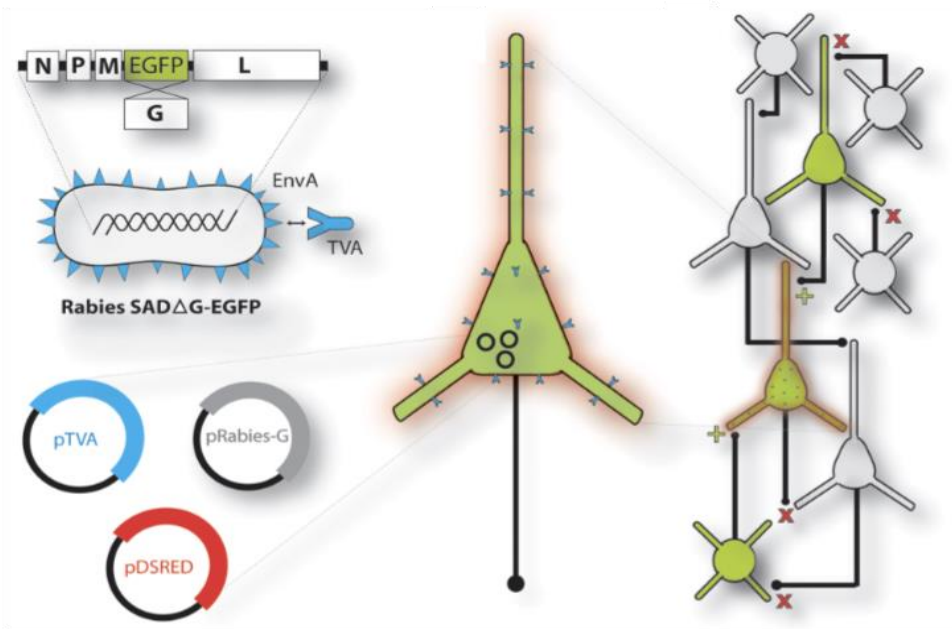

Figure 1.6: trans-synaptic labeling using deletion-mutant rabies viruses; pTVA plasmid for avian virus ASLV-A TVA receptor; EnvA envelope glycoprotein from ASLV-A; pRabies-G plasmid for rabies SAD-B19 glycoprotein; pDSRED reporter plasmid; SADΔG-EGFP deletion-mutant rabies virus contains five genes, with EGFP replacing native G, based on the inoculation strain SAD-B19 (adapted from Arenkiel & Ehlers 2009)

Constraints on original deletion-mutant rabies

As with many breakthroughs in the development of experimental tools, it can take several years of exploitation for a clear picture to emerge of the limitations of the technique, and several iterations before it reaches its potential. The invention of deletion-mutant rabies by Wickersham et al. (2007) similarly came with restrictions that constrained its use in many experimental applications. There has been continuous improvement to the original tool (Okasada, et al. 2010; Wickersham et al., 2013), in particular with a variety of increasingly sophisticated complementation reagents (Weissbourd, et al. 2014). One major restriction to which these improvements were addressed is the limited trans-synaptic spread of SAD-B19$^{\Delta G}$. This virus was typically limited to ten or fewer cells for every primary cell infected (Watabe-Uchida 2012; Wall et al., 2013; but see Rancz, et al. 2011). Another major restriction arose when SAD-B19$^{\Delta G}$ was

used to express functional proteins. The virus appeared to have a strong cytotoxic impact. The former led to incomplete static maps of the particular circuit in question, and the latter restricted the usage of the virus for *in vivo* experiments of the variety contemplated above for dynamic mapping. This led to the pursuit of several improvements to the base provided by Wickersham et al., using both improvement glycoproteins and entirely novel strains of deletion-mutant rabies. These are discussed at length in the following chapters.

Bibliography: Part 1

Alivisatos, A.P., Chun, M., Church, G.M., Greenspan, R.J., Roukes, M.L., and Yuste, R. (2012). The Brain Activity Map Project and the Challenge of Functional Connectomics. Neuron *74*, 970–974.

Arenkiel, B.R., and Ehlers, M.D. (2009). Molecular genetics and imaging technologies for circuit-based neuroanatomy. Nature *461*, 900–907.

Ascoli, G.A., Alonso-Nanclares, L., Anderson, S.A., Barrionuevo, G., Benavides-Piccione, R., Burkhalter, A., Buzsáki, G., Cauli, B., DeFelipe, J., Fairén, A., et al. (2008). Petilla terminology: nomenclature of features of GABAergic interneurons of the cerebral cortex. Nature Reviews Neuroscience *9*, 557–568.

Enquist, L.W. (1994). Infection of the mammalian nervous system by pseudorabies virus (PRV). Seminars in Virology *5*, 221–231.

Enquist, Husak, Banfield, and Smith (1998). PRV Bartha, an Example of a "Good" Tracing Virus. In Advances in Virus Research

Glover, J.C., Petursdottir, G., and Jansen, J.K.S. (1986). Fluorescent dextran-amines used as axonal tracers in the nervous system of the chicken embryo. Journal of Neuroscience Methods *18*, 243–254.

Golic, K.G., and Lindquist, S. (1989). The FLP recombinase of yeast catalyzes site-specific recombination in the drosophila genome. Cell *59*, 499–509.

Honig, M.G., and Hume (1986). Fluorescent carbocyanine dyes allow living neurons of identified origin to be studied in long-term cultures. The Journal of Cell Biology *103*, 171–187.

Kaifosh, P., Lovett-Barron, M., Turi, G.F., Reardon, T.R., and Losonczy, A. (2013). Septo-hippocampal GABAergic signaling across multiple modalities in awake mice. Nature Neuroscience *16*, 1182–1184.

Katz, L.C., Burkhalter, A., and Dreyer, W.J. (1984). Fluorescent latex microspheres as a retrograde neuronal marker for in vivo and in vitro studies of visual cortex. Nature *310*, 498–500.

Kelly, R.M., and Strick, P.L. (2000). Rabies as a transneuronal tracer of circuits in the central nervous system. J. Neurosci. Methods *103*, 63–71.

Kristensson, K., Olsson, Y., and Sjostrand, J. (1971). Axonal uptake and retrograde transport of exogenous proteins in the hypoglossal nerve. Brain Research *32*, 399–406.

Lichtman, J.W., and Denk, W. (2011). The Big and the Small: Challenges of Imaging the Brain's Circuits. Science *334*, 618–623.

Markram, H. (2006). The Blue Brain Project. Nature Reviews Neuroscience *7*, 153–160.

Nachmansohn, and Machado (1943). The Formation of Acetycholine. A New Enzyme: "Choline Acetylase." J. Neurophysiology *6*.

Osakada, F., Mori, T., Cetin, A.H., Marshel, J.H., Virgen, B., and Callaway, E.M. (2011). New Rabies Virus Variants for Monitoring and Manipulating Activity and Gene Expression in Defined Neural Circuits. Neuron *71*, 617–631.

Petreanu, L., Huber, D., Sobczyk, A., and Svoboda, K. (2007). Channelrhodopsin-2–assisted circuit mapping of long-range callosal projections. Nature Neuroscience *10*, 663–668.

Rancz, E.A., Franks, K.M., Schwarz, M.K., Pichler, B., Schaefer, A.T., and Margrie, T.W. (2011). Transfection via whole-cell recording in vivo: bridging single-cell physiology, genetics and connectomics. Nature Neuroscience *14*, 527–532.

Sauer, B. (1987). Functional expression of the cre-lox site-specific recombination system in the yeast Saccharomyces cerevisiae. Molecular and Cellular Biology *7*, 2087–2096.

Seung, H.S. (2011). Neuroscience: Towards functional connectomics. Nature *471*, 170–172.

Shepherd, G.M. (1991). Foundations of the neuron doctrine (New York: Oxford University Press).

Stretton, A.O.W., and Kravitz, E.A. (1968). Neuronal Geometry: Determination with a Technique of Intracellular Dye Injecion. Science *162*, 132–134.

Swanson, L.W. (2012). Brain architecture: understanding the basic plan (New York: Oxford University Press).

Thompson, R.L., Wagner, E.K., and Stevens, J.G. (1983). Physical location of a herpes simplex virus type-1 gene function(s) specifically associated with a 10 million-fold increase in HSV neurovirulence. Virology *131*, 180–192.

Tononi, G., and Koch, C. (2008). The Neural Correlates of Consciousness: An Update. Annals of the New York Academy of Sciences *1124*, 239–261.

Ugolini, G. (1995). Specificity of rabies virus as a transneuronal tracer of motor networks: Transfer from hypoglossal motoneurons to connected second-order and higher order central nervous system cell groups. The Journal of Comparative Neurology *356*, 457–480.

Ugolini, G. (2010). Advances in viral transneuronal tracing. J. Neurosci. Methods *194*, 2–20.

Wall, N.R., De La Parra, M., Callaway, E.M., and Kreitzer, A.C. (2013). Differential Innervation of Direct- and Indirect-Pathway Striatal Projection Neurons. Neuron *79*, 347–360.

Watabe-Uchida, M., Zhu, L., Ogawa, S.K., Vamanrao, A., and Uchida, N. (2012). Whole-Brain Mapping of Direct Inputs to Midbrain Dopamine Neurons. Neuron *74*, 858–873.

Watts, A.G., and Swanson, L.W. (2002). Anatomy of Motivation. In Stevens' Handbook of Experimental Psychology, H. Pashler, ed. (Hoboken, NJ, USA: John Wiley & Sons, Inc.),.

Webster, K. (1961). Cortico-striate interrelations in the albino rat.

Weissbourd, B., Ren, J., DeLoach, K.E., Guenthner, C.J., Miyamichi, K., and Luo, L. (2014). Presynaptic Partners of Dorsal Raphe Serotonergic and GABAergic Neurons. Neuron *83*, 645–662.

White, J.G., Southgate, E., Thomson, J.N., and Brenner, S. (1986). The structure of the nervous system of the nematode Caenorhabditis elegans. Philos. Trans. R. Soc. Lond., B, Biol. Sci. *314*, 1–340.

Wickersham, I.R., Lyon, D.C., Barnard, R.J.O., Mori, T., Finke, S., Conzelmann, K.-K., Young, J.A.T., and Callaway, E.M. (2007). Monosynaptic Restriction of Trans-synaptic Tracing from Single, Genetically Targeted Neurons. Neuron *53*, 639–647.

Wickersham, I.R., Sullivan, H.A., and Seung, H.S. (2013). Axonal and subcellular labelling using modified rabies viral vectors. Nature Communications *4*.

Zampieri, N., Jessell, T.M., and Murray, A.J. (2014). Mapping Sensory Circuits by Anterograde Trans-synaptic Transfer of Recombinant Rabies Virus. Neuron *81*, 766–778.

Zeier, Z., Aguilar, J.S., Lopez, C.M., Devi-Rao, G., Watson, Z.L., Baker, H.V., Wagner, E.K., and Bloom, D.C. (2009). A limited innate immune response is induced by a replication-defective herpes simplex virus vector following delivery to the murine central nervous system. Journal of Neurovirology *15*, 411–424.

Swanson et al (1996). Integrated systems of the CNS, part III. Cerebellum, basal ganglia, olfactory system (Amsterdam: Elsevier).

Neuronal Wiring of C. elegans: http://www.wormatlas.org/neuronalwiring.html. Retrieved April 27, 2016.

NIH Blueprint for Neuroscience: http://www.neuroscienceblueprint.nih.gov/factSheet/GENSAT.htm Retrieved April 27, 2016.

Part 2

Preface

It is conventional to consider the neocortex as the seat of consciousness and the root of volitional behavior. Cortex is adjacent to and tightly bound with the basal ganglia, and it is possible that all cortical output is available to the basal-ganglia. The striatum represents the major input region of the basal ganglia. Here, we consider cortex and striatum as a joint structure and offer an inquiry and early results about the nature of the unidirectional projection from cortex to striatum, based on mono-synaptic tracing studies.

Functions of dorsal striatum

The basal ganglia are the first structure that cortical neurons encounter as their axonal outputs course downward toward the spinal cord. The projection from cortex (or pallium) to the basal ganglia is conserved from primates all the way to "ancient" vertebrates such as the lamprey (Gerfen & Bolam, 2010; Grillner 2008, 2011). Proper function of this circuit is required for the acquisition of skilled motor behaviors (Dudman & Krakauer, 2016; Koralek et al., 2012; Yin et al., 2009). In rodents, operant tasks such as sequential lever presses require proper function of basal ganglia (Costa 2007). Dysfunction within the dorsal basal ganglia, most often due to dysregulation of ascending dopaminergic input, leads to profound motor deficits, most famously the symptoms observed in Parkinson's and Huntington's disease. The major recipient of the massive cortical projection to the basal ganglia are the input nuclei, the ventral and dorsal

stratum. These two input nuclei also receive by far the largest transmission of dopamine in the brain. The dorsal striatum is the target of the inquiry here.

From the first investigations into the tragedy of Phineas Gage to contemporary studies of cortically-lesioned patents, it is conventionally if not dogmatically thought that volitional behaviors emerge from frontal cortex. But evidence mounts that the interaction between cortex and the striatum is necessary for the proper acquisition of skilled movements, and we hold that skilled movements are the primary expression of volition. As is described below in detail, the cortical projection to striatum is nearly global, to the extent that striatum may receive a near-complete copy of cortical output (Dudman & Gerfen, 2015; J. Dudman personal correspondence). The striatum, to a first approximation, shadows cortex. If cortical processing is the heart of volition, we might say that cortico-striatal processing is key to the proper expression of volition.

Volitional behavior as used here focuses on skilled movements and includes tasks such as reaching for desired objects. These are motivated behaviors, neither reflexive nor repetitive, and require both planning and ongoing maintenance and compensation. Data increasingly suggest that plasticity in the cortico-striatal circuit are key to acquiring these skilled behaviors (Koralek et al., 2012).

Basal ganglia output emerges downstream of the striatum (Figure 2.1), from the globus pallidus (GP) and substantia nigra pars reticulata (SNr). Two output paths variably affect behavior: there are strong descending outputs to the superior colliculus and pontine nuclei which can serve to directly initiate and modulate motor behaviors, and ascending outputs to the thalamus. This latter forms the cortico-basal-ganglia loop, thought to affect ongoing maintenance

of movement among other integrative roles (Parent & Hazrati, 1995; Haber 2003; Costa et al., 2004; Cui et al., 2013).

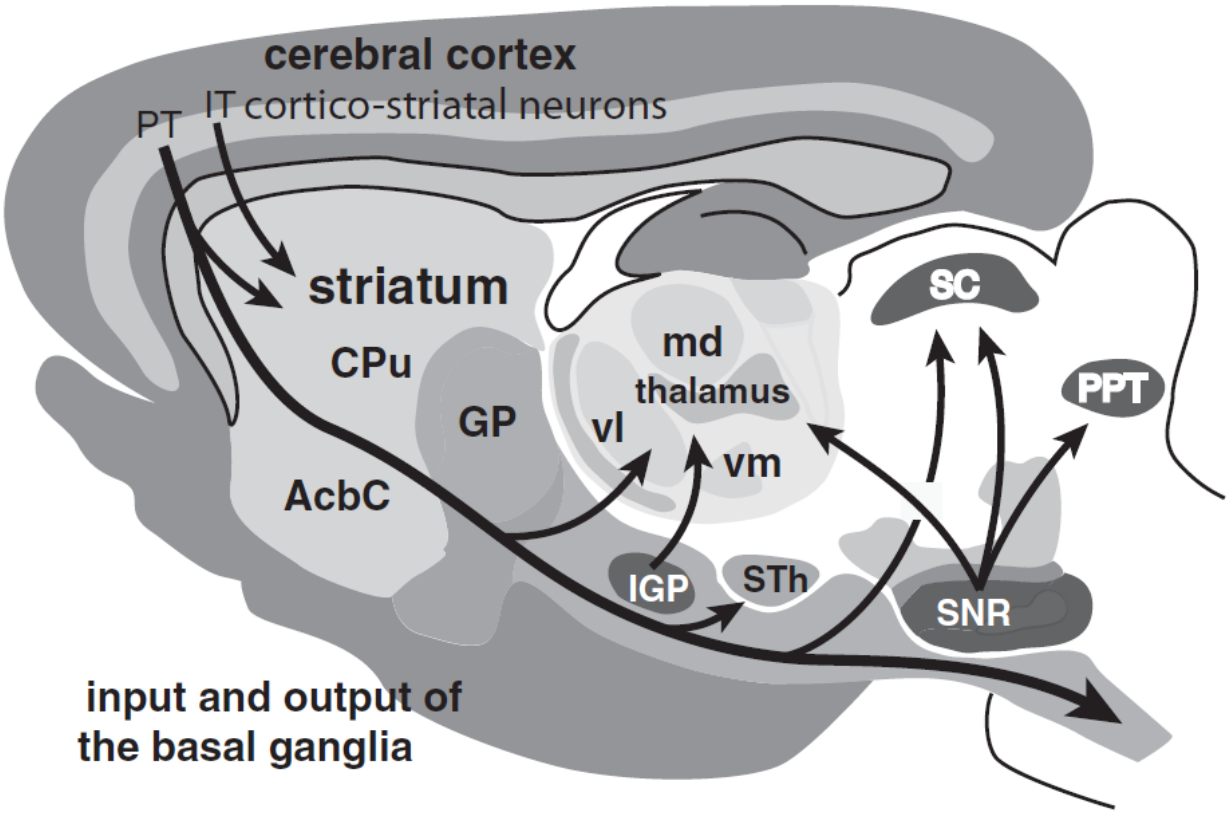

Figure 2.1: map of basal ganglia of the rodent, sagittal view, with striatum as primary input region of basal ganglia, GP and SNR as primary output; CPu caudate putamen or dorsal striatum, AcbC nucleus accumbens, GP globus pallidus, IGP global pallidus internal segment, vl/vm/md thalamic nuclei, STh subthalamic nucleus, SNR substantia nigra pars reticulata, SC superior colliculus, PPT pedunculopontine tegmental nucleus (adapted from Dudman & Gerfen 2015)

Architecture of the basal-ganglia: input and output

The striatum is composed primarily of medium spiny neurons (MSN), which form a GABAergic projection. The MSNs receive excitatory input from cortex and thalamus, with the former providing perhaps 80% of total input (Dudman & Gerfen 2015; personal observation

from retrograde tracing studies). Most famously, the striatum is the target for majority of dopamine released from the midbrain.

In rodents, the dorsal striatum is a unitary structure, whereas in primates it is divided into two portions, the putamen and caudate nucleus. The putamen corresponds to dorsolateral striatum in rodents, where the caudate corresponds to dorsomedial striatum. Our circuit analysis below will focus on dorsolateral striatum, thought to be a center for the consolidation of skilled motor actions as they become habit (Yin et al., 2005; Yin et al., 2009)

MSNs project to two downstream nuclei, the global pallidus (GP) and the substantia nigra (SN) via "direct" and "indirect" pathways (Figure 2.2). The GP itself has an output segment, GPi in primates and entopeduncular nucleus in rodents. GP outputs both onward to substantia nigra as well as outward to thalamus. The SN pars reticulata represents the last stage of output from the basal ganglia.

For purposes of model simplification, we leave aside the role of the subthalamic nucleus (STN) as both a zone of direct cortical input as well as a target for a portion of striatal output. Thus, with the exception of modulatory dopamine, all basal ganglia output is GABAergic and inhibitory.

In the canonical model of basal ganglia function, the inhibitory output is tonic while phasic excitation from cortex leads to disinhibition via the striatal projection neurons. That is, activation of striatonigral medium spiny neurons by cortical input results in inhibition of substantia nigra pars reticulata, thus disinhibiting its action on the thalamus, superior colliculus, and other targets. The indirect pathway is more complex but at its simplest may act in reverse. The key observation is that striatal neurons which project to one pathway or the other may work

antagonistically, which immediately begs the question of how medium spiny neurons receive input and what transformations they make in forming outputs.

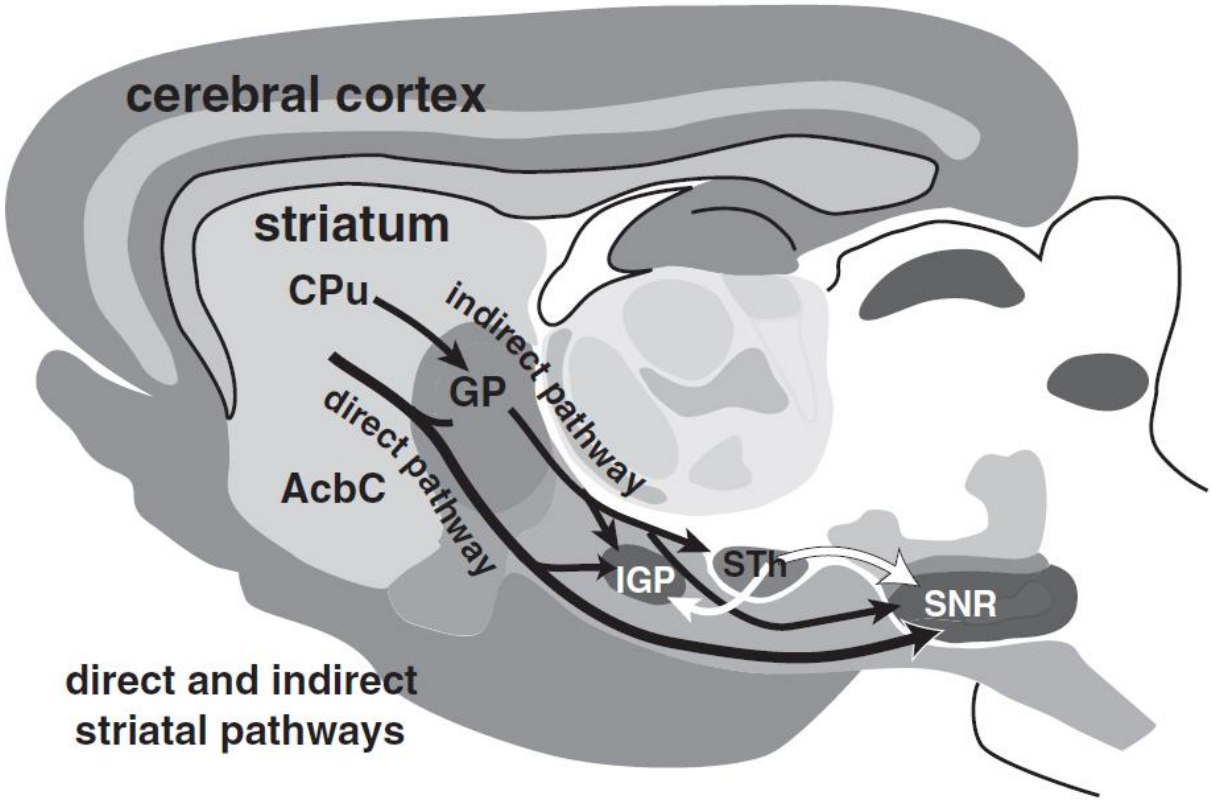

Figure 2.2: map of basal ganglia pathways in the rodent, sagittal view, with striatonigral projections for the direct pathway and striatopallidal projections for the indirect pathway (adapted from Dudman & Gerfen 2015)

Medium spiny neurons are the dominant striatal neuron

Conserved nature of cortico-striatal input and output

It is estimated that 95% or more of all neurons in the striatum are MSNs (higher in rodents, lower in primates), with the rest comprised of a small but important number of cholinergic, tonically active neurons as well as a vanishingly small number of GABAergic

interneurons (Dudman & Gerfen 2015). While MSNs are less prevalent in primates, this anatomical ratio of MSN abundance is conserved across the span of Mammalia from human to mouse, and further extends to avian, reptile, and aquatic species. It is highly conserved. Thus, what we discover about the nature of cortical innervation of striatum in rodents may yield insight into the role of the striatum in modifying or guiding "cortically initiated" behavior across many species. It may also reveal much about the evolution of cortex as it expanded to dominate the basal ganglia in generating behavior.

Cortical input to striatum is global

No region of the central nervous system receives more cortical input than the striatal nuclei. For sensory-motor and frontal areas of cortex, the projection is densest to dorsal striatum. There is evidence that these cortical projection neurons all make synapses onto dorsal striatum (Zheng & Wilson 2002; Dudman & Krakauer 2016; but see Donoghue & Kitai 1981) even as they continue on to pontine or spinal nuclei. In this light, the cortico-striatal projection can be seen as a total mapping of cortical output.

In a series of important studies from the Wilson laboratory (Cowan & Wilson, 1994; Kincaid & Wilson, 1996; Kincaid et al., 1998; Zheng & Wilson, 2002) we get clues as to the combinatorics that necessitate the view that the cortex fully maps to striatum. Each medium spiny neuron has roughly 7500 synapses, of which we assume 4000 are from cortex. Within the volume of a single MSN, there are nearly 400,000 cortical axons and 3000 other MSNs. Each cortical axon has boutons for 40 synapses within the volume of the dendritic field of the MSN, yielding a potential connection rate around 1%. Thus, the cortico-striatal connection is quite sparse, and even neighboring MSNs are unlikely to receive input from the same cortical neuron.

Functional organization of dorsal striatum: putative motor striatum

While the cortical projection to striatum may be "complete", it does not follow the functional homuncular organization of sensorimotor cortices. A cortical axon typical meanders and synapses across a vast range of striatum, while the regions of highest synaptic output, or focus, are organized along a ventromedial / dorsolateral axis (Voorn 2004) (Figure 2.3). For our purposes, this means that a putative "motor striatum" can be seen as that part of dorsolateral striatum upon which motor cortical areas make their greatest number of synaptic contact. Regardless, this organization is entirely unlike the homuncular organization that is typical used to describe cortex. Rather than a "foot" or "finger" focal area, individual MSNs within the dorsolateral striatum appear to mix a variety of somatotopic information. It should be noted that despite the assertion here, there is evidence of overlapping "focal" and "diffuse" cortico-striatal projection systems. For instance, Wright et al. (1999) showed that the highly organized output of adjacent barrels in mouse whisker sensory cortex yields two different forms of axon projections, one that is similarly focused in adjacent zones of striatum and another that spans across barrels. As will be seen below, our view is that the overwhelming majority of inputs to dorsal striatum are of the "mixed" variety (see Brown and Feldman 1992).

The striatal outputs visibly diverge down two separate axonal paths, leading dense but distinct fiber bundles into either GPe or SN. Axons of either pathway rise without obvious organization or anatomical preference from medium spiny neurons across the expanse of the striatum. Projection neurons of the striatum were thus classed as indirect (striatopallidal) or direct (striatonigral).

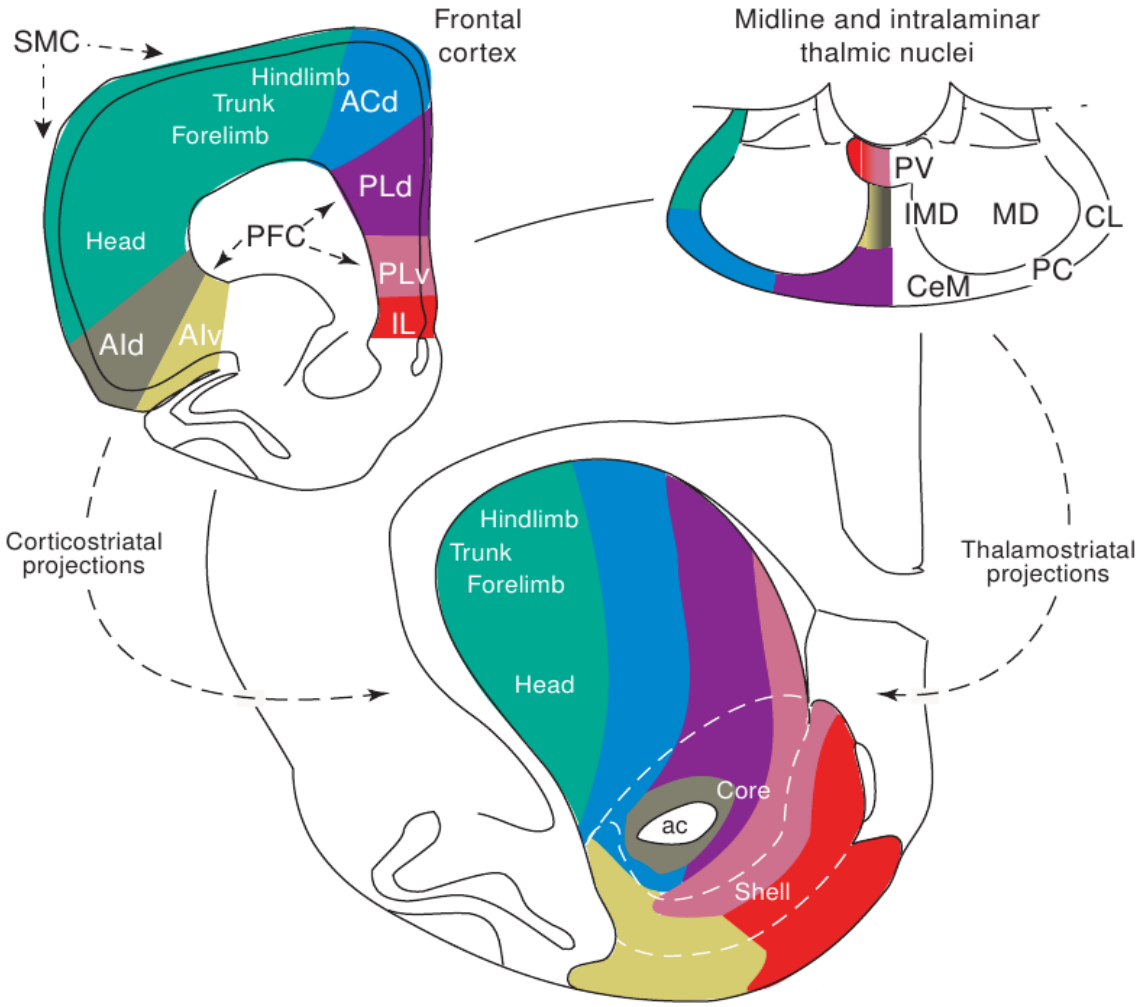

Figure 2.3: excitatory projection map from cortex and thalamus into striatum, including dorsal and ventral extents. (adapted from Voorn et al, 2004)

Striatum neurons lack obvious anatomical organization

While the outputs of the striatum present clear anatomical feature, the neurons which give rise to those outputs appear distributed evenly throughout the striatum. The first evidence of genetic separation of cell-types arose from the discovery of "patch" and "matrix" zones (Graybiel 1978) within the striatum, which contained relative differences in some receptors and neuropeptides but which did not separate neurons by projection targets. Patch and matrix do serve to organize cortical inputs, such that inputs from different cortical sublayers synapse differentially on each compartment (Gerfen, 1989). It is this fact which leads to the question of whether a similar organization might be found based on the identity and location of the two different outputs neurons of the striatum. But to understand whether cortical axons connected equally to the two different basal ganglia pathways required the discovery of markets for those neurons.

Direct and indirect pathways

After it emerged in the 1970's that most neurons of the striatum were projection neurons and that their outputs followed two distinct pathways, it was next shown that all projection neurons were of the medium spiny GABAergic variety. Starting in 1982, a series of immuno-histochemical tracing studies revealed a striking anatomical feature of the striatum, showing that the distinct projection pathways (Figure 2.4) corresponded to expression of different neuropeptides and, later, specific subtypes of dopamine receptors (Gerfen & Sawchenko, 1984; Izzo et al., 1987; Gerfen 1990).

Our work began with this question: how do projections neurons of the neocortex synapse onto the two major subclasses of neurons at the input of the basal ganglia? We investigated

whether cortical neurons, as distinguished by their somata, or starting location, may or may not drive the basal ganglia by differentially communicating with its two parallel pathways. While the basal ganglia play a role across a wide spectrum of vertebrate behavior, we concerned ourselves with skilled motor behaviors, and asked how the synaptic map from cortex to the striatum, the input nucleus of the basal ganglia, impacts motor behavior. It has been shown that activation of striatonigral neurons can promote locomotion, whereas activation of striatopallidal neurons can retard (Kravitz, et al., 2012; Kravitz et al., 2010). Changes in the relative innervation of these pathways produce striking effects and may underlie significant pathologies (Cazorla, et al., 2014). Further, phasic activity in these two populations was observed in skilled instrumental tasks (Xin & Costa, 2010).

We report our results and compare with others in subsequent sections.

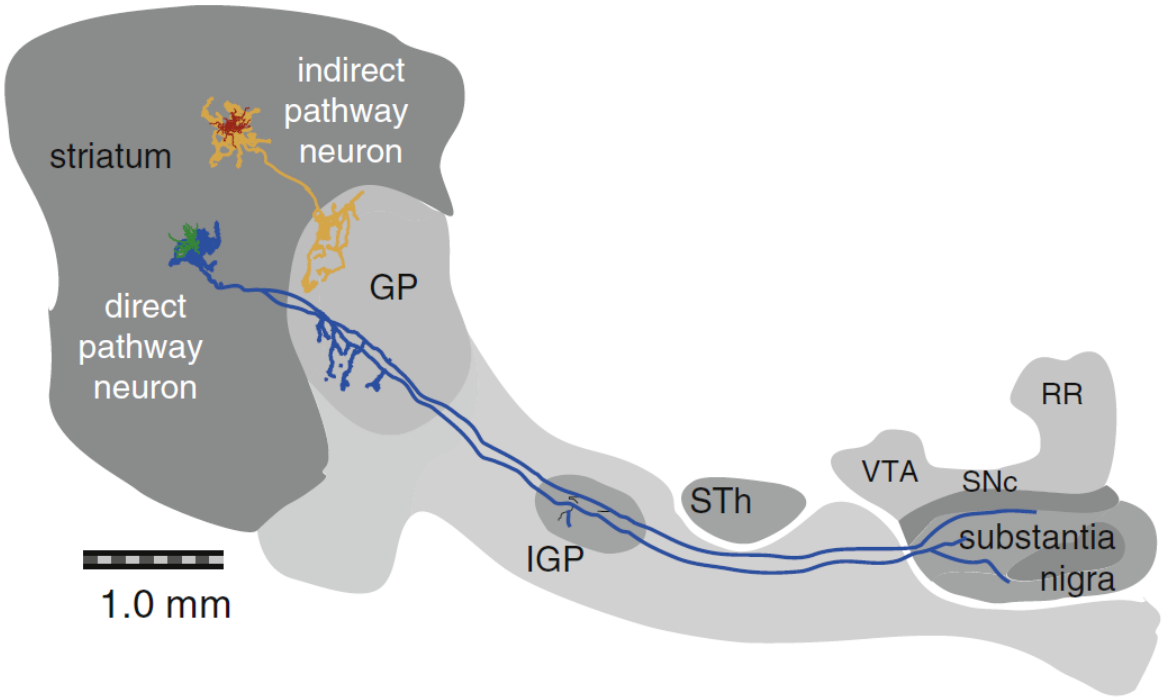

Figure 2.4: schematic of the two parallel pathways of the basal ganglia, sagittal view in rodent brain. Striatonigral medium spiny neurons project along the direct pathway while striatopallidal MSNs project along the indirect pathway. GP global pallidus, IGP globus pallidus internal segment, STh subthalamic nucleus, VTA ventral tegmental area, SNc substantia nigra pars compacta (adapted from Gerfen 2015)

Medium spiny neurons are identified by two genetic markers which coincide with axonal output

Following the initial insight that striatal neurons could be segregated by both the isolation of inputs from cortex as well as the expression of specific neuropeptides, a more significant discovery (Gergen 1990) was made regarding the output of MSNs: it had been shown the two different dopamine receptors were widely expressed in the striatum, but Gerfen discovered that MSNs which projected via the direct pathway exclusively expressed the D1 receptor while those projecting more dorsally into the pallidum expressed the D2 receptor (Figure 2.6), and that there was scant cross-expression (Figure 2.5). A number of studies then established that D1- and D2-receptor-expressing MSNs have different responses to dopamine, different basal physiological properties, and different morphological features (Gertler et al., 2008). Over the course of the next two decades, an explosion of research investigated the relative contribution of D1- and D2-expression neurons in sculpting normal and abnormal animal behavior (see discussions in Gerfen and Bolam, 2010; Howes et al., 2012).

While other genes also serve to mark the separation of these subpopulations (dynorphin and substance P versus enkephalin) is it the different expression of dopamine receptor subtypes that has drawn the most attention (Surmeier et al., 2007). Each of these receptors responds to binding of dopamine differently, with dopamine having marginally excitatory effects to D1-expressing cells and inhibitory to D2-expressing cells. Given the wide and still growing literature on reward and the effects of dopamine on behavior, this difference has provided the most

compelling models for how differential pathway output might serve as a basis for learned behaviors (Schulz 2002; Costa 2011; Vicente et al., 2016).

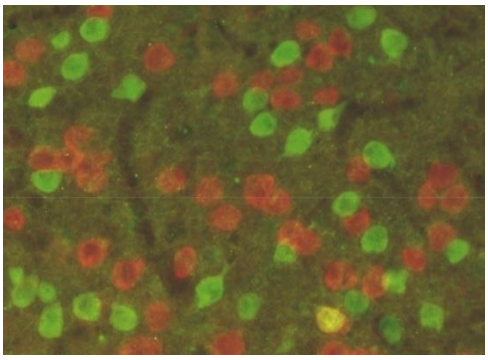

Figure 2.5: immunostaining illustrates the anatomical mixture of striatonigral (green) and striatopallidal (red) neurons, based on different G protein expression (from Gerfen et al. 2002)

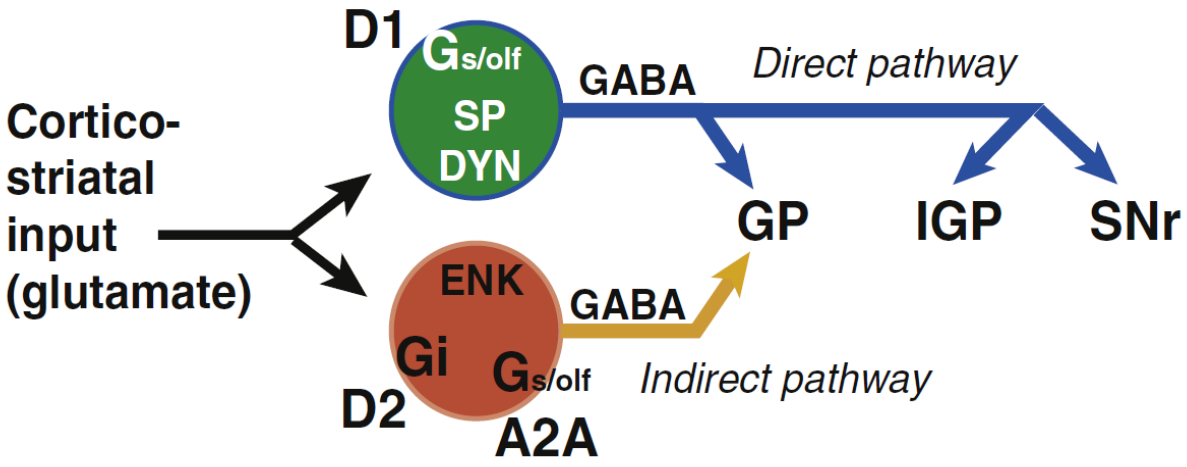

Figure 2.6: schematic representation of direct- and indirect-pathways of the basal ganglia. Cortical input feeds onto two subpopulations of medium spiny neurons. Striatonigral (direct-pathway) neurons express substance P, dynorphin and the dopamine receptor Drd1a, and project *en passant* to the globus pallidus on their way to terminations in the midbrain output nuclei of the basal ganglia; enkephalin, the adenosine receptor 2A, and the dopamine receptor Drd2 collectively mark the neurons of the striatopallidal (indirect-pathway) projection) (adapted from Gerfen 2015)

Other class groupings of medium spiny neurons may exist which are masked by identification using dopamine receptor expression

A major caveat to these models is the mixture of direct- and indirect-pathway neurons into patch and matrix. While it is clear from anterograde tracing (figure not shown; results from AAV-FLEX-synaptophysin_GFP labeling of synapses of D1-Cre expressing and A2AR-Cre expressing neurons) that indirect-pathway neurons project only to globus pallidus, and that direct-pathway axons make a lesser connection to globus pallidus on their way to substantia nigra and GPi, it is not understood if there are "pure" striatonigral connections. If a variety of subclasses exists for each pathway, it may be that differences in cortical innervation are masked by grouping classes at too large a granularity.

Genetic tools are required to separate inputs to MSNs

The striatum can be viewed as having two overlapping anatomical organizations: (1) patch and matrix, and (2) direct- and indirect-pathway. Patch and matrix can roughly be viewed as organizing inputs, for instance from different cortical layers or feedback from midbrain structures, while the pathways organize output. In each case, a set of genes are uniquely expressed. To date, there is minimal evidence that patch and matrix have much impact on pathway identity. (Dudman & Gerfen, 2015).

Given the mixing of pathway neurons, traditional synthetic tracers, and even biological tracers such as wheat-germ-agglutinin (WGA), cannot help untangle whether there is an underlying organization of cortical inputs based on striatal pathway output identity.

How convergent or divergent are synapses onto medium spiny neurons?

Several models of cortical axon arborization have been described for the striatal afferents. It is not clear whether these are actual genetic subtypes of cortical neurons (Gerfen 1989; Greig 2013). The two simplest models are focal and diffuse (Kincaid et al., 1998). In either case, it does not appear that focal arborization leads to more convergent or multiplicative contact onto target neurons. Rather, the sparse model of Zheng and Wilson (2002) and Parent and Parent (2006) appears to be dominant. Under that model, we expect only single contacts from passing cortical axons, and further expect that adjacent MSNs do not receive common cortical input.

It may be that the synaptic organization of inputs to MSNs is merely obscured by the non-laminar structure of the striatum, much the same way that non-laminar structure of pallial tissue (closely related to neocortex in evolution) obscures the input structure of projections neurons in animals such as passeriform songbirds (Gerfen & Surmeier 2011).

An important caveat about convergence is that relative amount of total input that striatonigral and striatopallidal neurons receive. It has been suggested that neurons of the direct-pathway are modestly less compact, electrotonically, than indirect-pathway neurons, owing to a substantially increase in surface area (Figure 2.7). This latter observation, while controversial, implies 50% more spine (cortical projection neurons synapse exclusively on dendritic spines of MSNs) onto the direct-pathway (Gerfen & Surmeier 2011; Day et al 2008; Planert et al., 2013). All data presented below, from myself as well as similar reports from Wall et al. (2013), ignore this possibility, which would represent an otherwise substantial and important normalization of the data we do present.

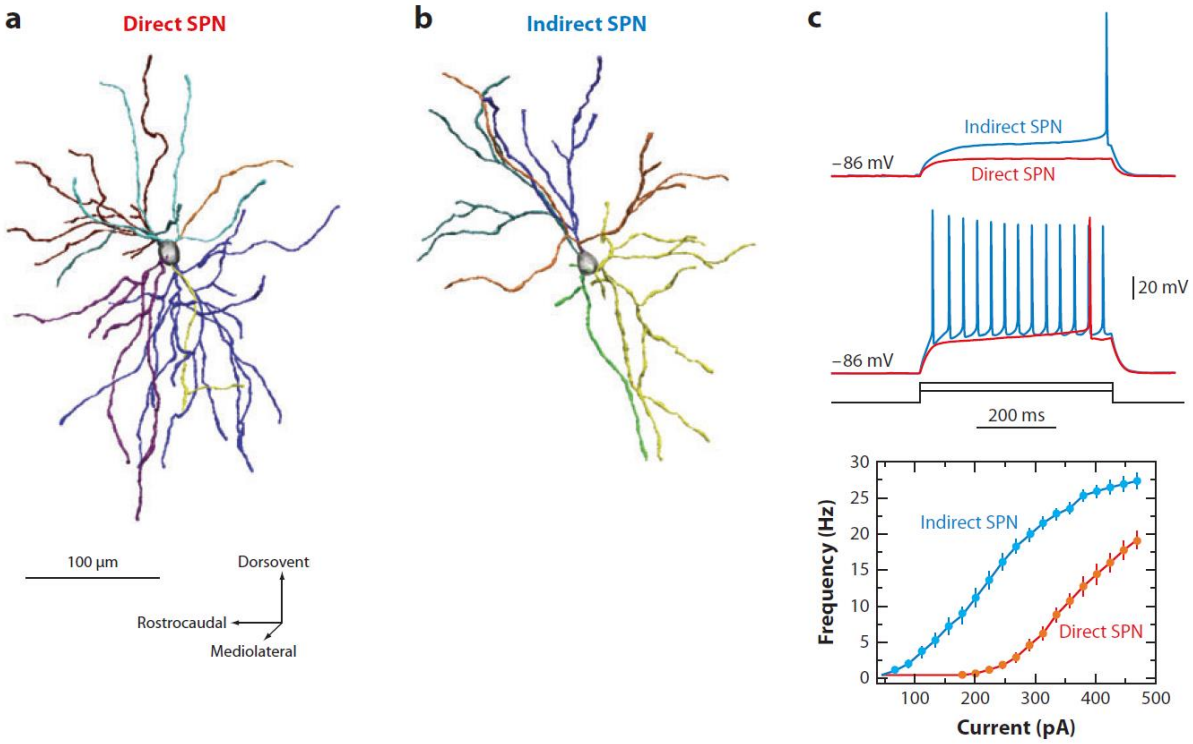

Figure 2.7: (a) reconstruction of representative striatonigral medium spiny projection neuron; (b) same from striatopallidal (c) response of each type of MSN to somatic current steps; indirect-pathway MSNs are more excitable, possibly due to overall membrane compactness (adapted from Gertler et al., 2008)

Open questions regarding cortical input: specifists and generalists

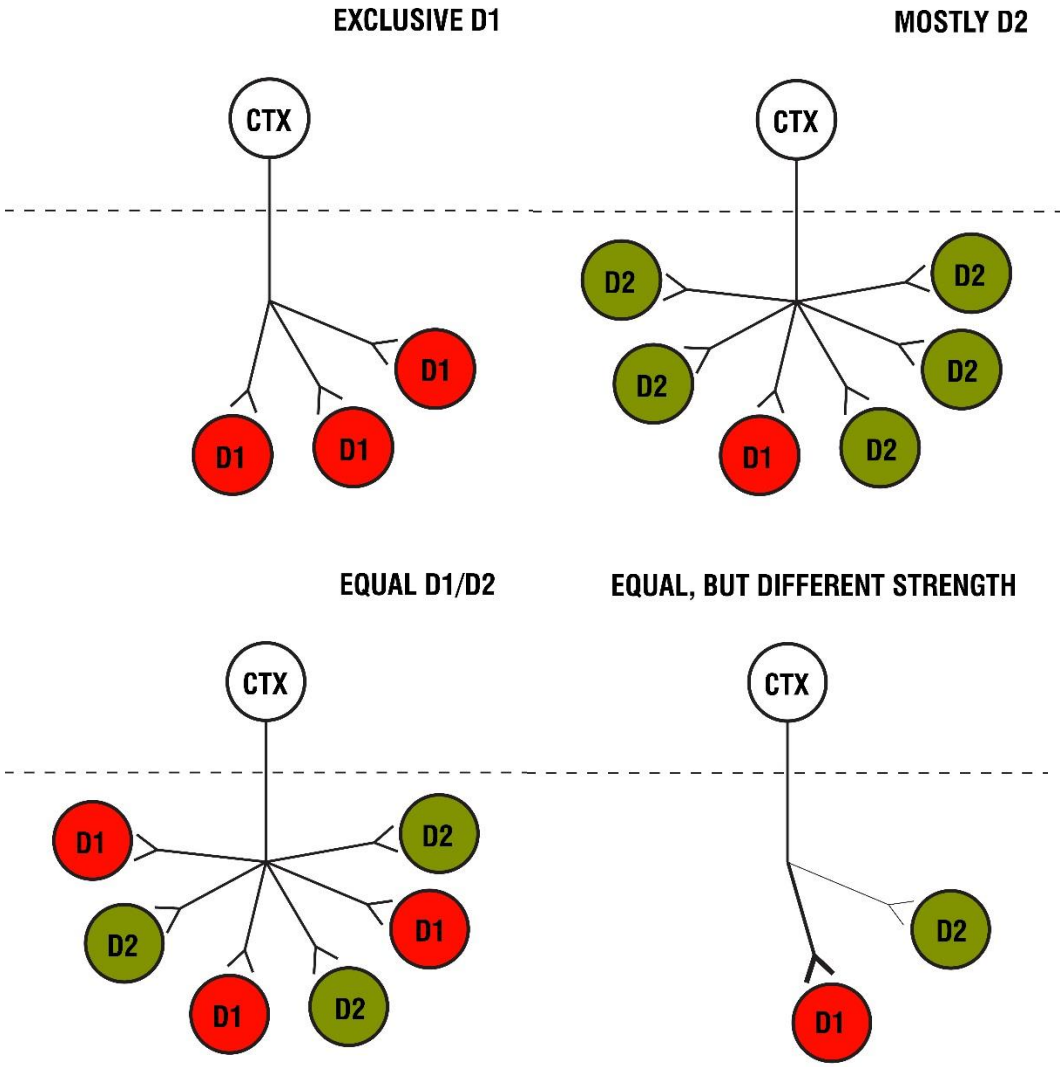

Figure 2.8: four example models of cortico-striatal connectivity based on D1 and D2 classes)

A series of questions can be asked about the cortical input onto MSNs (Figure 2.8):

1) Are cortical-striatal neurons specifists? A putative specifist would be a cortical neuron which only contacts striatal neurons which project to one pathway or the other.
2) Are cortical neurons generalists? A generalist would contact striatal neurons of both pathways indiscriminately, which statistics of contact simply to a random matrix.

3) What are the properties for clustering cortico-striatal neurons within a spectrum of specificity to generality? Possibilities include a strong preference for synaptic contact, but not exclusivity; differences in relative strength of synaptic contacts; differences in location of synaptic contacts; for instance spine versus shaft of dendrite; or distal versus proximal dendrite (Gerfen & Surmeier 2011)
4) Do cortical neurons cluster within these possible biases based on projection type (intra-telencephalic versus pyramidal-tract), laminar origin, and cortical region.

While there is clear evidence of laminar bias in the cortical inputs to patch and matrix of the striatum, at the time this study commenced there was no evidence supporting a similar bias for connections onto direct- and indirect-pathway projection neurons. The first question we set out to answer was whether there is evidence for pure specifists.

No evidence for binary specifists

To explore whether there is binary specificity in the cortico-striatal projection (Figure 2.8), we use optogenetic techniques in combination with double-mutant mice find common inputs onto neighboring striatonigral and striatopallidal neurons. Mice expressing tdTomato under the control of the D1R promoter (Shuen et al., 2008), selectively expressed by striatonigral neurons, were bred with mice expression Cre under the control of the A2AR promoter, selectively expressed by striatopallidal neurons. A novel SAD-B19-based RABV$^{\Delta G}$-hChR2-YFP (channelrhodopsin) was injected into dorsal striatum following priming infections AAV-EF1a-FLEX-hGFP-CVS*B19(G) and AAV-FLEX-TVA-mCherry (see below for description of chimeric glycoprotein CVS*B19). Initially, only striatopallidal neurons and expressed

channelrhodopsin. After a period of 5-7 days, a significant number of cortical neurons were infected trans-synaptically and also expressed channelrhodopsin. By recording post-synaptic responses in neighboring striatonigral neurons, we could assess whether cortical neurons known to project (via trans-synaptic marker) to one class of MSN also project to the other.

We estimate that approximately 200 striatal neurons were infected in the priming infection, and that on the order of 2000 cortical neurons were trans-synaptically infected. In contrast with the findings of Cowan and Wilson (2002) and the view espoused in Dudman & Gerfen (2015), we found that neighboring MSNs received common cortical input in all but one of eleven neurons tested. This may be due to a significant population of cortical axons (thousands) simultaneously expressing channelrhodopsin.

Results using new RABV strategies: SAD-B19$^{\Delta G}$, CVS*B19(G), and CVS-N2c$^{\Delta G}$.

Our initial efforts at retrograde tracing from dorsal striatum and cortex relied on the same SAD-B19$^{\Delta G}$-GFP virus described by Wickersham et al. (2007), but complemented via a mouse mutant which conditionally expressed SAD-B19(G) glycoprotein as well as the avian TVA800 receptor (Takatoh et al., 2013). However, this system yielded very low trans-synaptic spread of virus, on the order of 4 secondary neurons for each primary neuron. By trying a variety of AAV-based approaches to complementation, a "cocktail" approach was ultimately chosen which mixes several Cre-conditional viruses together in one infection. Unlike the system used in Watabe-Uchida et al. (2012), we chose to include a reporter of primary infection (see description of the necessity of this approach in Part 3), which allowed us to normalize viral spread to the number of

primary starter neurons. Under these conditions we never obtained more than 8 neurons for each primary neuron. Figure 2.9 shows a typical animal where the ratio of viral spread was 6.9.

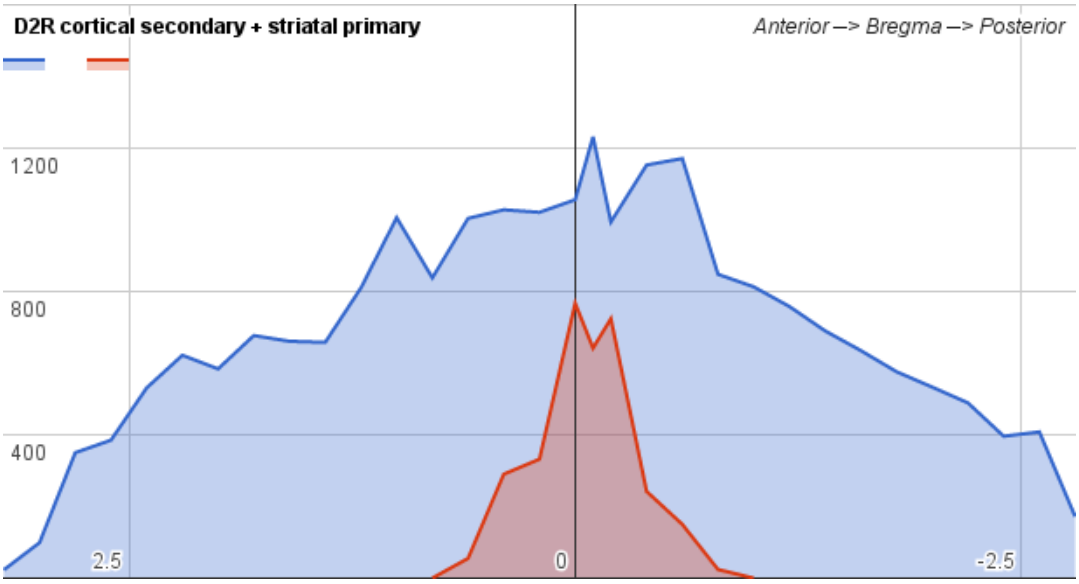

Figure 2.9: analysis of spread of SAD-B19$^{\Delta G}$ from a single D2R-Cre mouse following injection by AAV-FLEX-TVA and AAV-FLEX-hGFP-SADB19(G). Red primary, blue secondary. Total secondary 22221, total primary 3226.

Viral spread of less than 10 secondary neurons implies a labeling rate of cortical neurons of well under 1%. We were concerned that this number was so low that the system overall was vulnerable to biases in labeling (see Discussion in Part 6) or very high animal-to-animal variability, or both. As well, the ratio of contralateral to ipsilateral connectivity was nearly undetectable, and significantly below the level estimated by Webster (1961) in rodents and Parent & Hazrati (1995) in primates, perhaps by an order of magnitude. (Figure 2.10)

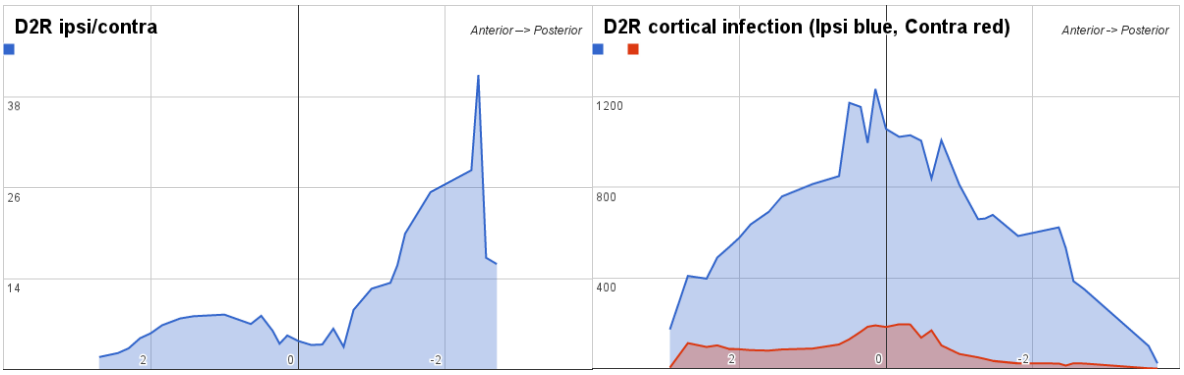

Figure 2.10: retrograde, trans-synaptic spread of SAD-B19$^{\Delta G}$ using SAD-B19(G), showing ipsilateral to contralateral ratio. Left: ipsilateral/contralateral ratio, with Bregma at 0. Right: red contralateral and blue ipsilateral secondary neuron count.

Updated and improved AAV complementation vectors have expanded the spread ratio to dozens in ideal scenarios (Weissbourd et al 2014). To further improve spread, we pursued a strategy wherein a synthetic glycoprotein is created from the "head" of CVS-11(G) and the "tail" of SAD-B19(G), thus preserving the ability of the glycoprotein to bind to RABV M protein and form a functional virion while altering the receptor affinity of the resulting virion. Roughly, this lead to a 10-fold increase in total trans-synaptic spread. (Figure 2.11). Notably, the increase in contralateral spread lagged far behind the increase in ipsilateral, implying either a bias for class (e.g., cortical lamina) or projection length of pre-synaptic neurons. This is addressed in more depth in Part 3.

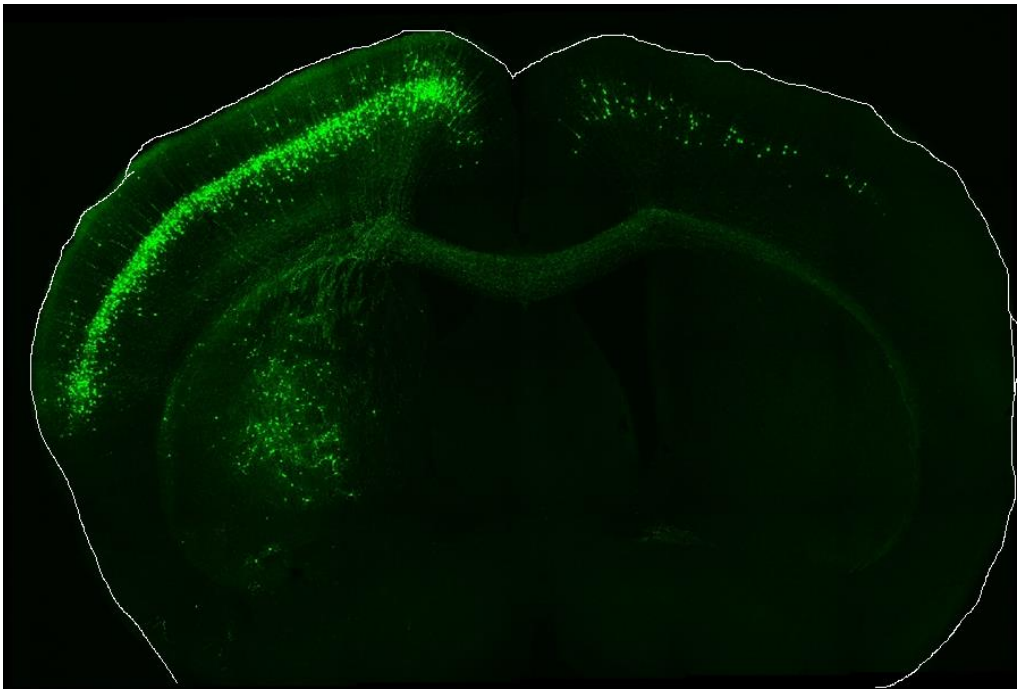

Figure 2.11: representative image from CVS*B19(G) complementation of first-generation $RABV^{\Delta G}$; retrograde labeling from dorsal striatum, in A2AR-Cre animal, showing cortical cells projecting onto striatopallidal neurons. Note the relative ratio of ipsilateral to contralateral labels

Because our experiments relied on the use of a complementation AAV which expresses a nuclear GFP reporter (histone2B-GFP fusion), we were able to count primary starter neurons and normalize secondary presynaptic counts to starter counts.

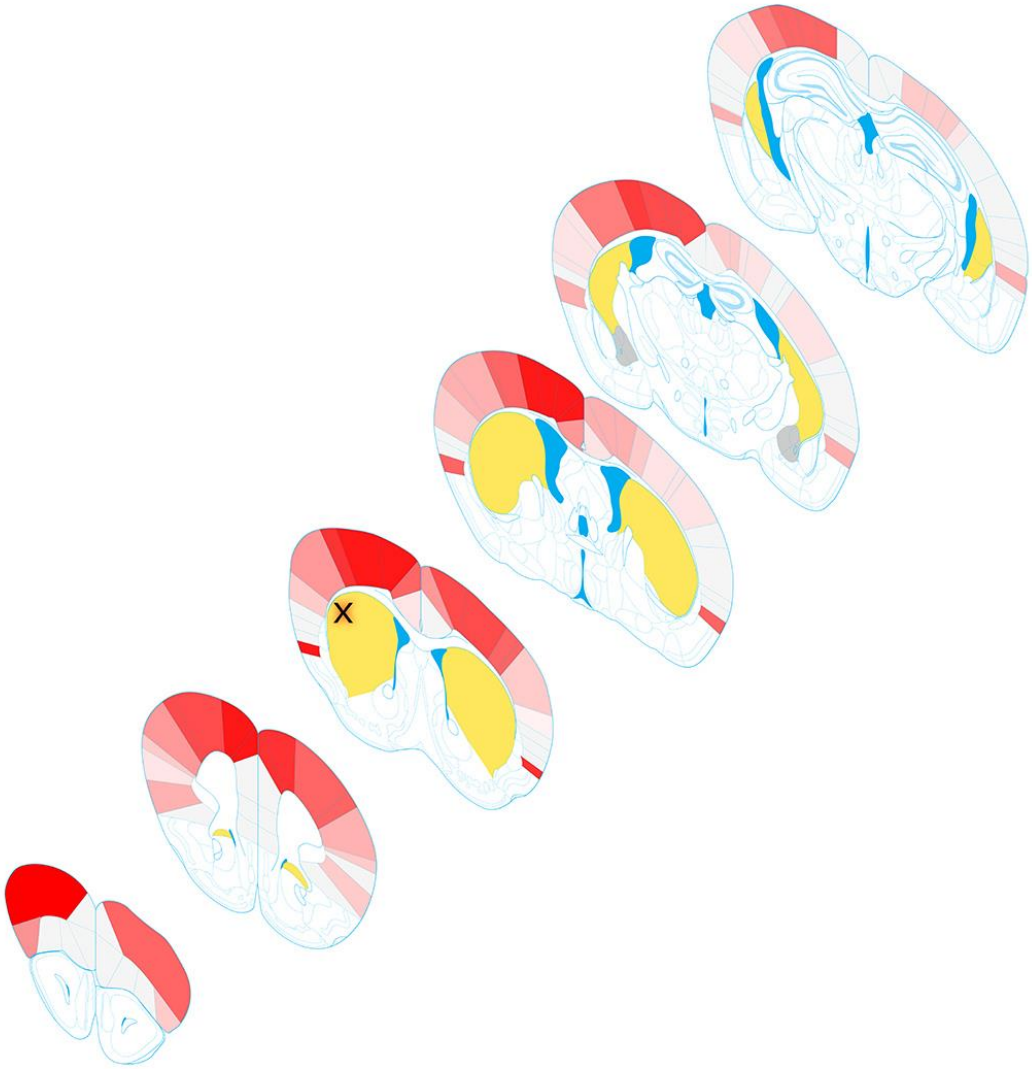

Figure 2.12: full anatomical projection map of cortical input to direct-pathway medium spiny neurons. ‘X’ marks primary starter infection. Data was hand-scored on 0-100 intensity scale, and averaged across 3 animals for each condition.

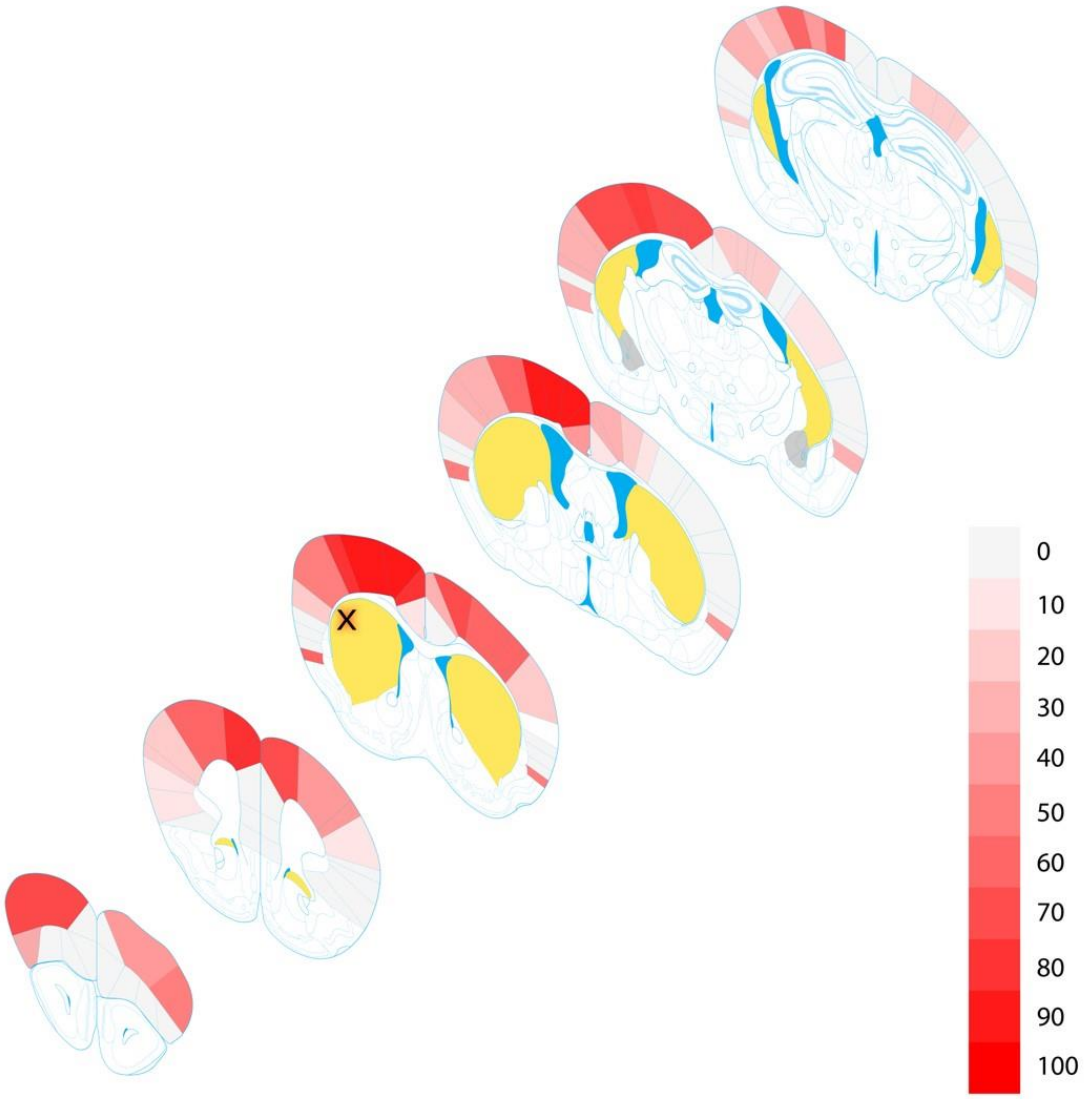

Figure 2.13: full anatomical projection map of cortical input to indirect-pathway medium spiny neurons. (top) Direct (bottom) Indirect**.** 'X' marks primary starter infection. Data was hand-scored on 0-100 intensity scale, and averaged across 3 animals for each condition.

In a final set of experiments, we repeated our anatomical investigation using the complete CVS-N2c system described in Part 3. Based on the significant increase in trans-synaptic spread, we arrived at new conclusions regarding the level of cortical innervation of striatonigral and striatopallidal neurons. A key feature in our analysis relative to previously published work is

that our data cover approximately 60,000 labeled cortical neurons vs 200 as seen in Wall et al. We saw a significant shift in prefrontal and motor areas towards the direct-pathway striatonigral neurons. Somatosensory areas, in particular barrel cortex, favored striatopallidal connections (Figure 2.12)

Earlier Results from Wall, et al. (2013) using legacy RABV$^{\Delta G}$

In the course of the study presented above, another report emerged describing the cortico-striatal circuit. Wall et al. used the first-generation rabies tracing tools based on SAD-B19 to trace relative cortical synaptic contact to striatonigral and striatopallidal neurons. The published data showed the number of secondary neurons per animal (presumably spread from hundreds of primary neurons) was only in the range of 150-200. Using the mono-synaptic tracing system first seen in Wickersham et al (2007), they created a priming infection in the central dorsal striatum (Figure 2.14), and followed that with pseudotyped rabies infection which spread to presynaptic sites. This was the first published attempt to map presynaptic partners for both striatonigral and striatopallidal neurons.

The key result of their inquiry was that, for most cortical areas, the relative outputs are balanced across both striatal pathways. The largest differences are seen among the midline cortical areas, with a strong preference among primary motor cortex for striatopallidal neurons and among the more midline areas (retrosplenial, cingulate) for striatonigral (Figure 2.15, 2.16, 2.17, 2.18).

Traditionally, the dorsal striatum in rodents is segregated in lateral and medial extents, which correspond to anatomically distinct anatomical components of primate striatum (putamen and caudate, respectively). However, Wall et al. deliberately chose to probe a central striatal

site, which may obscure cortico-striatal organization that is better delineated within the traditional structures.

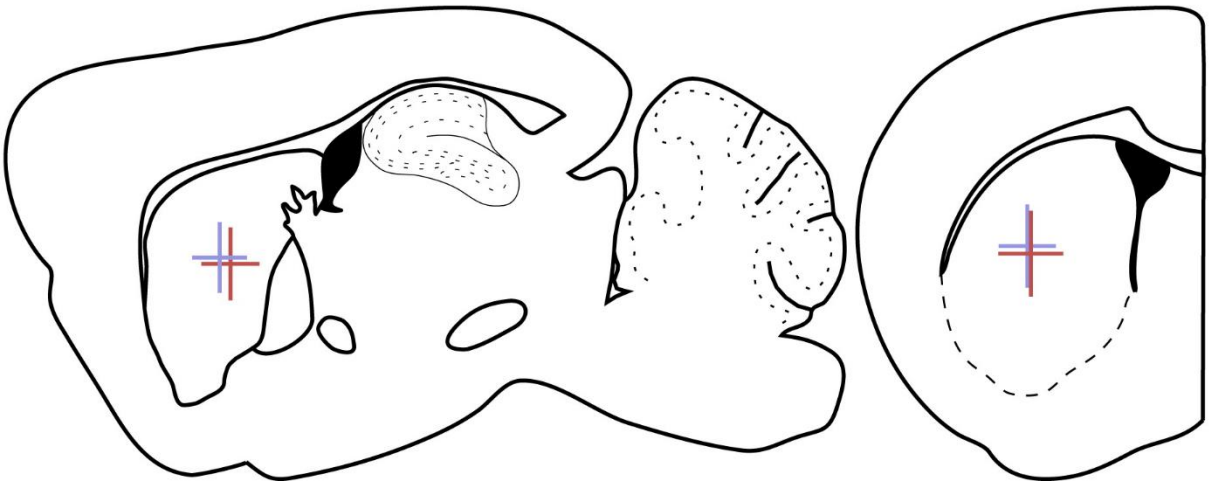

Figure 2.15: location of primary starter infection within dorsal striatum, the presumed locus of all presynaptic labeling shown in the following figure. These priming infections are more medial and more ventral than that seen in Figure 2.12, by approximate 500um in both directions. (from Wall et al., 2013)

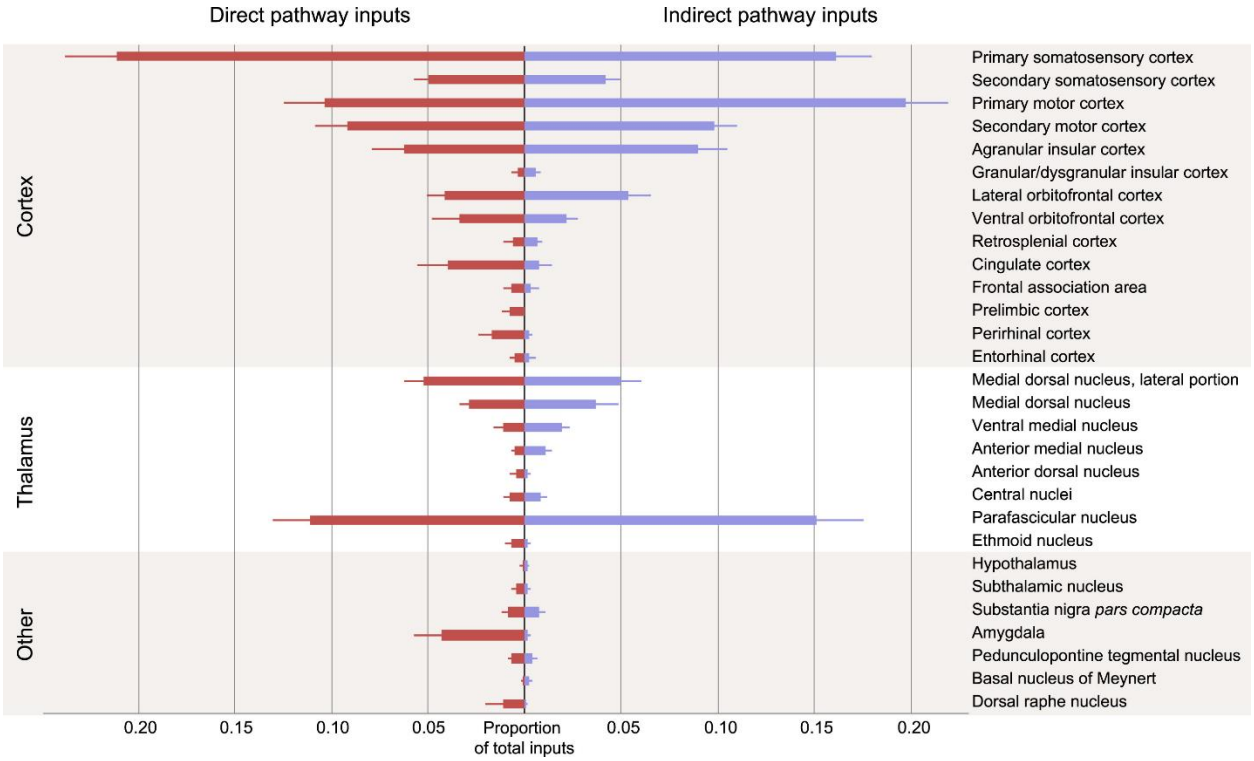

Figure 2.16: relative map of inputs onto medium spiny neurons in dorsal striatum (from Wall et al., 2013)

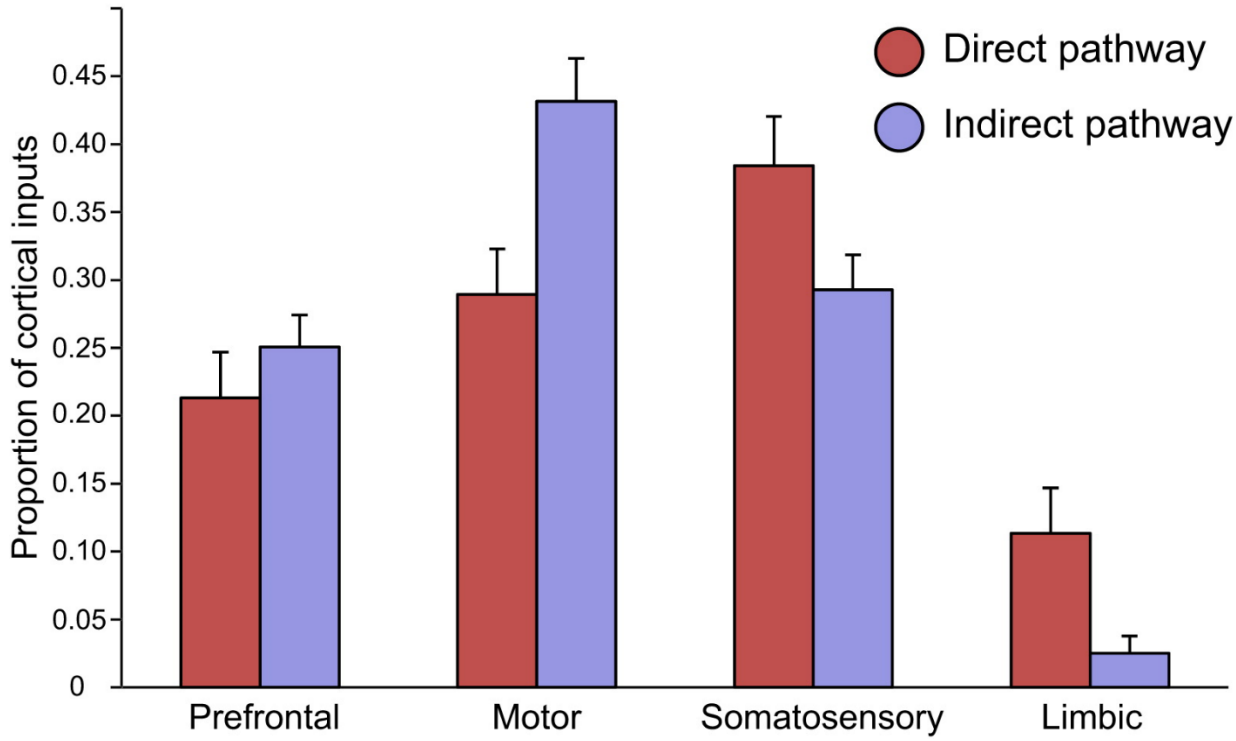

Figure 2.17: cortico-striatal input biases. p-values removed, error bars are 1 SEM (modified from Wall et al. 2013)

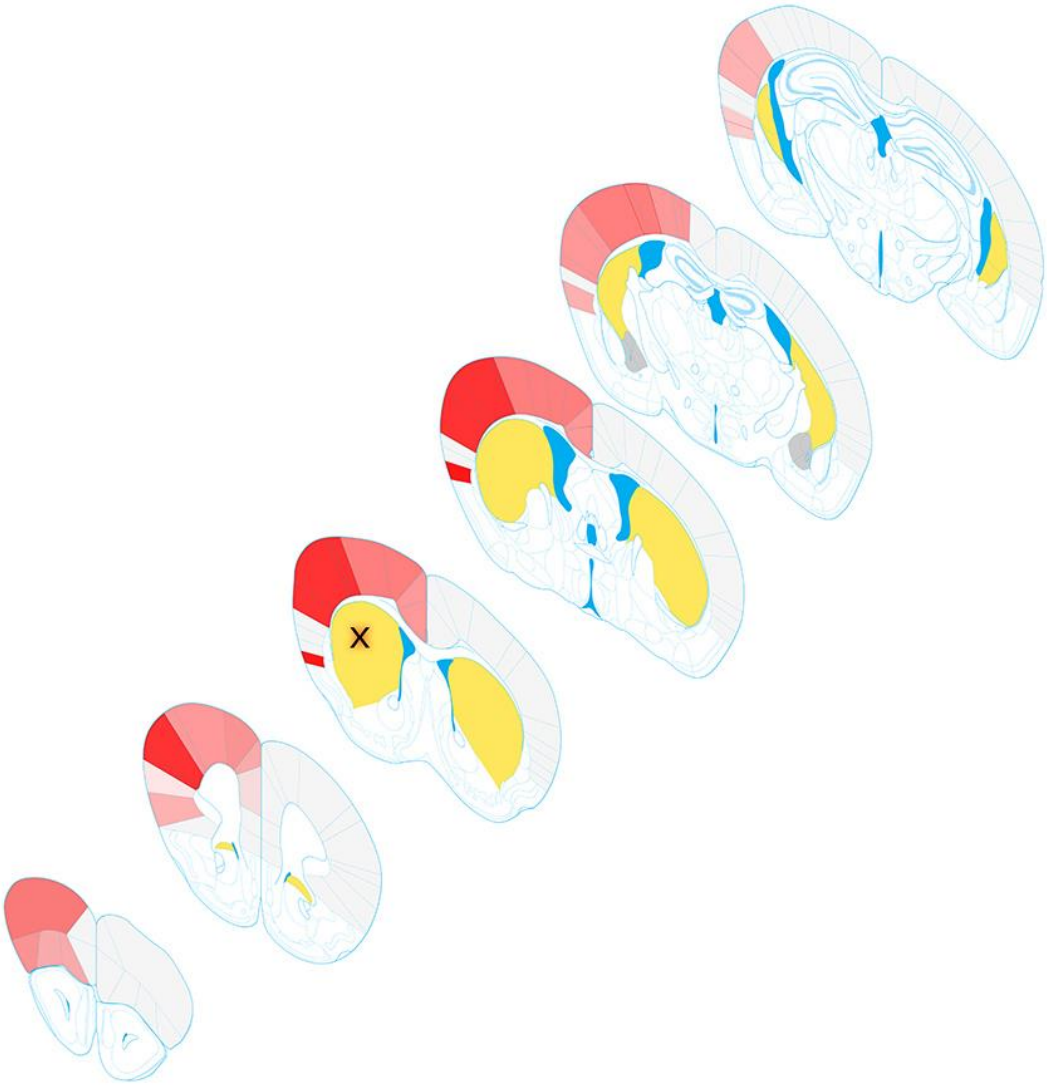

Figure 2.18: relative density of cortico-striatal projection to direct-pathway striatal neurons, based on Wall et al. (2013). 'X' marks the primary infection (Franklin-Paxinos mouse atlas; projection data as interpreted from Wall et al.)

Notes and Conclusions on the updated cortico-striatal projection map

Transgenic TVA is not efficiently expressed at axon terminals, and thus does not efficiently support uptake of RABV$^{\Delta G}$ when pseudotyped with EnvA. This is both a restriction

and feature. As a feature, it means that we do not have to account for low-levels of expression of Cre in cortical neurons. As a restriction, it keeps us from attempting to distinguish the subclass of direct-pathway neurons that make substantial contact in GPe from those that make little or no contact. We could find no difference in efficiency of uptake of SAD-B19 vs. CVS-N2c when pseudotyped with EnvA. Injections of pseudotyped virus into the terminal fields did not sustain infection in the striatum.

We labeled 300-fold more cortical neurons, a number which is so different that it is difficult to ascertain or even assert that our results are comparable. It is entirely possible that the spread of rabies infection depends on non-linear thresholds which are established by the nature of the underlying connectivity. For instance, it may be that the new method of CVS*B19(G) complementation crosses a "reliability" threshold or activity threshold such that synaptic biases inherent to SAD-B19 are overcome, or vice-versa, that CVS*B19(G) exploits a certain special class of synapses and misrepresents, as a sample, total synaptic input. We offer no evidence that our method fixes biases inherent to the original method, nor do we offer evidence that our method has biases not in the original method.

Regardless, our results contain several significant departures as compared to Wall et al.: the dramatic increase in presynaptic labeling, the reduction in animal-to-animal variability, and the discovery that cortical neurons do not seem to exist in specifist subpopulations—at least not if one considers the direct- and indirect-pathways as the dominant organizing feature of the striatum. Let us deal with each of these departures separately.

First, the dramatic increase in presynaptic labeling strongly hints at the truth of the conjecture that cortex completely "maps" (in the sense of mathematical project) the striatum. Somewhat surprisingly, despite some variability in the priming infection, the presynaptic maps

were actually less variable. We would have expected that a dramatic increase in spread would magnify the differences in cortical regional preferences, regardless of pathway. Seen in this light, it is clearer now that the ipsilateral projection dominates the contralateral projection and that this effect grows moving from "later" processing areas in anterior cortex as compared to "earlier" areas in posterior cortex. One striking exception to this rule is the strong bilateral projection from gustatory cortices (lateral insular AI and GI). The other sensory modalities do not share this bilaterality, suggesting that gustatory information is mixed into a wide range of cortical output presented to the striatum. Given the role of the striatum in processing and responding to dopaminergic reward signals (Schultz 2002), and the primacy of food as reward, this makes some sense.

Intriguingly, there is a subtle but consistent bias for stronger contralateral connectivity to the direct pathway. If those neurons, especially in motor areas, are similarly bias-connected to direct pathway neurons in the opposing hemisphere, then we suggest a model that optimizes for simultaneous activation (rather than suppression) of contralateral motor programs, based on the evidence that direct pathway activation promotes motor initiation.

The data is clear, however, that exclusive specificity of connectivity (direct- or indirect-only inputs) does not exist. This strongly suggests that medium spiny neurons are performing calculations with mixed information and that synaptic weights and plasticity in the striatum of those weights are a fundamental part of controlling skilled motor activity.

Problems exposed, opportunities to improve cortico-striatal map

Both the original investigation by Wall et al. as well as our two similar experiments using updated viruses leave significant open questions and expose problems in the use of tracing tools which map genetically-identified neural circuits. First, within the striatum, there is very high animal-to-animal variability in cortical projections as seen from similar striatal locations. Second, bulk delivery of AAV used for complementation almost always spans across functional boundaries within the striatum and blurs what could be a strong organization of inputs within functional subzones of dorsal striatum. Third, ideal comparisons in this either/or system, should leverage the two hemispheres to make intra-animal comparisons of cortical innervation of striatonigral and striatopallidal neurons.

Figure 2.8 proposes four different scenarios that a map of the cortico-striatal projection should attempt to answer. Only by combining fluorescent labels with activity reporters such as GCaMP and manipulation reagents such as channelrhodopsin will we able to satisfactorily address each scenario. In particular, the scenario wherein cortex makes equivalent number of synapses onto each of the two striatal populations, but with different synaptic weights, requires the use of tools which manipulation the functional output of cortical neurons.

To improve these maps, we propose that:

1) Priming infection be limited to less than 10 neurons. The sparsity of cortico-striatal connectivity described extensively in the literature (see summary in Dudman & Gerfen 2015) is likely overcome when the priming infection increases to hundreds of neurons.
2) Additional pseudotypes of $RABV^{\Delta G}$ be used, deploying EnvB coats in addition to EnvA in use today. The dual population of striatal neurons is the ideal scenario for dual EnvA/EnvB tracing. The biggest obstacle to this approach is the lack of alternative conditional recombinase mutants, such as Flpo under the control of A2AR promoter.

3) Definitive average synapse number for striatonigral and striatopallidal neurons be established. It is difficult to assign value to relative innervation of each striatal population when the total innervation is unknown.
4) Functional zones with the striatum be mapped independently. The organization proposed by Voorn et al (2004) should be followed. This implicitly requires (1) above.

It is important to note that while our investigation into the nature of the cortico-striatal map focused on outputs and inputs associated with skilled movement, we believe this is only a means of attacking the overriding mystery: are cortex and striatum so synaptically and functionally intertwined that we ought to consider cortico-striatal processing as another "layer" to add to the canonical six-layer cortex.

Bibliography: Part 2

Brown, L.L., and Feldman, S.M. (1993). Chapter 16 The organization of somatosensory activity in dorsolateral striatum of the rat. In Progress in Brain Research, (Elsevier), pp. 237–250.

Cazorla, M., de Carvalho, F.D., Chohan, M.O., Shegda, M., Chuhma, N., Rayport, S., Ahmari, S.E., Moore, H., and Kellendonk, C. (2014). Dopamine D2 Receptors Regulate the Anatomical and Functional Balance of Basal Ganglia Circuitry. Neuron *81*, 153–164.

Costa, R.M. (2007). Plastic Cortico-striatal Circuits for Action Learning: What's Dopamine Got to Do with It? Annals of the New York Academy of Sciences *1104*, 172–191.

Costa, R.M. (2011). A selectionist account of de novo action learning. Current Opinion in Neurobiology *21*, 579–586.

Costa, R.M., Cohen, D., and Nicolelis, M.A.L. (2004). Differential Cortico-striatal Plasticity during Fast and Slow Motor Skill Learning in Mice. Current Biology *14*, 1124–1134.

Cowan, R.L., and Wilson, C.J. (1994). Spontaneous firing patterns and axonal projections of single cortico-striatal neurons in the rat medial agranular cortex. J. Neurophysiol. *71*, 17–32.

Cui, G., Jun, S.B., Jin, X., Pham, M.D., Vogel, S.S., Lovinger, D.M., and Costa, R.M. (2013). Concurrent activation of striatal direct and indirect pathways during action initiation. Nature *494*, 238–242.

Donoghue, J.P., and Kitai, S.T. (1981). A collateral pathway to the neostriatum from corticofugal neurons of the rat sensory-motor cortex: An intracellular HRP study. The Journal of Comparative Neurology *201*, 1–13.

Dudman, and Gerfen (2015). The Basal Ganglia. In The Rat Nervous System, (Elsevier),.

Dudman, J.T., and Krakauer, J.W. (2016). The basal ganglia: from motor commands to the control of vigor. Current Opinion in Neurobiology.

Gerfen, C.R. (1988). Synaptic organization of the striatum. J Electron Microsc Tech *10*, 265–281.

Gerfen, C.R. (1989). The neostriatal mosaic: striatal patch-matrix organization is related to cortical lamination. Science *246*, 385–388.

Gerfen, C.R., and Bolam, J.P. (2010). The Neuroanatomical Organization of the Basal Ganglia. In Handbook of Behavioral Neuroscience, (Elsevier), pp. 3–28.

Gerfen, C.R., and Surmeier, D.J. (2011). Modulation of Striatal Projection Systems by Dopamine. Annual Review of Neuroscience *34*, 441–466.

Gerfen, C., and Sawchenko, P. (1984). An anterograde neuroanatomical tracing method that shows the detailed morphology of neurons, their axons and terminals: Immunohistochemical localization of an axonally transported plant lectin,Phaseolus vulgaris leucoagglutinin (PHA-L). Brain Research *290*, 219–238.

Gerfen, C., Engber, T., Mahan, L., Susel, Z., Chase, T., Monsma, F., and Sibley, D. (1990). D1 and D2 dopamine receptor-regulated gene expression of striatonigral and striatopallidal neurons. Science *250*, 1429–1432.

Gertler, T.S., Chan, C.S., and Surmeier, D.J. (2008). Dichotomous Anatomical Properties of Adult Striatal Medium Spiny Neurons. Journal of Neuroscience *28*, 10814–10824.

Gong, S., Doughty, M., Harbaugh, C.R., Cummins, A., Hatten, M.E., Heintz, N., and Gerfen, C.R. (2007). Targeting Cre Recombinase to Specific Neuron Populations with Bacterial Artificial Chromosome Constructs. Journal of Neuroscience *27*, 9817–9823.

Graybiel, A.M., and Ragsdale, C.W. (1978). Histochemically distinct compartments in the striatum of human, monkeys, and cat demonstrated by acetylthiocholinesterase staining. Proc. Natl. Acad. Sci. U.S.A. *75*, 5723–5726.

Greig, L.C., Woodworth, M.B., Galazo, M.J., Padmanabhan, H., and Macklis, J.D. (2013). Molecular logic of neocortical projection neuron specification, development and diversity. Nature Reviews Neuroscience *14*, 755–769.

Grillner, S. (2011). Control of Locomotion in Bipeds, Tetrapods, and Fish. In Comprehensive Physiology, R. Terjung, ed. (Hoboken, NJ, USA: John Wiley & Sons, Inc.),.

Grillner, S., Wallén, P., Saitoh, K., Kozlov, A., and Robertson, B. (2008). Neural bases of goal-directed locomotion in vertebrates—An overview. Brain Research Reviews *57*, 2–12.

Haber, S.N. (2003). The primate basal ganglia: parallel and integrative networks. Journal of Chemical Neuroanatomy *26*, 317–330.

Howes, O.D., Kambeitz, J., Kim, E., Stahl, D., Slifstein, M., Abi-Dargham, A., and Kapur, S. (2012). The Nature of Dopamine Dysfunction in Schizophrenia and What This Means for Treatment: Meta-analysis of Imaging Studies. Archives of General Psychiatry *69*.

Izzo, P.N., Graybiel, A.M., and Bolam, J.P. (1987). Characterization of substance P- and [MET]enkephalin-immunoreactive neurons in the caudate nucleus of cat and ferret by a single section golgi procedure. Neuroscience *20*, 577–587.

Jin, X., and Costa, R.M. (2010). Start/stop signals emerge in nigrostriatal circuits during sequence learning. Nature *466*, 457–462.

Kincaid, A.E., and Wilson, C.J. (1996). Cortico-striatal innervation of the patch and matrix in the rat neostriatum. The Journal of Comparative Neurology *374*, 578–592.

Kincaid, A.E., Zheng, T., and Wilson, C.J. (1998). Connectivity and convergence of single cortico-striatal axons. J. Neurosci *18*, 4722–4731.

Koralek, A.C., Jin, X., Long II, J.D., Costa, R.M., and Carmena, J.M. (2012). Cortico-striatal plasticity is necessary for learning intentional neuroprosthetic skills. Nature *483*, 331–335.

Kravitz, A.V., Freeze, B.S., Parker, P.R.L., Kay, K., Thwin, M.T., Deisseroth, K., and Kreitzer, A.C. (2010). Regulation of parkinsonian motor behaviours by optogenetic control of basal ganglia circuitry. Nature *466*, 622–626.

Kravitz, A.V., Tye, L.D., and Kreitzer, A.C. (2012). Distinct roles for direct and indirect pathway striatal neurons in reinforcement. Nature Neuroscience.

Parent, A., and Hazrati, L.-N. (1995). Functional anatomy of the basal ganglia. I. The cortico-basal ganglia-thalamo-cortical loop. Brain Research Reviews *20*, 91–127.

Schultz, W. (2002). Getting Formal with Dopamine and Reward. Neuron *36*, 241–263.

Shuen, J.A., Chen, M., Gloss, B., and Calakos, N. (2008). Drd1a-tdTomato BAC Transgenic Mice for Simultaneous Visualization of Medium Spiny Neurons in the Direct and Indirect Pathways of the Basal Ganglia. Journal of Neuroscience *28*, 2681–2685.

Surmeier, D.J., Ding, J., Day, M., Wang, Z., and Shen, W. (2007). D1 and D2 dopamine-receptor modulation of striatal glutamatergic signaling in striatal medium spiny neurons. Trends in Neurosciences *30*, 228–235.

Takatoh, J., Nelson, A., Zhou, X., Bolton, M.M., Ehlers, M.D., Arenkiel, B.R., Mooney, R., and Wang, F. (2013). New Modules Are Added to Vibrissal Premotor Circuitry with the Emergence of Exploratory Whisking. Neuron 77, 346–360.

Vicente, A.M., Galvão-Ferreira, P., Tecuapetla, F., and Costa, R.M. (2016). Direct and indirect dorsolateral striatum pathways reinforce different action strategies. Current Biology *26*, R267–R269.

Voorn, P. (2004). Putting a spin on the dorsal-ventral divide of the striatum. Trends in Neurosciences *27*, 468–474.

Wall, N.R., De La Parra, M., Callaway, E.M., and Kreitzer, A.C. (2013). Differential Innervation of Direct- and Indirect-Pathway Striatal Projection Neurons. Neuron *79*, 347–360.

Watabe-Uchida, M., Zhu, L., Ogawa, S.K., Vamanrao, A., and Uchida, N. (2012). Whole-Brain Mapping of Direct Inputs to Midbrain Dopamine Neurons. Neuron *74*, 858–873.

Weissbourd, B., Ren, J., DeLoach, K.E., Guenthner, C.J., Miyamichi, K., and Luo, L. (2014). Presynaptic Partners of Dorsal Raphe Serotonergic and GABAergic Neurons. Neuron *83*, 645–662.

Wickersham, I.R., Lyon, D.C., Barnard, R.J.O., Mori, T., Finke, S., Conzelmann, K.-K., Young, J.A.T., and Callaway, E.M. (2007). Monosynaptic Restriction of Trans-synaptic Tracing from Single, Genetically Targeted Neurons. Neuron *53*, 639–647.

Wright, A.., Norrie, L., Ingham, C.., Hutton, E.A.., and Arbuthnott, G.. (1999). Double anterograde tracing of outputs from adjacent "barrel columns" of rat somatosensory cortex. Neostriatal projection patterns and terminal ultrastructure. Neuroscience *88*, 119–133.

Yin, H.H., Ostlund, S.B., Knowlton, B.J., and Balleine, B.W. (2005). The role of the dorsomedial striatum in instrumental conditioning. European Journal of Neuroscience *22*, 513–523.

Yin, H.H., Mulcare, S.P., Hilário, M.R.F., Clouse, E., Holloway, T., Davis, M.I., Hansson, A.C., Lovinger, D.M., and Costa, R.M. (2009). Dynamic reorganization of striatal circuits during the acquisition and consolidation of a skill. Nature Neuroscience *12*, 333–341.

Zheng, T., and Wilson, C.J. (2002). Cortico-striatal Combinatorics: The Implications of Cortico-striatal Axonal Arborizations. Journal of Neurophysiology *87*, 1007–1017.

Part 3. Updating deletion-mutant rabies: improving trans-synaptic spread

Virally-based trans-synaptic tracing technologies are powerful experimental tools for neuronal circuit mapping. The glycoprotein-deletion variant of the SAD-B19 vaccine strain rabies virus (RABV) has been the reagent of choice in monosynaptic tracing, since it permits the mapping of synaptic inputs to genetically marked neurons. Since its introduction, new helper viruses and reagents that facilitate complementation have enhanced the efficiency of SAD-B19$^{\Delta G}$ trans-synaptic transfer, but there has been little focus on improvements to the core RABV strain. Here we generate a new deletion-mutant strain, CVS-N2c$^{\Delta G}$, and examine its neuronal toxicity and efficiency in directing retrograde trans-synaptic transfer. We find that by comparison with SAD-B19$^{\Delta G}$, the CVS-N2c$^{\Delta G}$ strain exhibits a reduction in neuronal toxicity and a marked enhancement in trans-synaptic neuronal transfer. We conclude that the CVS-N2c$^{\Delta G}$ strain provides a more effective means of mapping neuronal circuitry and of monitoring and manipulating neuronal activity *in vivo* in the mammalian central nervous system.

Introduction

The quest to understand the organization and function of neural circuits has been aided by the development of genetic techniques that link neuronal connectivity and animal behavior. Recombinant viruses have emerged as powerful tools for analyzing circuit structure and function (Nassi et al., 2015). When used with genetic markers for a large repertoire of neuronal types, recombinant trans-synaptic viruses permit the construction of precise maps of synaptic input and output, and provide an entry point for identification and manipulation of targeted neurons. The efficacy of such viruses depends on three main features: selectivity of expression in pre-defined

neuronal classes, long-term neuronal viability, and efficient marking of neuronal inputs or targets.

Rabies virus- (RABV) based techniques have achieved particular prominence in circuit mapping (Coulon et al., 1989, Ugolini, 2010) because they enable retrograde-, and for primary sensory neurons anterograde-, trans-synaptic neuronal tracing (Ugolini, 1995; Zampieri et al., 2014). Moreover, the use of glycoprotein [G] deletion-mutant RABV$^{\Delta G}$ restricts viral budding and transfer, permitting selective mapping of first-order presynaptic neurons (Wickersham et al., 2007a,b). First-generation RABV$^{\Delta G}$ tools, based largely on the attenuated vaccine strain SAD-B19 (Schnell et al., 1994; Wickersham et al., 2007b), have two significant limitations: inefficiency of trans-synaptic transfer and neurotoxicity with longer-term infection (Schnell et al., 2009; Callaway and Luo, 2015; Ghanem and Conzelmann, 2015) (see schematic Figure 3.1A). Toxicity could reflect high levels of viral gene expression combined with inherent mechanisms for stabilizing viral glycoprotein (Morimoto et al., 2000; Palusa et al., 2012). Limitations to the efficiency of viral transfer could, in turn, be a function of weak viral neurotropism (Schnell et al., 2009; Conzelmann and Hagendorf, 2011). To address these limitations, we have explored whether the use of a different RABV strain might reduce toxicity (see Part 4) and achieve improved trans-synaptic transfer - permitting more accurate analysis of the organization of neural circuits in the mammalian central nervous system (CNS).

Many studies have documented laboratory RABV strains that exhibit varying degrees of pathogenicity. These strains range from virulent, highly neurotropic and neuroinvasive challenge

viruses to apathogenic vaccine strains which have almost completely lost their neurotropism and neuro-invasiveness (Finke and Conzelmann, 2005; Jackson, 2013; Dietzschold et al., 2008). These laboratory strains exhibit predictable tropism and transmission speed, and are termed "fixed" viruses. The vaccine strain SAD-B19 was selected for its thermal stability, high titer in cell culture, low residual pathogenicity in small rodents and immunogenicity *in vivo* (Geue, et al., 2008) and was adopted as a neural circuit tracer (Kelly & Strick, 2000). In a search for alternative RABV strains, we focused our attention on "fixed" strains that have been selected for neuronal affinity and rapid transport *in vivo*, potentially making them better suited than vaccine strains for the analysis of neural circuitry. Amongst these fixed strains, the challenge virus CVS-N2c exhibits strong neurotropism and reduced cytotoxicity (Morimoto et al., 1998; Ugolini, 2010; Conzelmann and Hagendorf, 2011) and has been used previously, in a replication-competent form, for multisynaptic circuit mapping in primates (Hoshi et al., 2005). In addition, the availability of reverse-genetically rescued CVS-N2c (Wirblich and Schnell, 2011) enables the design of replication-incompetent strains that can be rendered non-virulent and potentially more suitable for laboratory usage.

We report here the features of a glycoprotein-deficient CVS-N2c$^{\Delta G}$ strain derived from a virulent and highly neurotropic parental strain. Direct comparison with SAD-B19$^{\Delta G}$ reveals that CVS-N2c$^{\Delta G}$ exhibits lower levels of neurotoxicity and enhanced retrograde trans-synaptic transfer. The enhanced efficacy of CVS-N2c$^{\Delta G}$ does not seem to be restricted to specific classes of neuron or circuits, in that we detected enhanced trans-synaptic transfer in both cortico-striatal and spinal premotor circuits. Neuronal viability is well maintained following infection by CVS-N2c$^{\Delta G}$ variants that express proteins that permit monitoring and manipulation of neurons, as

demonstrated in the septo-hippocampal pathway and in the parabrachial projection to the ventral tegmental area (VTA). The new CVS-N2c$^{\Delta G}$ strain maintains compatibility with many of the helper viruses and complementation constructs used for SAD-B19, and thus constitutes a more effective reagent with which to probe the organization, physiology and behavioral relevance of neural circuits in the mammalian CNS.

Results

Recovery and pseudotyping of CVS-N2c$^{\Delta G}$

To provide a RABV strain for comparison with SAD-B19 derivatives, we explored the properties of a deletion mutant CVS-N2c strain, designated CVS-N2c$^{\Delta G}$, in which the glycoprotein gene (G) has been removed and complemented *in trans* by the deleted G gene, to permit retrograde monosynaptic transfer. The strong neurotropism of CVS-N2c may reflect the adaptation of virus to continued passage in mouse brain and cultured neuronal cell lines (Morimoto et al., 1998, 1999). We rescued and amplified virus exclusively in Neuro2A neuroblastoma cells, as a proxy for replication in primary neurons (see Experimental Procedures). Two Neuro2A-based lines were created for packaging: one expressing CVS-N2c(G) for use in amplification (Figure 3.1B), and the other expressing EnvA for use in pseudotyping (Figure 3.1C). To monitor viral transfer and neuronal viability, we created variants of CVS-N2c$^{\Delta G}$ expressing the fluorescent reporters dsRed or GFP (Figure 3.1B; Supplementary Figure 3.1). We noted that the maximum attainable titer of CVS-N2c$^{\Delta G}$ using our packaging cells was always lower than that achieved with SAD-B19$^{\Delta G}$ (Supplementary Table 3.1).

Enhanced trans-synaptic transfer of CVS-N2c$^{\Delta G}$ virus

We compared the efficiency of retrograde monosynaptic transfer of the CVS-N2c$^{\Delta G}$ and SAD-B19$^{\Delta G}$ strains under similar infection conditions in cortico-striatal and spinal premotor circuits, assessing the spread of these viruses from primary infected, to trans-synaptically-infected secondary neurons.

To achieve selective monosynaptic RABV transfer we used two priming (helper) reagents introduced *in trans*, one to complement the deleted RABV glycoprotein (G) gene and the other to express the pseudotyping receptor TVA. To induce complementation, we developed Cre-conditional adeno-associated viruses (AAV) expressing RABV(G) and a nuclear marker, human histone2B-GFP (nGFP) (Kanda et al., 1998; Sun et al., 2014). Two versions of the virus, designated AAV-FLEX-nGFP-2A-RABV[G], were used to express either SAD-B19(G) or CVS-N2c(G) – proteins identical in length but differing in 60 amino acid residues. After Cre recombination, both viruses directed glycoprotein expression to similar levels, assessed by immunofluorescence (Supplementary Figure 3.2). Selectivity was established by targeting neuronal subtypes for EnvA/TVA pseudotyped RABV$^{\Delta G}$ infection (Wickersham et al., 2007b) using a Cre-conditional virus, AAV-FLEX-TVA-mCherry, to achieve TVA receptor expression (Watabe-Uchida et al., 2012).

To provide a background control we injected all viruses into wild-type mice and assayed non-targeted expression. Neither of the AAV-FLEX-nGFP-2A-RABV[G] variants exhibited spontaneous recombination or expression, as revealed by complete absence of nGFP^{+} neurons. We detected little to no "leaky" expression of TVA from our AAV-FLEX-TVA-mCherry, as revealed by the detection of <5 RFP^{+} neurons after over-infection with either RABV$^{\Delta G}$-dsRed[EnvA] virus, indicating that EnvA/TVA infections were highly selective. As a final control, a separate injection of EnvA-pseudotyped CVS-N2c$^{\Delta G}$ into the spinal cord resulted in a maximum of one infected neuron per animal, supporting the selectivity of infection (for viral controls see Experimental Procedures).

To assess trans-synaptic transfer efficiency, neuronal infection with a mixture of the TVA and RABV(G) priming viruses (Figure 3.2A-C) was followed two weeks later by injection of matching EnvA-pseudotyped RABV$^{\Delta G}$-dsRed, either SAD-B19$^{\Delta G}$ or CVS-N2c$^{\Delta G}$. We used the maximum attainable titer for both the SAD-B19$^{\Delta G}$ and CVS-N2c$^{\Delta G}$ strains (Supplementary Table 1). Primary neurons were defined by co-expression of nGFP from RABV(G) priming virus and dsRed driven by RABV$^{\Delta G}$, whereas trans-synaptically infected secondary neurons expressed dsRed alone. After an additional 10 days post-infection, primary and secondary neurons were counted and the extent of transfer determined from the ratio of secondary to primary infection numbers.

In the cortico-striatal pathway, medium spiny neurons (MSN) of the striatum receive extensive excitatory input from cortical projection neurons (Gerfen and Bolam, 2010), prompting us to compare the degree of retrograde trans-synaptic transfer from striatal to cortical neurons. To restrict priming infection, we used mice expressing Cre-recombinase under the control of the *adenosine receptor 2A* (Adora2A) promoter, which is active in approximately half of all MSNs (Gong et al., 2007) (Figure 3.2B,C). In each animal, we counted all primary labeled neurons and sampled secondary labeled neurons from the same five cortical regions. For both RABV$^{\Delta G}$ strains we observed a relatively linear increase in transfer ratio as the number of primary neurons increased (primary/secondary neuronal numbers: CVS-N2c$^{\Delta G}$: 34/434, 57/810, 126/1240; SAD-B19$^{\Delta G}$: 126/44, 132/58, 450/400). These transfer counts indicate that CVS-N2c$^{\Delta G}$ virus exhibits a 22-fold higher (range 11- to 40-fold) incidence of retrograde trans-synaptic transfer into cortical projection neurons than SAD-B19$^{\Delta G}$ virus (Figure 3.2D-F).

MSNs represent a near-homogenous and densely interconnected neuronal population, such that local intra-striatal transfer of RABV is expected. But in this circuit the determination of local viral transfer with current methods is not possible, for two reasons. First, TVA-mCherry is not detectable with native fluorescence (Watabe-Uchida et al., 2012; Krashes et al., 2014). Nevertheless, antibody amplification of the mCherry signal will likely cross-react with RABV encoded dsRed, making primary vs secondary neuron identification ambiguous. Second, and more importantly, direct and trans-synaptic infection by RABV$^{\Delta G}$ cannot be distinguished within the population of TVA-expressing striatal cells, making secondary infection counts unreliable.

This problem led us to evaluate the efficiency of trans-synaptic viral transfer in a spinal circuit within which local transfer can be cleanly assayed, permitting the analysis of viral transfer as a function of axonal projection distance. We focused on spinal premotor circuits, where primary infected motor neurons transfer virus to premotor interneurons. Since motor neurons are anatomically and genetically distinguishable from surrounding spinal interneurons, the use of selective Cre mouse lines makes it possible to distinguish primary EnvA/TVA labeled motor neurons from both local and distant secondary trans-synaptically-infected interneurons.

To target spinal motor neurons, we used mice expressing Cre under control of the *choline acetyltransferase* (ChAT) promoter. Paired TVA and RABV(G) priming viruses were injected into the ventral horn of L3 and L4 lumbar spinal segments, followed two weeks later by L3 and L4 injection of RABV$^{\Delta G}$-dsRed[EnvA] (Figure 3.3A). Primary infection was limited to motor neurons, as identified by their distinct morphology and ventral position and nuclear expression of

GFP by RABV(G) priming virus. We compared the total number of secondary infected neurons as a function of primary starter cell number for each strain, and found that SAD-B19$^{\Delta G}$ was transferred to 7.0 ± 0.5 secondary cells (mean ± s.e.m.; Figure 3.3E), a number comparable to that found in previous studies using related helper viruses (Watabe-Uchida et al., 2012; Sun et al., 2014; Pollak Dorocic et al., 2014; Ogawa et al., 2014). By comparison, each CVS-N2c$^{\Delta G}$ primary neuron yielded 60.2 ± 16.3 secondary neurons (Figure 3.3E), close to an order of magnitude increase in the efficiency of total trans-synaptic transfer.

We also analyzed the transfer ratio as a function of the distance of secondary neurons from the injection site. At local lumbar levels, we detected a ~80% reduction in primary infection by CVS-N2c$^{\Delta G}$ compared to SAD-B19$^{\Delta G}$, likely a result of the lower initial CVS-N2c$^{\Delta G}$ titer (Figure 3.3B,E,F, Supplementary Table 1). Despite this difference, the total number of secondary infected neurons detected at local lumbar levels was similar with both viral strains (Figure 3.3B,F), indicative of a ~4-fold enhancement from CVS-N2c$^{\Delta G}$ mediated local trans-synaptic transfer. But for more distant interneurons found in thoracic and cervical spinal cord segments and in the hindbrain, pairwise comparison revealed a 16- to 50-fold enhancement in efficiency of CVS-N2c$^{\Delta G}$- over SAD-B19$^{\Delta G}$-mediated transfer (Figure 3.3C,D,G).

Thus, trans-synaptic transfer of the CVS-N2c$^{\Delta G}$ strain exhibits an order of magnitude enhancement over SAD-B19$^{\Delta G}$, and an especially strong improvement in transfer efficacy into spinal premotor neurons with distant somata.

Restricted trans-synaptic transfer of CVS-N2c$^{\Delta G}$

Resolving whether the transfer of CVS-N2c$^{\Delta G}$ is restricted to trans-synaptic means is critical to the interpretation of anatomical tracing and connectivity maps. One report offered some evidence of synaptically restricted spread for SAD-B19 (Wickersham et al., 2007b). But the lack of conclusive evidence that any RABV strain is transferred exclusively across synapses makes it crucial to resolve whether CVS-N2c virus spreads by additional, non-synaptic, means.

We tested the exclusivity of CVS-N2c transfer at proprioceptive sensory synapses with spinal motor neurons, given that information on the normal pattern of connectivity in this circuit is available at high enough resolution to match experimental data with predictions about the selectivity of viral transfer. Within this circuit, proprioceptive sensory afferents make direct connections with spinal motor neurons that project to the same muscle (forming homonymous connections) and weaker connections to motor neurons innervating muscles with synergistic functions, termed heteronomous connections (Mendelsohn et al., 2015; Frank and Westerfield, 1983). In addition, despite the proximity of sensory terminals and motor neuron dendrites, proprioceptive sensory neurons do not form direct connections with motor neurons that innervate antagonistic muscles (Figure 3.4A,B; Eccles et al., 1957; Frank and Westerfield, 1983; Hongo et al., 1984; Mendelsohn et al., 2015). The conservation of sensory-motor synaptic selectivity across mammalian species provided the basis for a 'homonymous vs antagonist' assay to test the exclusivity of synaptic viral transfer in mice.

To examine the exclusivity of CVS-N2c$^{\Delta G}$ transfer we examined sensory-motor connectivity between ankle extensor gastrocnemius [GS] and ankle flexor tibialis anterior [TA] antagonist circuits. Motor neurons that innervate these two muscle groups possess dendrites that are interleaved in the ventral spinal cord (Figure 3.4B), permitting the detection of potential non-synaptic routes of transfer. We injected paired TVA and CVS-N2c(G) priming viruses into the GS muscle of *ChAT*-Cre mice, directing CVS-N2c(G) and TVA expression selectively in GS motor neurons (Figure 3.4C). Two weeks later EnvA-pseudotyped CVS-N2c$^{\Delta G}$-dsRed was injected into spinal segments L3-L6, selectively infecting GS motor neurons. We then examined the pattern of fluorescent protein labeling in peripheral sensory endings derived from homonymous GS and antagonist TA group Ia proprioceptive sensory afferents.

We detected dsRed-labeled sensory endings in contact with intrafusal muscle spindle fibers in 75% of GS muscles, but did not observe any dsRed-labeled spindle-associated sensory endings in the TA muscle (4 mice, n = 8 muscles; Figure 3.4D,E). This finding implies a tightly controlled and exclusively synaptic process of CVS-N2c$^{\Delta G}$ transfer from motor neurons to sensory terminals that form monosynaptic contacts with their target motor neuron pool.

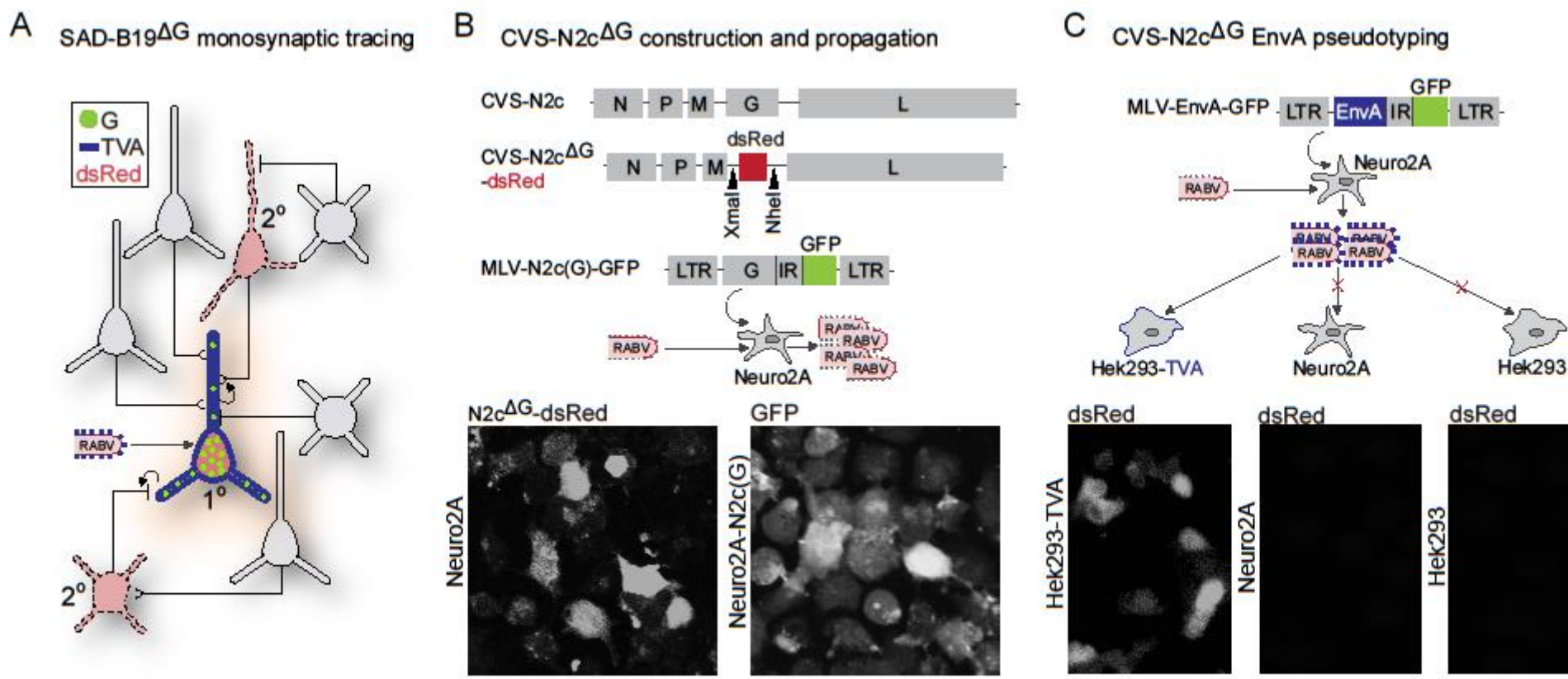
A
SAD-B19ΔG monosynaptic tracing
G
TVA
dsRed
2°
1°
2°
RABV
B
CVS-N2cΔG construction and propagation
CVS-N2c
N
P
M
G
L
CVS-N2cΔG
-dsRed
dsRed
XmaI
NheI
MLV-N2c(G)-GFP
LTR
G
IR
GFP
LTR
RABV
Neuro2A
N2cΔG-dsRed
GFP
Neuro2A
Neuro2A-N2c(G)
C
CVS-N2cΔG EnvA pseudotyping
MLV-EnvA-GFP
LTR
EnvA
IR
GFP
LTR
Neuro2A
RABV
Hek293-TVA
Neuro2A
Hek293
dsRed
dsRed
dsRed
Hek293-TVA
Neuro2A
Hek293

Figure 3.1

FIGURE 3.1. Construction and Packaging of CVS-N2c$^{\Delta G}$ for monosynaptic tracing

The CVS-N2c deletion mutant was created in the manner pioneered by Wickersham et al (2007a,b). A key difference is the use of a neural cell line for viral packaging. **(A)** Schematic illustrating monosynaptic restriction of viral spread from starter to secondary neurons. **(B)** CVS-N2c genome and recombinant CVS-N2c$^{\Delta G}$ vector with XmaI/NheI insert restriction sites flanking dsRed insert as well as rescued virus expressing dsRed in Neuro2A cells (top) and complementation vector expressing CVS-N2c glycoprotein inside murine leukosis virus (MLV) (middle) stably transfected into Neuro2A cells for amplification of virus CVS-N2c$^{\Delta G}$ to create the line Neuro2A-N2c(G). Levels of GFP expression correspond to expression of N2c(G) (bottom). **(C)** Complementation vector expressing a chimeric EnvA glycoprotein with short CVS glycoprotein tail (top) transfected into Neuro2A cells for packaging of pseudotyped virus. 293-TVA cells show infection by EnvA-pseudotyped CVS-N2c$^{\Delta G}$ and Neuro2A and Hek293 cells lacking the TVA receptor show no infection by the same virus (bottom).

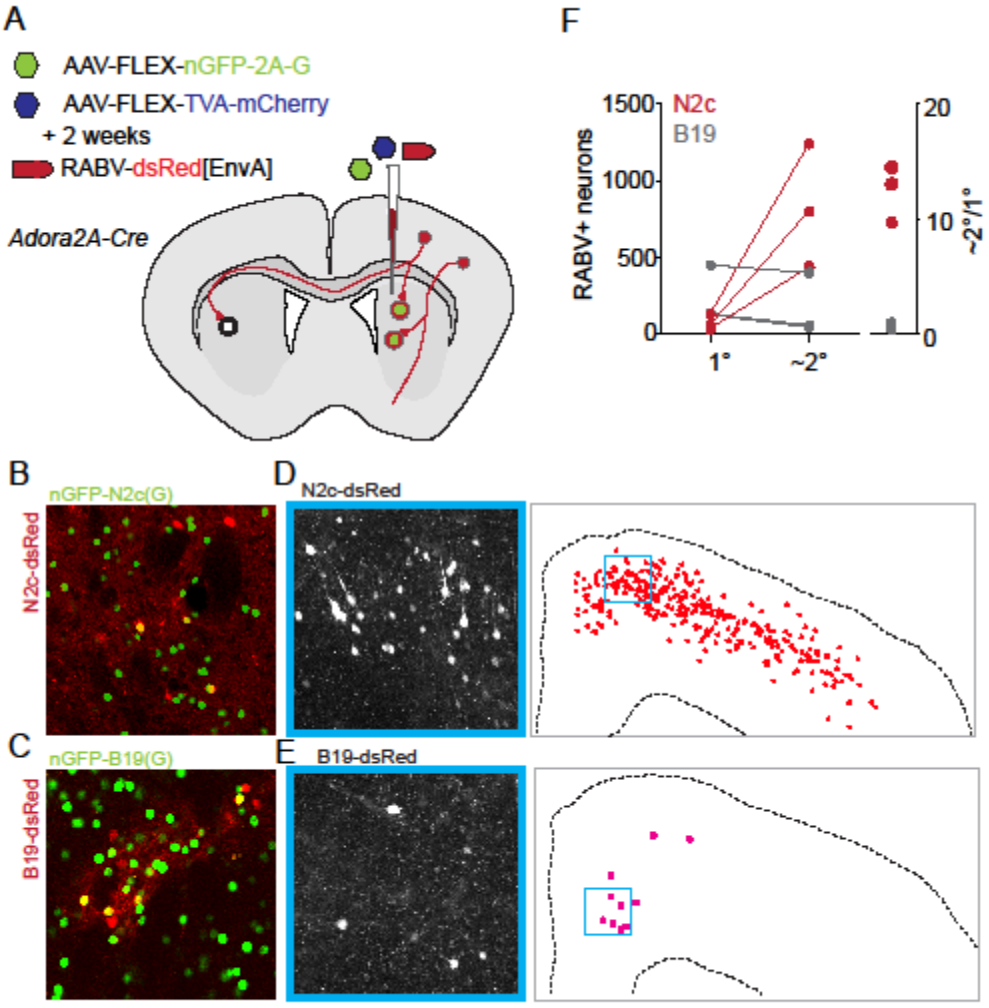

Figure 3.2

FIGURE 3.2. Greater trans-synaptic transfer for CVS-N2c than SAD-B19 in the forebrain

(A) Schematic for cortico-striatal retrograde trans-synaptic infection. Primary neurons in striatum infected by conditional AAV expressing RABV(G) and nuclear GFP (histone2B-GFP fusion: nGFP) and AAV expressing TVA and mCherry after recombination via germline *Adora2a*-Cre, and re-infected two weeks later by pseudotyped RABV$^{\Delta G}$–dsRed[EnvA]. **(B-C)**

Confocal images of primary infection for SAD-B19 and CVS-N2c. Primary cells display both nGFP as well as dsRed. **(D-E)** Representative image of monosynaptic viral spread with 20x confocal image inset from anatomical plot showing all RABV+ neurons. **(F)** Plot of infection spread from primary striatal to secondary cortical neurons in 6 mice, 3 for each viral strain. Primary infection was marked by expression of both dsRed from RABV and nGFP from the AAV complementation vector. Primary infection was constrained to small populations in the same region of anterior dorsal striatum. Secondary infection was calculated by sampling the same 5 coronal sections from each animal as identified by position relative to Bregma. Pan-cortical secondary infection is greater, but scales with numbers shown here.

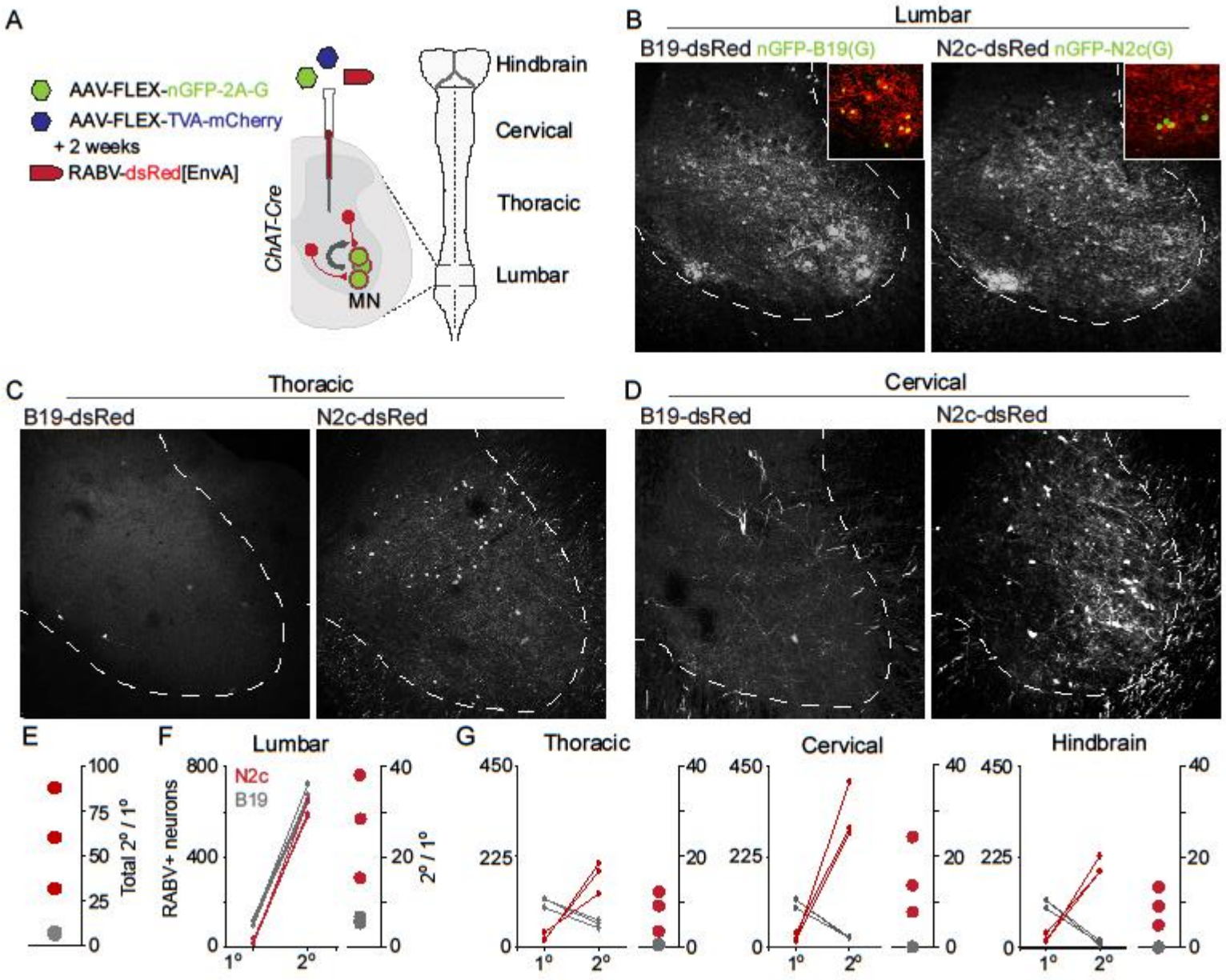
A
AAV-FLEX-nGFP-2A-G
AAV-FLEX-TVA-mCherry
+ 2 weeks
RABV-dsRed[EnvA]
ChAT-Cre
MN
Hindbrain
Cervical
Thoracic
Lumbar
B
Lumbar
B19-dsRed nGFP-B19(G)
N2c-dsRed nGFP-N2c(G)
C
Thoracic
B19-dsRed
N2c-dsRed
D
Cervical
B19-dsRed
N2c-dsRed
E
Total 2° / 1°
F
Lumbar
RABV+ neurons
N2c
B19
2° / 1°
G
Thoracic
Cervical
Hindbrain
1°
2°

Figure 3.3

FIGURE 3.3. CVS-N2c$^{\Delta G}$ from lumbar motor neurons shows enhanced trans-synaptic spread compared to SAD-B19$^{\Delta G}$

(A) Schematic of RABV-monosynaptic tracing from lumbar motor neurons. **(B-D)** Representative images for each viral strain showing trans-synaptically transferred infection at lumbar **(B)**, thoracic **(C)** and cervical **(D)** levels. **(E)** Total primary to secondary ratios for SAD-B19$^{\Delta G}$ (grey) and CVS-N2c$^{\Delta G}$ (red). **(F,G)** Plot of infection spread from primary to secondary neurons in 6 mice, 3 for each viral strain, at local lumbar **(F)**, and **(G)** distant thoracic, cervical and hindbrain levels.

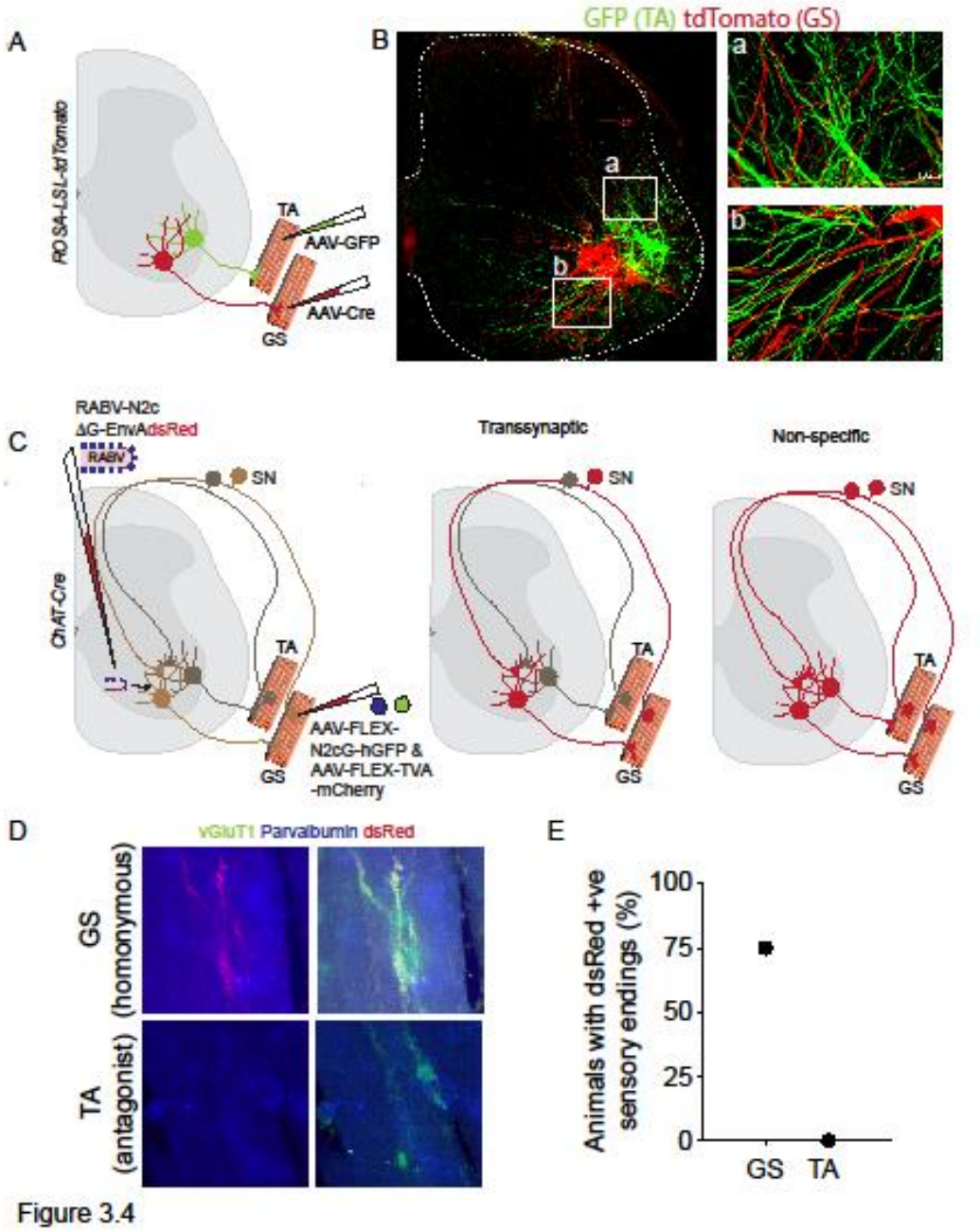

Figure 3.4

FIGURE 3.4. Restricted trans-synaptic transfer of CVS-N2c$^{\Delta G}$

(A) Experimental design to examine overlap of GS and TA motor neuron dendrites. (B) Fluorescent labeled motor neurons showing overlap of GS and TA dendrites. (C) Assay

to test for selective trans-synaptic transfer of RABV. (D) Example images of GS and TA muscle spindles showing dsRed positive sensory endings in GS (top) but not TA (bottom). (E) Quantitation of labeled sensory endings in GS or TA muscles.

Supplemental Information

A summary of figures and important controls follows.

Supplementary Figure 3.1, related to Figure 3.1: Neuro2a cells infected with CVS-N2c$^{\Delta G}$.

Supplementary Figure 3.2, related to Figure 3.1: RABV glycoprotein immunofluorescence after transfection with AAV constructs.

Supplementary Figure 3.3, related to Figures 3.1-3.3: Control experiments for the EnvA-pseudotyped CVS-N2c$^{\Delta G}$ and the AAV constructs.

Supplementary Table 3.1: Titer of viruses used in this study.

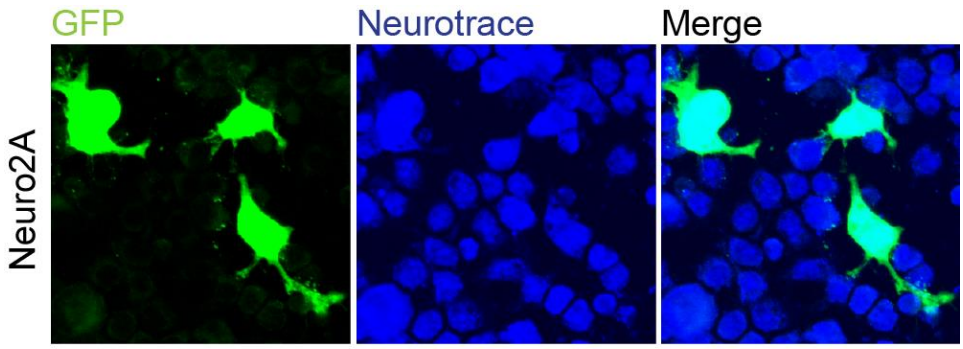

Supplementary Figure 3.1, related to Figure 3.1: Infection of Neuro2A cells with CVS-N2cΔG.

Neuro2A cells infected with CVS-N2c$^{\Delta G}$, expression after 4 days.

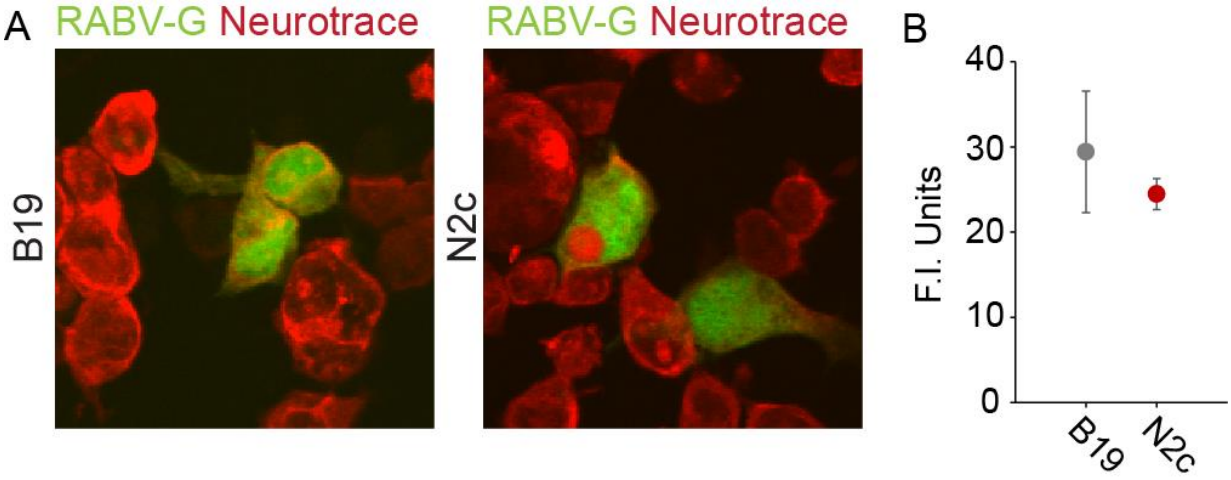

Supplementary Figure 3.2, related to Figure 3.1: Glycoprotein expression from AAV helpers. (A) Example images of Neuro2A cells infected with AAVs driving B19-G (left) or N2c-G (right). (B) Plot of rabies glycoprotein fluorescence intensity.

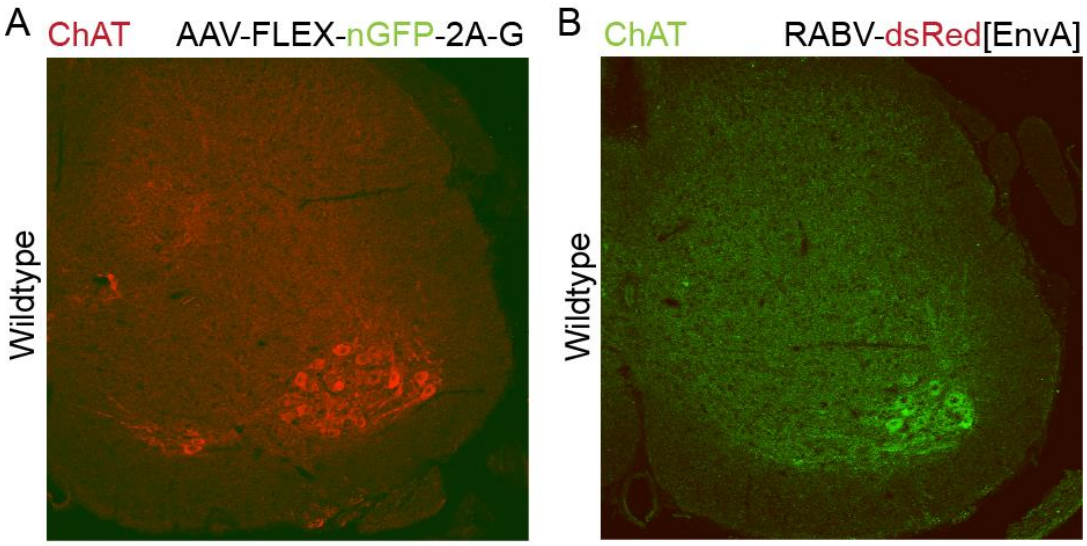

Supplementary Figure 3.3, related to Figures 3.1-3.3: Selectivity of FLEX AAVs and EnvA-pseudotyped rabies virus. (A) Injection of AAV-FLEX-nGFP-2A-G into spinal cord of wild-type mice. (B) Injection of RABV$^{\Delta G}$-N2c-dsRed[EnvA] into spinal cord of wild-type mice.

Virus Type	Name	Gene(s)	Titer (units/ml)	First described	Estimated production time from rescue
RABV-B19	SAD-B19ΔG-GFP	GFP	$1x10^9$ (WTG) $1x10^8$ (EnvA)	Wickersham et al. (2007)	3-4 weeks*
RABV-N2c	CVS-N2cΔG-GFP	GFP	$3x10^8$ (WTG) $2x10^7$ (EnvA)	Here	6-8 weeks WTG + 2 weeks
RABV-B19	SAD-B19ΔG-dsRed	dsRed	$1x10^9$ (WTG) $1x10^8$ (EnvA)	Osakada et al., 2011	3-4 weeks*
RABV-N2c	CVS-N2cΔG-dsRed	dsRed	$2x10^8$ (WTG) $1x10^7$ (EnvA)	Here	6-8 weeks WTG + 2 weeks
RABV-B19	SAD-B19ΔG-ChR2-eYFP	ChR2 & eYFP	$1x10^9$ (WTG)	Osakada et al., 2011	3-4 weeks*
RABV-N2c	CVS-N2cΔG-ChR2-eYFP	ChR2 & eYFP	$1x10^7$ (WTG)	Here	6-8 weeks WTG + 2 weeks
RABV-B19	SAD-B19ΔG-GCaMP6f	GCaMP6f	$2x10^9$ (WTG)	Here, but see Osakada et al., 2011 for B19-GCaMP3	3-4 weeks*
RABV-N2c	CVS-N2cΔG-GCaMP6f	GCaMP6f	6x107 (WTG)	Here	6-8 weeks WTG + 2 weeks
AAV2/1	AAV2/1-FLEX-nGFP-2A-B19G	HistoneGFP and B19G	$2x10^9$	Kaifosh et al., 2013 (and Addgene 37452, 2012)	1 week
AAV2/1	AAV2/1-FLEX-nGFP-2A-N2cG	HistoneGFP and N2cG	$2x10^9$	Here	1 week
AAV2/1	AAV2/1-FLEX-TVA-mCherry	TVA and mCherry	$2x10^9$	Watabe-Uchida et al., 2012	1 week

Supplementary Table 3.1: Viral vectors and titers used in this study. Titers are expressed as infectious units/ml. * see Wickersham et al., 2010.

Part 4. Updating deletion-mutant rabies: reducing the toxicity

Using the CVS-N2c$^{\Delta G}$ introduced in Part 3, we also wished to examine its cytotoxic properties. As explained previously, one hypothesis holds that rabies "uses stealth" to spread in the nervous system (Schnell 2009), and relies on minimizing early immune response. We thus hypothesized that a strain of rabies which spreads particularly well would show relatively reduced cytotoxic effects.

Results

Reduced expression and neurotoxicity of CVS-N2c$^{\Delta G}$ virus *in vitro*

To characterize CVS-N2c$^{\Delta G}$ for use in functional experiments we examined the level of RABV gene expression elicited by the SAD-B19$^{\Delta G}$ and CVS-N2c$^{\Delta G}$ strains. Neuro2A cells were infected with RABV$^{\Delta G}$-GFP, under conditions in which the multiplicity of infection (MOI) was kept below 0.1, to avoid cellular infection by multiple copies of virus. Two days after infection, both RABV$^{\Delta G}$ strains directed GFP expression at similar levels; but after four days, the level of GFP expression directed by SAD-B19$^{\Delta G}$ was significantly higher than that conferred by CVS-N2c$^{\Delta G}$ (unpaired Student's t-test; $p = 0.045$, Figure 4.1A-C).

We next examined whether the SAD-B19$^{\Delta G}$ and CVS-N2c$^{\Delta G}$ strains differed in their ability to impose cytotoxic damage to Neuro2A cells. To assess this, we monitored the incidence of incorporation of propidium iodide (PI), a cell-impermeable DNA intercalating agent that is passively transferred through the plasma membrane of dead or dying cells. In uninfected Neuro2A cells, PI labeled 21% of cells, and in Neuro2A cells infected with CVS-N2c$^{\Delta G}$-GFP 22% of cells were PI labeled. But for Neuro2A cells infected with SAD-B19$^{\Delta G}$-GFP, 49% were PI labeled (Figure 4.1D-F) ($p = 0.037$, unpaired Student's t-test). Thus, SAD-B19$^{\Delta G}$ exerts a greater toxicity *in vitro* than CVS-N2c$^{\Delta G}$ strain, even with a comparatively inert fluorophore.

Manipulating and monitoring neural activity with CVS-N2c$^{\Delta G}$ virus

We next compared CVS-N2c$^{\Delta G}$ and SAD-B19$^{\Delta G}$ strains for their ability to express proteins to monitor and manipulate neuronal activity. To achieve this, we created RABV$^{\Delta G}$ variants expressing humanized channelrhodopsin2 (hChR2), or a genetically encoded calcium indicator, GCaMP6f (Zhang et al., 2006; Chen et al., 2013). In this set of experiments we controlled the duration of infection by injecting native-envelope RABV$^{\Delta G}$ viruses such that they directly infected the terminals of projection neurons in cortico-striatal and hippocampal-septal circuits.

To explore the utility of SAD-B19$^{\Delta G}$ and CVS-N2c$^{\Delta G}$ as vectors for manipulating neural activity through hChR2 expression (Zhang et al., 2006) we first analyzed levels of neurotoxicity for each strain. Injection of RABV$^{\Delta G}$ into the dorsal striatum resulted in retrograde infection of cortical projection neurons. After 6 days, SAD-B19$^{\Delta G}$-hChR2-YFP infected neurons exhibited an

aberrant neuronal morphology with distal dendrites exhibiting noticeable disruption, and the surrounding neuropil containing neuronal debris (Figure 4.2A,C). In contrast, near-normal cortical neuronal morphology was observed 6 days after infection with CVS-N2c$^{\Delta G}$-hChR2-YFP (Figure 4.2B,C).

We examined the ability of RABV$^{\Delta G}$-hChR2-YFP expression, to confer photo-excitability, assaying responses over a four-week period (Figure 4.2D,E,F). Using SAD-B19$^{\Delta G}$-hChR2-YFP virus, we detected few fully intact cortical neurons after 7 days of infection, precluding physiological analysis (6 animals; Figure 4.2A; data not shown). In contrast, photo-illumination at 473 nm wavelength of cortical neurons infected by CVS-N2c$^{\Delta G}$-hChR2-YFP reliably elicited action potentials in infected cortical neurons in acute forebrain slices (Figure 4.2E,F), for up to 28 days after infection. Spike frequency increased with the duration of viral expression over the first 10 days (Figure 4.2F,G). Moreover, recordings from nearby YFP^{off} uninfected cortical neurons revealed excitatory postsynaptic currents elicited by presynaptic photo-stimulation (Figure 4.2H). Stable whole-cell recordings from CVS-N2c$^{\Delta G}$-infected cortical neurons were obtained at a rate similar to that of uninfected neurons. Resting potentials (V_m) for infected and uninfected cells in the same animal were statistically similar over the infection period (-58.7mV ± 2.2, n = 7 versus -56.8mV ± 1.5, n = 16); without a clear trend for changes in V_m as a function of infection time. These results document the efficacy of CVS-N2c$^{\Delta G}$ in expressing hChR2 under conditions that permit optogenetic manipulation of neuronal activity.

We next assessed the efficacy of CVS-N2c$^{\Delta G}$ and SAD-B19$^{\Delta G}$ as monitors of neural activity through expression of GCaMP6f (Chen et al., 2013). In this analysis we focused on hippocampal-septal circuits in which locomotion evokes robust hippocampal neuronal activity (Somogyi and Klausberger, 2008; Jinno et al., 2007). We first assayed neurotoxicity of each RABV$^{\Delta G}$ strain. Following injection of SAD-B19$^{\Delta G}$-GCaMP6f virus into the medial septum, infected hippocampal projection neurons exhibited marked signs of degeneration, most notably pronounced blebbing of neuronal processes 10 days after infection (Figure 4.3A,C). In contrast, septal neurons infected with CVS-N2c$^{\Delta G}$-GCaMP6f for one week exhibited near-normal morphology and only a modest disruption at two weeks (Figure 4.3B,C).

The activity of hippocampal-septal projection neurons after retrograde infection with CVS-N2c$^{\Delta G}$-GCaMP6f was determined through *in vivo* two-photon Ca^{2+} imaging (Figure 4.3E). We detected hippocampal neuronal GCaMP6f-Ca^{2+} transients in mice during treadmill locomotion, with a tight temporal coincidence in locomotor episodes and neuronal burst activity (Lovett-Barron et al., 2014) (Figure 4.3G). In addition, we found that the magnitude of treadmill based locomotion-evoked Ca^{2+} signals recorded from hippocampal-septal projection neurons was constant over the first two post-injection weeks (Figure 4.3F). Repeated recordings from identified neurons were possible for the entire usable duration of the cranial imaging window, at least 17 days post-infection. These findings establish that CVS-N2c$^{\Delta G}$ confers durable, and physiologically non-disruptive, expression of GCaMP6f, permitting analysis of neuronal activity *in vivo* for at least several weeks.

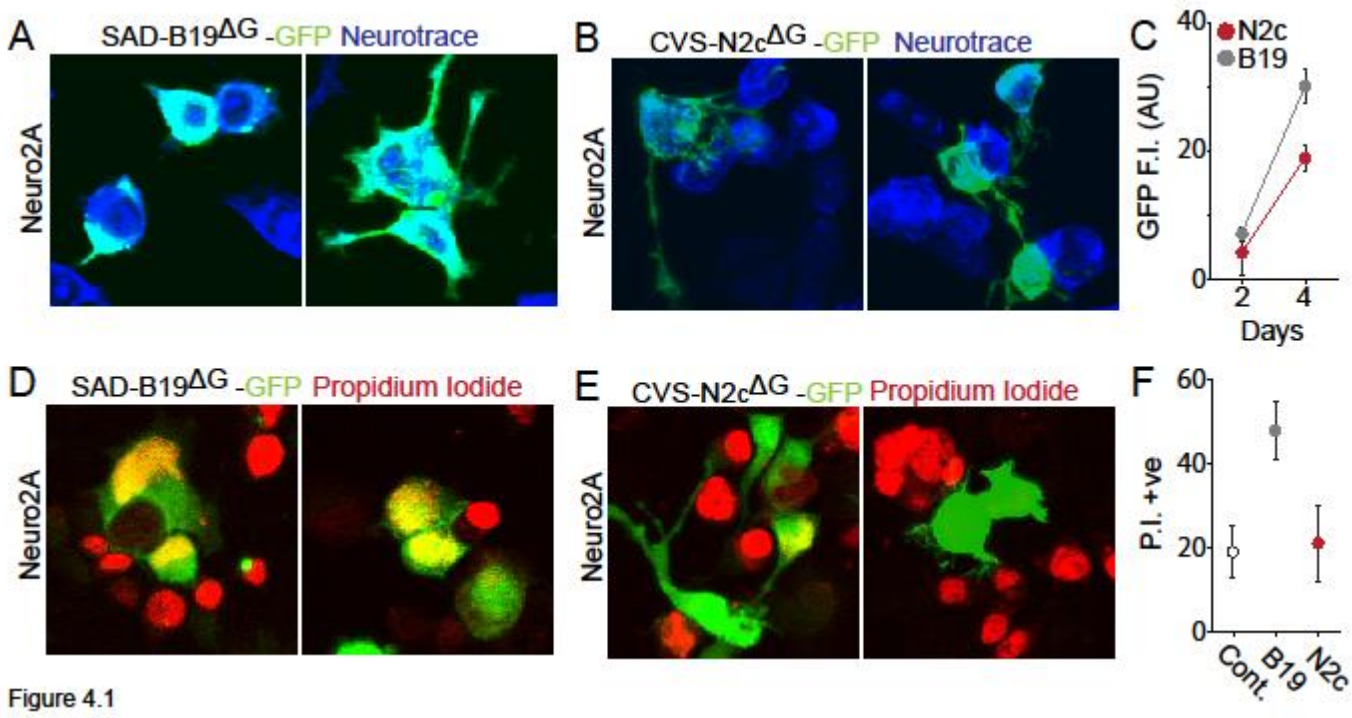

FIGURE 4.1. Reduced expression level and cytotoxicity of CVS-N2c compared to SAD-B19

(A) Neuro2A cells infected by GFP-expressing SAD-B19$^{\Delta G}$ or **(B)** CVS-N2c$^{\Delta G}$. **(C)** Intensometric plot of GFP expressed by each RABV strain at 2 and 4 days post-infection, normalized to single infected cells. **(D)** Neuro2A cells infected with SAD-B19$^{\Delta G}$ or **(E)** CVS-N2c$^{\Delta G}$ after 4 days and treated with propidium iodide, a proxy marker for cell death at 4 days post-infection. **(F)** Relative cell death after infection by each RABV strain. Error bars in C and F represent ± SEM.

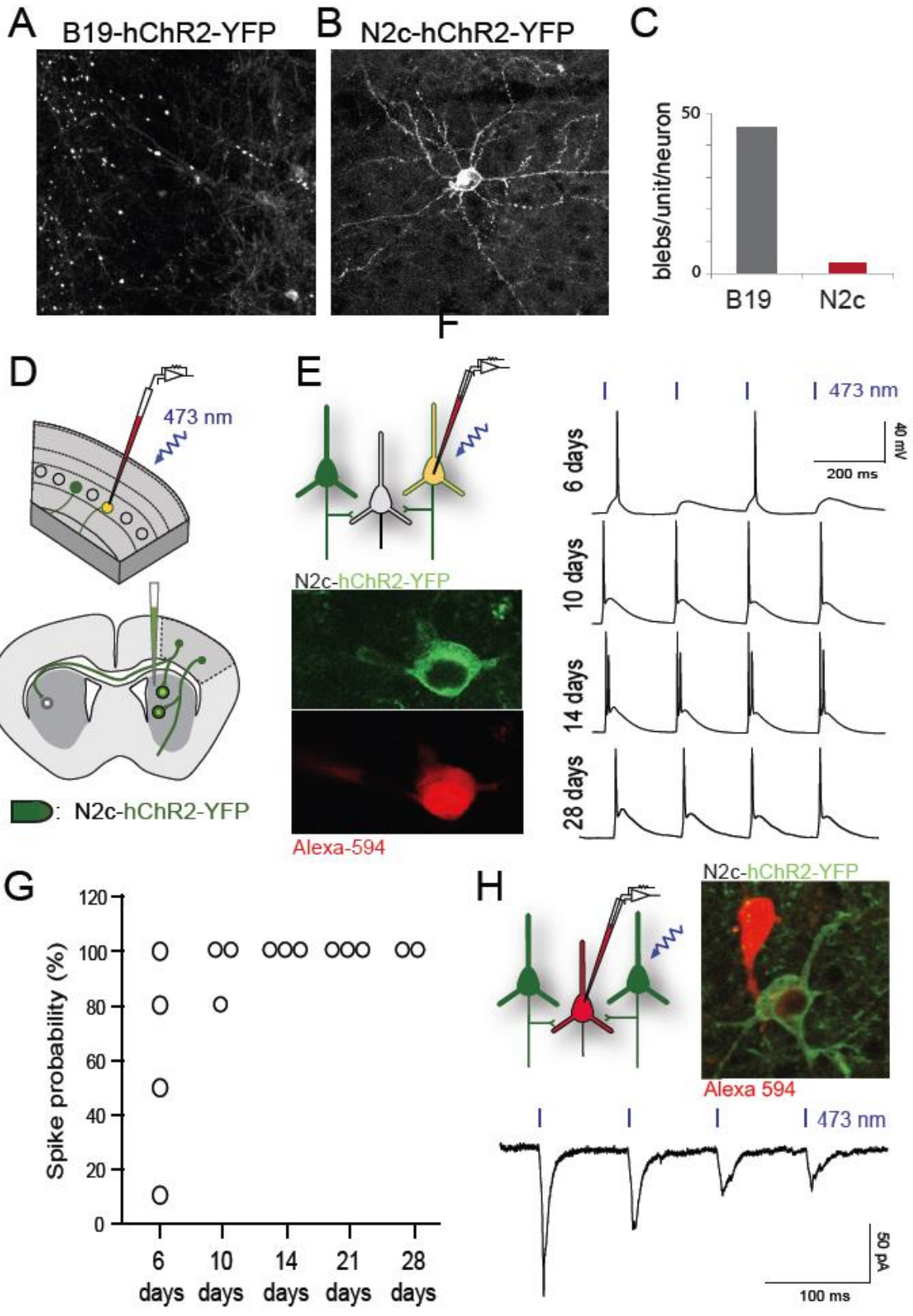
A
B19-hChR2-YFP
B
N2c-hChR2-YFP
C
blebs/unit/neuron
50
0
B19
N2c
D
473 nm
: N2c-hChR2-YFP
E
N2c-hChR2-YFP
Alexa-594
F
473 nm
40 mV
200 ms
6 days
10 days
14 days
28 days
G
Spike probability (%)
120
100
80
60
40
20
0
6 days
10 days
14 days
21 days
28 days
H
N2c-hChR2-YFP
Alexa 594
473 nm
50 pA
100 ms

Figure 4.2

FIGURE 4.2. CVS-N2c$^{\Delta G}$ is an effective trans-synaptic vector for optogenetic manipulation

(A) Confocal image of neurons after 7 days of infection by SAD-B19$^{\Delta G}$ virus expressing hChR2-YFP (cortex). **(B)** Same proteins via virus CVS-N2c$^{\Delta G}$. **(C)** Assay of cell health by morphological irregularity, blebs along proximal dendrites per RABV-infected neuron. **(D)** Schematic of cortico-striatal retrograde infection using CVS-N2c$^{\Delta G}$-hChR2-YFP in the dorsal striatum in wild type mice and retrograde spread into cortex (top) and patch-clamp recording of infected cortical neurons (bottom). **(E)** Schematic of whole-cell current-clamp recordings obtained from neurons in acute cortical slices (top). In vitro two-photon images of a recorded cortical neuron retrogradely infected by CVS-N2c$^{\Delta G}$-hChR2-YFP (green) and filled with fluorescent dye from patch pipette (red). **(F)** Example hChR2-photostimulation-evoked voltage responses recorded from CVS-N2c$^{\Delta G}$-hChR2-YFP-infected neurons at 6, 10, 14, and 28 days post infection as seen in (*B*). **(G)** Spike probability at each 6/10/14/21/28 DPI showing increasing effectiveness of hChR2 expressed by the CVS-N2c$^{\Delta G}$ vector. **(H)** Schematic and *in vitro* two-photon image showing CVS-N2c$^{\Delta G}$-infected (green) neuron in the vicinity of a non-infected cortical neuron filled with red fluorescent dye via patch pipette (top). Example averaged postsynaptic responses recorded from the non-infected neuron confirming effective synaptic release at 8 days post infection (bottom).

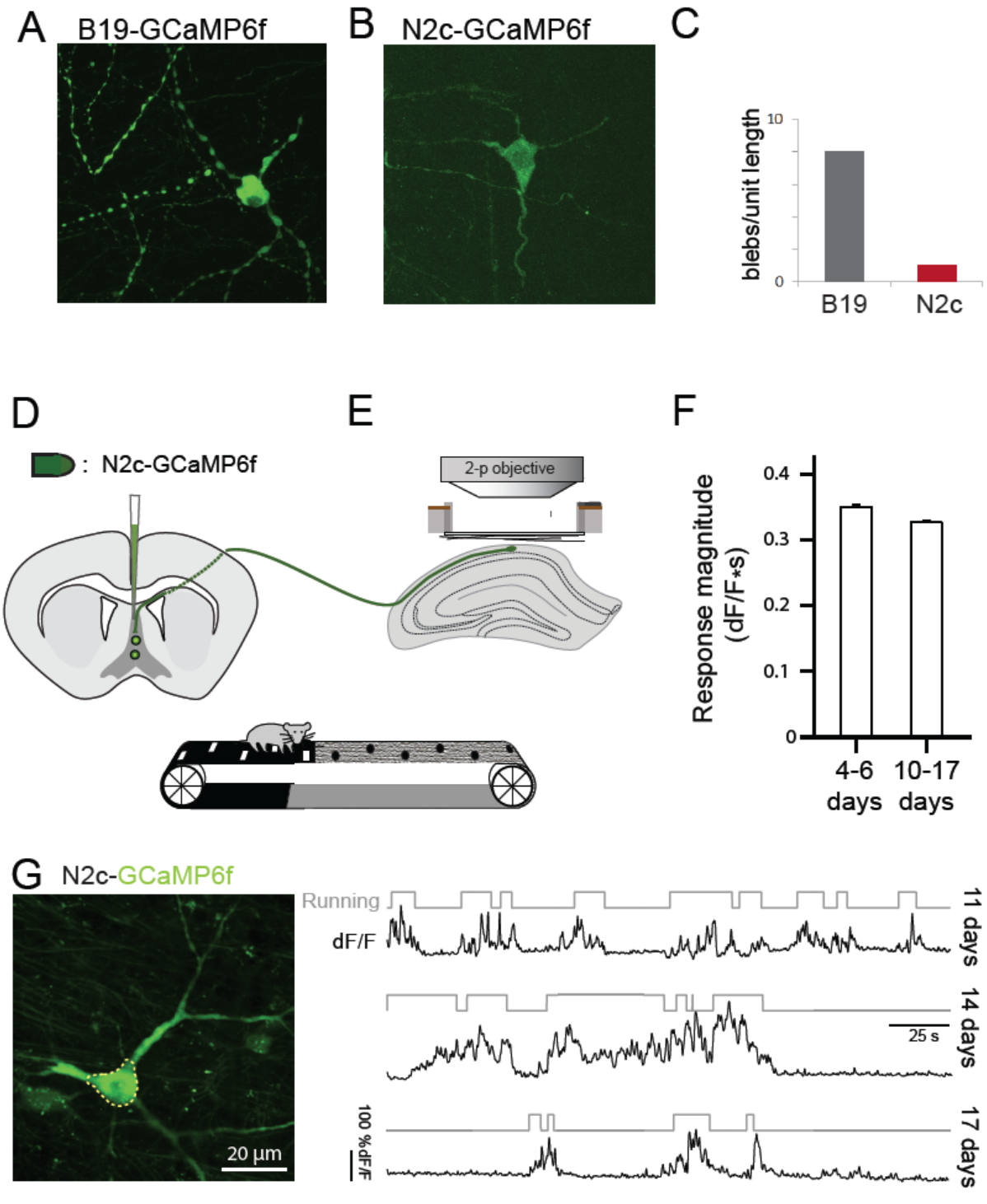
A
B19-GCaMP6f
B
N2c-GCaMP6f
C
blebs/unit length
10
0
B19
N2c
D
: N2c-GCaMP6f
E
2-p objective
F
Response magnitude (dF/F*s)
0.4
0.3
0.2
0.1
0
4-6 days
10-17 days
G
N2c-GCaMP6f
20 µm
Running
dF/F
11 days
14 days
25 s
100 %dF/F
17 days

Figure 4.3

FIGURE 4.3. CVS-N2c$^{\Delta G}$ is an effective trans-synaptic vector for optogenetic monitoring

(A) Confocal image of neurons after 10 days of infection by SAD-B19$^{\Delta G}$ virus expressing GCaMP6f (medial septum). **(B)** Same protein via virus CVS-N2c$^{\Delta G}$. **(C)** Assay of cell health by morphological irregularity, blebs along proximal dendrites per RABV-infection neuron. **(D)** Schematic of infection of CVS-N2c$^{\Delta G}$-GCaMP6f in medial septum and retrograde spread to the dorsal hippocampus. **(E)** Schematic of head-fixed two-photon imaging of dorsal hippocampus of mouse running on an environmentally enriched treadmill (top), *in vivo* two-photon image of an example septal projecting neuron imaged for activity in the area CA1 of the dorsal hippocampus (middle), and time-series of neural activity, expressed as relative changes in GCaMP6f fluorescence ($\Delta F/F$, black traces) of neuron during running bouts (grey traces) on belt, imaged via *in vivo* two-photon microscopy (bottom). **(F)** Population summary of the magnitude of running-evoked of Ca^{2+} signals indicating comparable responses over extended periods after infection (4-6 DPI: n = 13 cells in n = 2 animal; 10-17 DPI: n = 31 cells in n = 3 animals, Wilcoxon-Mann-Whitney two sample rank test, p = 0.592). **(G)** *In vivo* two-photon image of the same septal-projecting neuron in area CA1 of the dorsal hippocampus (left), and GCaMP6f fluorescence Ca^{2+} signals ($\Delta F/F$, black traces) recorded from the same neuron during running (grey traces) at 11, 14, and 17 days post-injection (right). Error bars in F represent ± SEM.

Part 5. Updating deletion-mutant rabies: alternate tools

Leveraging the same CVS-N2c$^{\Delta G}$ rabies strain introduced in Part 3, we created several new variants with utility to experimental neuroscience. Here is describe versions which can be used to neuroanatomical investigations at the level of electron microscopy, as well as versions which can be used to drive genetic recombination in other viruses and germline mutants.

Results

Conditional recombination with Cre and Flpo:
CVS-N2c expression level is sufficient to direct transgene recombination

CVS-N2c$^{\Delta G}$ infection directs comparatively low levels of gene expression, and thus it is unclear whether Cre or Flpo proteins can be expressed at concentrations sufficient to exert efficient enzyme-mediated recombination. To address this issue we constructed -mCherry-2A-Flpo and -mCherry-2A-Cre driver viruses for CVS-N2c$^{\Delta G}$ transduction. CVS-N2c$^{\Delta G}$-mCherry-2A-Flpo virus was injected into the lumbar spinal cord of mice harboring a Flp-GFP reporter (Figure 5.1A) and the incidence of retrogradely-infected neurons was examined in thoracic spinal cord. Germ-line expression of GFP served as an indicator of recombination, and was detected in all neurons infected with CVS-N2c$^{\Delta G}$-mCherry-2A-Flpo, revealed by expression of mCherry (Figure 5.1B). Thus, the level of Flpo expression achieved with CVS-N2c$^{\Delta G}$ transduction is sufficient to direct target gene recombination in an efficient manner.

In a similar manner, we investigated whether CVS-N2c$^{\Delta G}$ directs Cre-mediated recombination. We injected CVS-N2c$^{\Delta G}$-mCherry-2A-Cre into the ventral tegmental area (VTA)

of wild type mice, and in parallel injected a Cre-conditional AAV expressing GFP (AAV-FLEX-GFP) into the parabrachial nucleus (PBN) (Figure 5.1C). We found that ~50% of mCherry^{+} RABV-infected neurons expressed GFP (Figure 5.1D), consistent with the sparsity of infection of PBN neurons and indicative of the efficacy of Cre expression.

Electron-microscopy using APEX2

A recurring problem when performing tracing experiments with electron microscopy (EM) is the degeneration of neural tissue, and synapses in particular, during preparation of samples for imaging. Attempting to register the same neurons across light and confocal microscopy with EM is a Herculean task, as the preparation of samples degrades optical signals at the same time that it degrades tissue. One solution to this is the use of a unified reporter that allows for detection without extensive preparation. Genetically expressed proteins which can be directly detected with EM following minimal preparation include peroxidases such as HRP. However, HRP is not efficiently expressed (in proper conformation) by mammalian neurons. Alternative peroxidases offer that possibility (Matrell et al., 2012; Lam et al., 2014). We generated new CVS-N2c$^{\Delta G}$ rabies viruses that express the engineered ascorbate peroxidase APEX2. This new class of EM reporters are sensitive to expression levels, so we sought to determine whether CVS-N2c$^{\Delta G}$-APEX2-Venus would be expressed at too low a level to be detected or such a high level that it induced cytotoxicity and dysmorphia.

We tested the virus in cultured HEK-293 cells as well as *in vivo*, and found that it expressed well and yielded both detectable fluorescence as well as EM-detectable membrane signals (Figure 5.2)

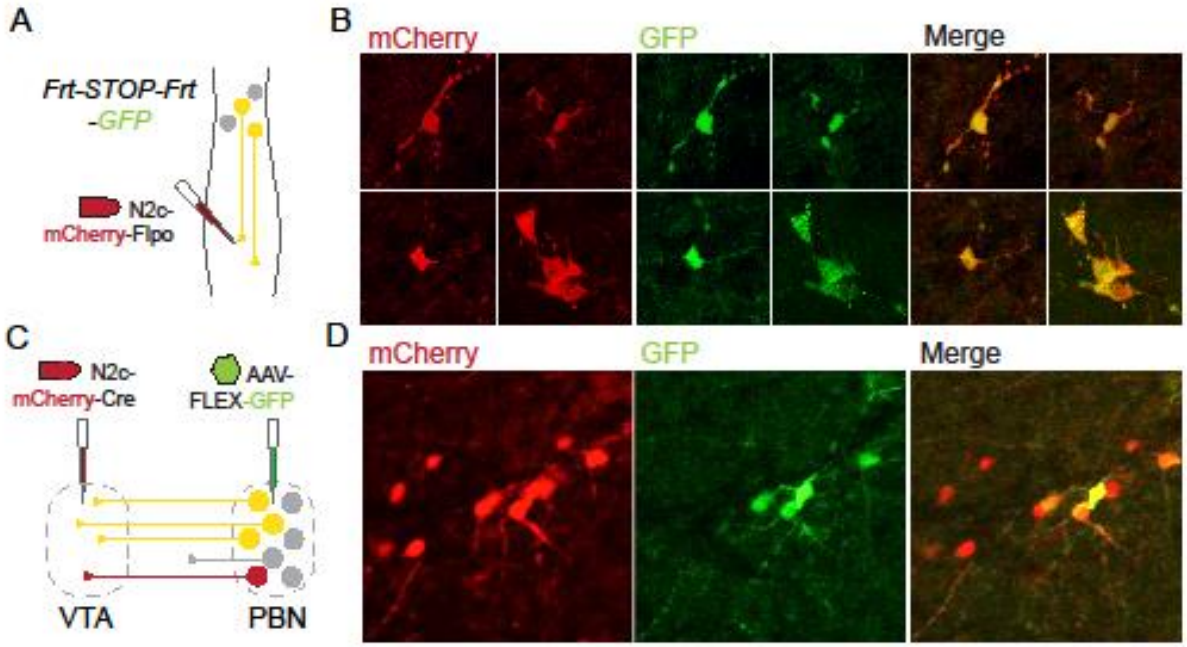

Figure 5.1

FIGURE 5.1. CVS-N2c$^{\Delta G}$ drives Cre- or Flp-dependent recombination

(A) Schematic depicting injection of CVS-N2c$^{\Delta G}$-mCherry-Flpo and recombination in Frt-STOP-Frt-GFP mouse line. **(B)** Confocal images of thoracic spinal cord showing recombination in retrogradely infected neurons. **(C)** Schematic depicting injection and recombination by CVS-N2c$^{\Delta G}$-mCherry-Cre. **(D)** Images in parabrachial nucleus (PBN) showing neurons after recombination and expression from a local AAV-FLEX-GFP injection and a corresponding infection in VTA and retrograde uptake of Cre-expressing virus by PBN neurons.

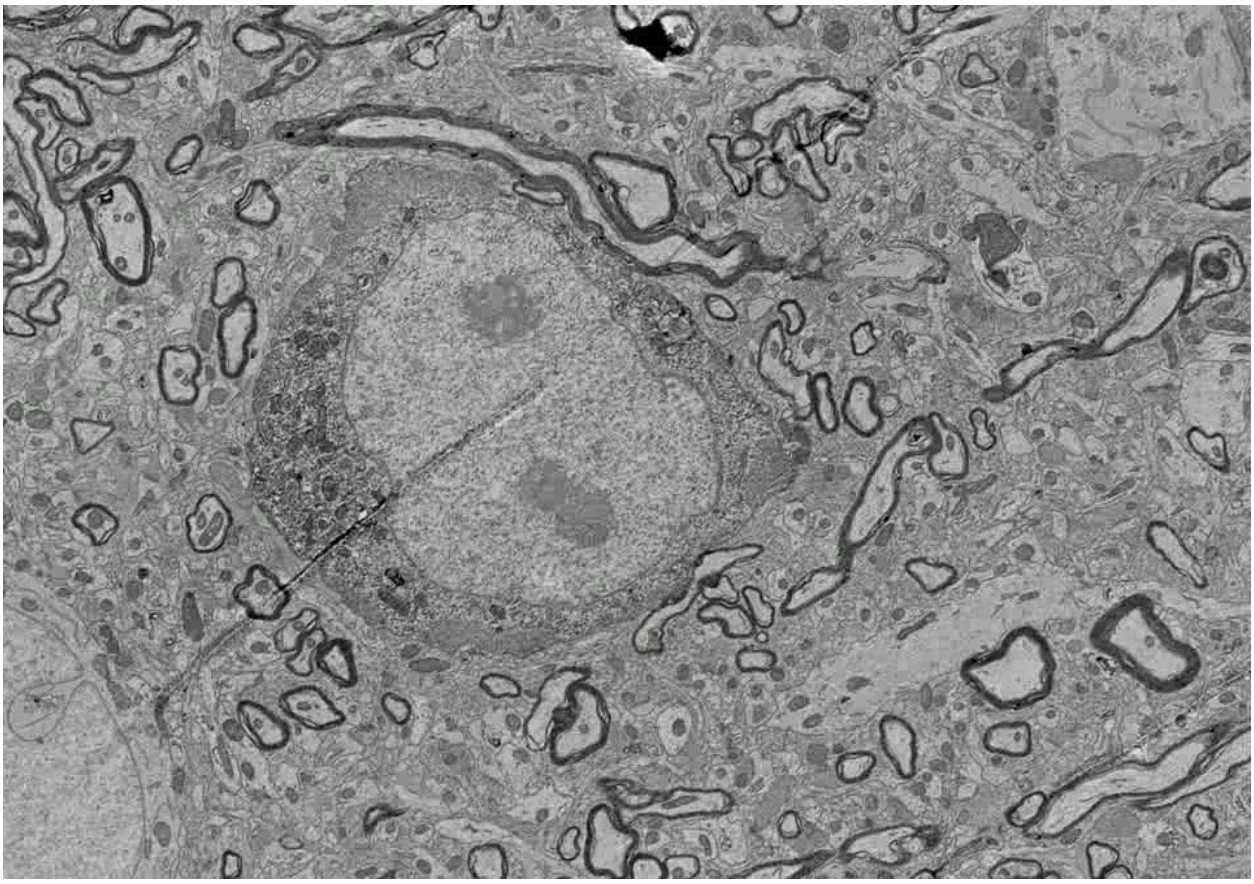

FIGURE 5.2: **electron micrograph of a neuron infected with CVS-N2c$^{\Delta G}$-APEX2-Venus** cellular membrane is well-preserved, allowing for fine-scale reconstruction of synaptic contacts

Part 6. CVS-N2c-$^{\Delta G}$ and future innovations for rabies and viral tools

Discussion of CVS-N2c-$^{\Delta G}$ investigation

Recombinant viruses facilitate the anatomical and functional analysis of mammalian neural circuits. We have explored the features of a recombinant strain of rabies virus, CVS-N2c$^{\Delta G}$, which permits monosynaptic tracing from genetically-defined neurons, as with the widely-used SAD-B19$^{\Delta G}$ strain. CVS-N2c$^{\Delta G}$ exhibits a marked reduction in neurotoxicity, both *in vitro* and *in vivo*, facilitating its application in monitoring and manipulating neural circuits. Moreover, direct comparison of CVS-N2c$^{\Delta G}$ and existing SAD-B19$^{\Delta G}$ strains reveals that CVS-N2c$^{\Delta G}$ provides at least an order of magnitude enhancement in trans-synaptic transfer to presynaptic neurons, with an even greater enhancement in transfer to long-range inputs (Table 1). CVS-N2c-based tools may therefore enable access to circuits that have so far proven refractory to RABV interrogation.

Enhanced trans-synaptic tracing with CVS-N2c$^{\Delta G}$.

Two major drawbacks in the application of attenuated RABV-based tools are high neurotoxicity (Morimoto et al., 1999) and inefficiency of trans-synaptic transfer (Callaway and Luo, 2015). Early generations of monosynaptic RABV-based vectors were primarily variants of the attenuated vaccine strain SAD-B19 (Schnell et al., 1994; Callaway and Luo, 2015; Ghanem and Conzelmann, 2015; Wickersham et al., 2007a,b), which is weakly neurotropic and strongly immunogenic. By contrast, most virulent RABV strains are highly neurotropic, neuroinvasive and, somewhat counter-intuitively, exhibit reduced immunogenicity and neurotoxicity by virtue

of their sequestration in neurons and evasion of surveillance by immune cells (Schnell et al., 2009).

The contrasting features of the SAD-B19 and CVS-N2c strains may stem from differences in growth and selection conditions. SAD-B19 was developed as a vaccine vector through serial passaging on non-neuronal cells. In contrast, CVS-N2c was developed through exclusive passaging in neonatal mouse brain and murine neuroblastoma cells as a challenge virus for testing RABV vaccines (Morimoto et al., 1998). As a result, CVS-N2c is highly neuroinvasive, has selective tropism for neuronal cells, lower replication and protein expression, and faster transport through the CNS (Bostan et al., 2010). These traits diverge from those of SAD-B19, which has a lower tropism for neurons, but a higher affinity for non-neuronal cells and faster replication. The consequence of accelerated replication is a greater number of viral particles and a strong induced immune response (see Schnell et al., 2009; Ghanem and Conzelmann, 2015; Morimoto et al., 1998 and Morimoto et al., 1999 for discussion on relative tropism and virulence of different RABV strains). These observations led us to consider whether a more virulent RABV strain might hold promise for circuit analysis. In addition, the reverse genetic rescue of the virulent CVS-N2c strain (Wirblich and Schnell, 2011) has eased the task of generating a glycoprotein deficient virus for use in monosynaptic tracing, as well as evading the biohazards inherent in working with virulent RABV.

We also provide evidence that CVS-N2c$^{\Delta G}$ is transferred retrogradely through an exclusive trans-synaptic route. The analysis of sensory-motor connectivity shows that CVS-

N2c$^{\Delta G}$ does not transfer to nearby, non-connected, synapses – with the implication that the enhancement in secondary neuron labeling occurs via an increase in synaptic transfer, rather than adventitious viral infection. The strength of glycoprotein complementation vector (Callaway and Luo, 2015), increased viral budding (Mebastion et al., 1996), enhanced glycoprotein neurotropism, reduced immunogenicity, and reduced viral toxicity (Schnell et al., 2009) may, separately or together, underlie the efficiency of RABV transfer and expression.

Of these variables, an increased neurotropism that maps to the viral glycoprotein is a plausible explanation for the increased transfer efficiency of CVS-N2c (Morimoto et al., 1998). We and others have replaced the SAD-B19 glycoprotein with that of CVS-N2c when complementing SAD-B19$^{\Delta G}$ virus and found that it increases trans-synaptic transfer, although not to the levels observed with fully complemented CVS-N2c$^{\Delta G}$ virus (Kaifosh et al. 2013; Velez-Fort et al., 2014; Reardon, Murray, Jessell, and Losonczy, unpublished data). By implication, the CVS-N2c glycoprotein may enhance trans-synaptic viral transfer. After CVS-N2c$^{\Delta G}$ infection the lack of infiltrating T-cells, antibodies and other antiviral immune effectors (Roy and Hooper, 2008; Schnell et al., 2009) may also increase the efficiency of viral transfer through the CNS. Finally, neuronal viability could extend the duration of competence for trans-synaptic transfer, as well as maintain host accessory proteins that assist in RABV transfer. We note that our work relies on the same complementation strategy as Wickersham et al, (2007b), and thus any improvements to that system, such as enhancement in TVA/EnvA selectivity or glycoprotein expression vectors, can easily be applied to the CVS-N2c strain.

Selection of appropriate RABV vectors for circuit analysis

In our studies, CVS-N2c$^{\Delta G}$ showed at least an order of magnitude enhancement in trans-synaptic spread compared to the SAD-B19$^{\Delta G}$ strain, and was particularly effective in trans-synaptic infection of neurons with long-range projections. A similar improvement was seen in two distinct CNS circuits, suggesting that CVS-N2c$^{\Delta G}$ lacks neuronal subtype constraints as a trans-synaptic tracer. Thus for anatomical studies CVS-N2c$^{\Delta G}$ appears to have major advantages over SAD-B19$^{\Delta G}$ and other prominent vaccine strains (Mori and Morimoto, 2014). Although it is conceivable that the trans-synaptic efficiency of SAD-B19 could be improved with modifications to the complementation vectors (e.g. DeNardo et al., 2015) or the use of alternate complementation methods (Rancz et al., 2011; Wertz et al., 2015) it is highly likely that the spread of CVS-N2c could be improved in the same way. Thus the use of the CVS-N2c$^{\Delta G}$ viral strain for anatomical studies has the potential to uncover aspects of neuronal connectivity inaccessible through the use of SAD-B19$^{\Delta G}$.

The ability to manipulate and monitor the activity of neurons within large networks, on behaviorally relevant timescales, sets CVS-N2c$^{\Delta G}$ apart from currently available RABV vectors. CVS-N2c$^{\Delta G}$ can drive tolerated levels of optogenetic activators, as well as recombinase proteins for selective recombination in presynaptic cells – opening the way for application of the full repertoire of conditional genetic tools in behaving animals. Previous studies have expressed optogenetic and recombinase proteins via SAD-B19$^{\Delta G}$ strains (Osakada et al., 2011) but neuronal manipulations were typically restricted to short post-infection times, typically 5-7 days (Kiritani et al., 2012; Namburi et al., 2015).

We have found that use of SAD-B19$^{\Delta G}$ precludes functional analysis of neuronal activity, as a consequence of premature neuronal dysfunction or death. The high levels of protein expression achieved by SAD-B19$^{\Delta G}$ may be a major contributor to its viral toxicity (Morimoto et al., 1999; Morimoto et al., 2000; Schnell et al., 2009). In particular, high expression levels of optogenetic proteins may facilitate cell death faster than would be observed when SAD-B19$^{\Delta G}$ is used to express relatively inert fluorescent proteins (Lin, 2011; Cetin and Callaway, 2014). In contrast, CVS-N2c$^{\Delta G}$ permits viable expression and long-term functional analysis using GCaMP6f or hChR2. Indeed, GCaMP calcium transients were detectable in hippocampo-septal neurons for up to 17 days, and cortical neurons expressing hChR2 under CVS-N2c$^{\Delta G}$ control maintained normal cell physiology and functional responses for 28 days after infection. We cannot exclude that over longer post-infection times, CVS-N2c$^{\Delta G}$ may also induce neuronal dysfunction (Scott et al., 2008), but the existing time-window opens potential new avenues for functional and behavioral experiments not available through use of SAD-B19$^{\Delta G}$.

CVS-N2c$^{\Delta G}$ seems to have major advantages over SAD-B19$^{\Delta G}$ in terms of anatomical tracing and functional analysis of circuit organization. But there are circumstances whereby SAD-B19$^{\Delta G}$ remains a relevant reagent. The higher protein levels produced after SAD-B19$^{\Delta G}$ infection make it more suitable for use as an acute vector, when fast expression of the transgene is important. SAD-B19$^{\Delta G}$ drives protein expression just one day post-infection, which is not achievable with CVS-N2c$^{\Delta G}$. In addition, the higher SAD-B19$^{\Delta G}$ directed protein expression levels permit visualization of fine neuronal morphologies (Wickersham et al. 2007a,b).

Moreover, the generation of viral particles in the laboratory is currently easier with SAD-B19$^{\Delta G}$ than with CVS-N2c$^{\Delta G}$. Titers on the order of $1x10^9$ infectious particles per milliliter can typically be achieved with SAD-B19$^{\Delta G}$, in a period of one to two weeks. CVS-N2c$^{\Delta G}$ titers used here were usually two orders of magnitude lower and generation of concentrated stocks of the virus can take four to six weeks. Given that full-length CVS-N2c can be grown in laboratory to similar titers as SAD-B19, it is possible that future refinement of CVS-N2c$^{\Delta G}$ packaging cells will improve attainable titers to the same level as SAD-B19$^{\Delta G}$.

Our findings therefore establish CVS-N2c$^{\Delta G}$ as an efficient monosynaptic retrograde reagent, one which overcomes many of the drawbacks inherent in the use of SAD-B19-based strains. Additionally, the enhanced ability of functional CVS-N2c$^{\Delta G}$ variants to monitor and manipulate presynaptic neuronal populations may also make it easier to link the organization of neural circuits to their encoded behaviors.

Summary of deletion mutant SAD-B19 and CVS-N2c

	SAD-B19	**CVS-N2c**
Type	Vaccination strain	Challenge strain
Packaging		
Native-coat G	Standard cell culture in BHK-21 cells; 7 days production time.	Specialized culture in Neuro2A cells; 28 day production time.

Pseudotyped EnvA	7-10 days for production	14 to 28 days for production.
Complementation	Commercially available viruses, transgenic animals available, requires B19-specific glycoprotein complementation	N2c-specific glycoprotein vectors required, and available. Transgenic animals not yet available.
Titers		
Native-coat G	Low 10^9 typical	Mid 10^7 typical
Pseudotyped EnvA	Low 10^8 typical, native-coat background 10^2 typical	Low 10^7 typical, no detectable native-coat background.
Expression		
Onset	Visible fluorescence within 24 hours.	Requires ≥4 days for visible fluorescence.
Specificity	Infects glia, limited reports of retrograde *in vivo* specificity.	No glial infection, demonstrated retrograde *in vivo* specificity.
Toxicity	Modest with fluorophores, higher with optogenetic proteins.	Low with fluorophores; survival up to 28 days even with optogenetic proteins.
Applications		
Trans-synaptic Transfer	7-40 presynaptic neurons typical with AAV complementation. Poor transfer to long-range inputs.	60-400 presynaptic neurons. Good transfer to long-range inputs.
Optogenetic manipulation (eg. ChR)	Short-term utility (1-5 days). Toxicity apparent ≥5 days.	Medium-term utility (7-28 days longest tested).
Optogenetic monitoring (eg. GCaMP)	Short-term utility (1-10 days). Toxicity apparent ≥10 days.	Medium-term utility (7-21 days longest tested).

Table 1: Comparison of packaging, titers, expression and application of SAD-B19 $^{\Delta G}$ and CVS-N2c $^{\Delta G}$ RABV strains. See text for further details.

What does rabies tell us?

The evidence presented in Part 3 proves, for the first time with high confidence, that the retrograde spread of at last one rabies strain, CVS-N2c, is exclusively trans-synaptic *in vivo* (see Zampieri, et al. (2014) for anterograde data). Clearly, in culture, other means of viral egress are supported, or the manufacture of virus would be untenable. But one overriding question remains: how does rabies infect neurons? While many attempts have been made (Lafon 2005), no definitive answer exists. This leaves us to question the nature of rabies spread and the biases and opportunities that creates:

1) Does the density of synaptic contact influence spread? Do multiple synaptic contacts from one cell increase the odds of viral transfer relative to singly-connected neurons?
2) Does the virus prefer weak or strong synapses?
3) Does it prefer symmetric or asymmetric synapses?
4) Does synaptic activity enhance or retard viral spread?
5) Does the length of projection influence spread?
6) Are there non-linear thresholds that change the amount of spread, such that a small sublinear improvement in one kinetic features of the virus (say, axonal trafficking) leads to an order-of-magnitude increase in spread.

It appears that at least (5) and (6) above might be true. For instance, in the cortico-spinal circuit, we notice a near 200-fold increase in spread with one strain versus another, while local circuits only experience a 4-fold increase.

How much does it map?

Currently, even with CVS-N2c-based tools, rabies only labels a minority of pre-synaptic inputs. But is there a level at which the sample size is sufficient for us to virtually recreate the entire map of the circuit? For the cortico-striatal study in Part 2, we propose that such a threshold exists due to the sparsity of excitatory synaptic connections. At a number close to 20% of presynaptic-contacts-labeled, we expect to at least separate sparsely and multiple connected neurons, if the range of contacts is 1-5, as speculated in Dudman & Gerfen (2015).

Evidence of activity dependence

As discussed above, a significant concern regarding experimental use of rabies viruses to build maps of neural connections is the possibility that the virus prefers to traverse active synapses. A reasonable but unproven hypothesis regarding rabies holds that since the virus is exclusively trans-synaptic in transport, it is likely dependent on synaptic proteins or the process of synaptic release to jump across a synapse. This has been widely discussed in the literature of virology, but has only been directly examined *in vitro* (Ghanem & Conzelmann, 2015; Bergami et al., 2015). Evidence from *in vitro* studies shows that the virus can spread effectively in the absence of neural activity. But since we know that the virus is promiscuous during *in vitro* manufacture, the evidence in Bergami et al. and elsewhere is not entirely satisfying. We propose

that the virus uses entirely different means of budding and uptake during its *in vivo* life-cycle.

We explored this phenomenon in two experiments shown below.

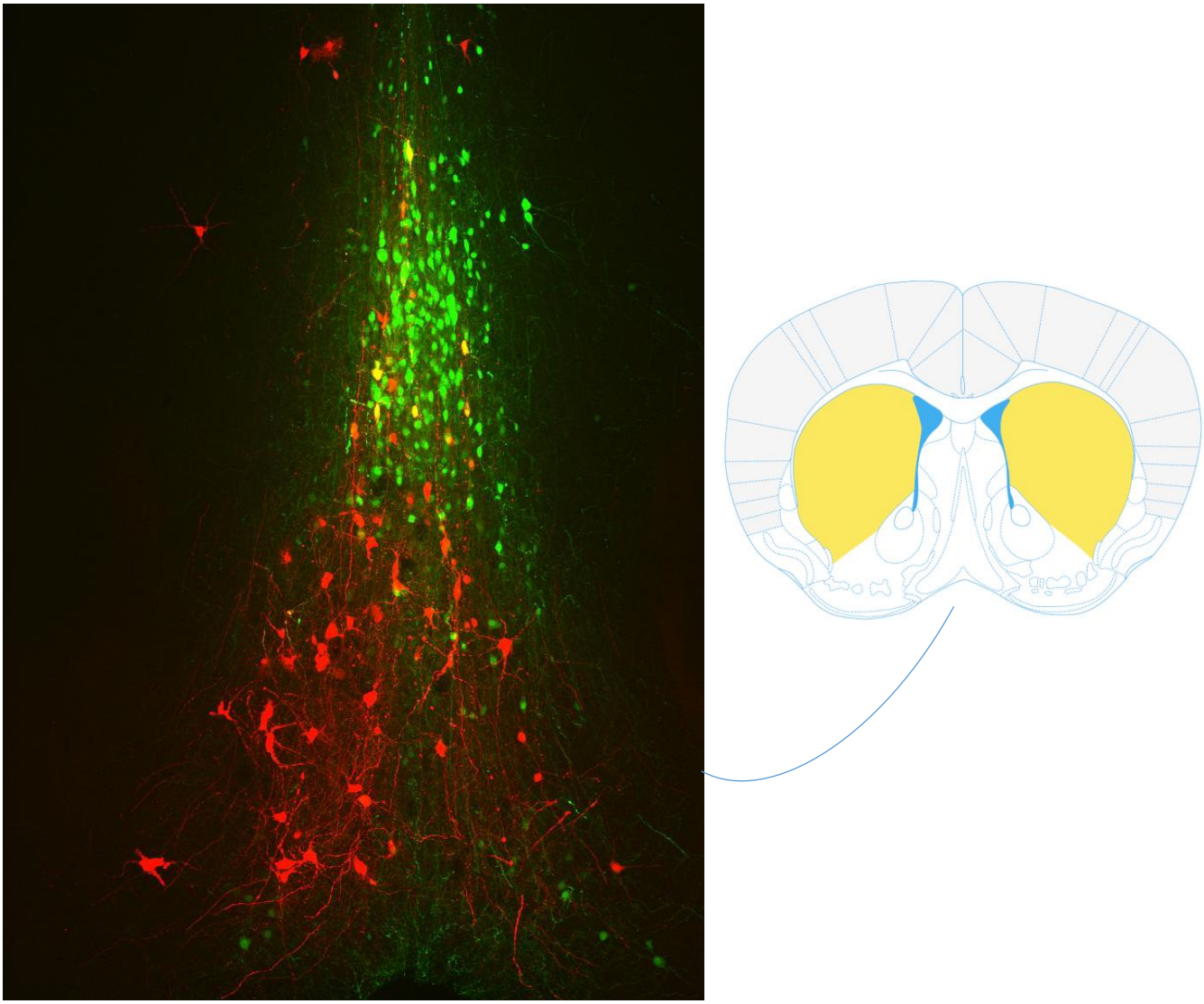

Figure 6.1: example of double-labeled neurons in the medial septum. Left: in a PV-Cre+ mouse, cells were infected by AAV-FLEX-EGFP and SAD-B19$^{\Delta G}$-dsRed.

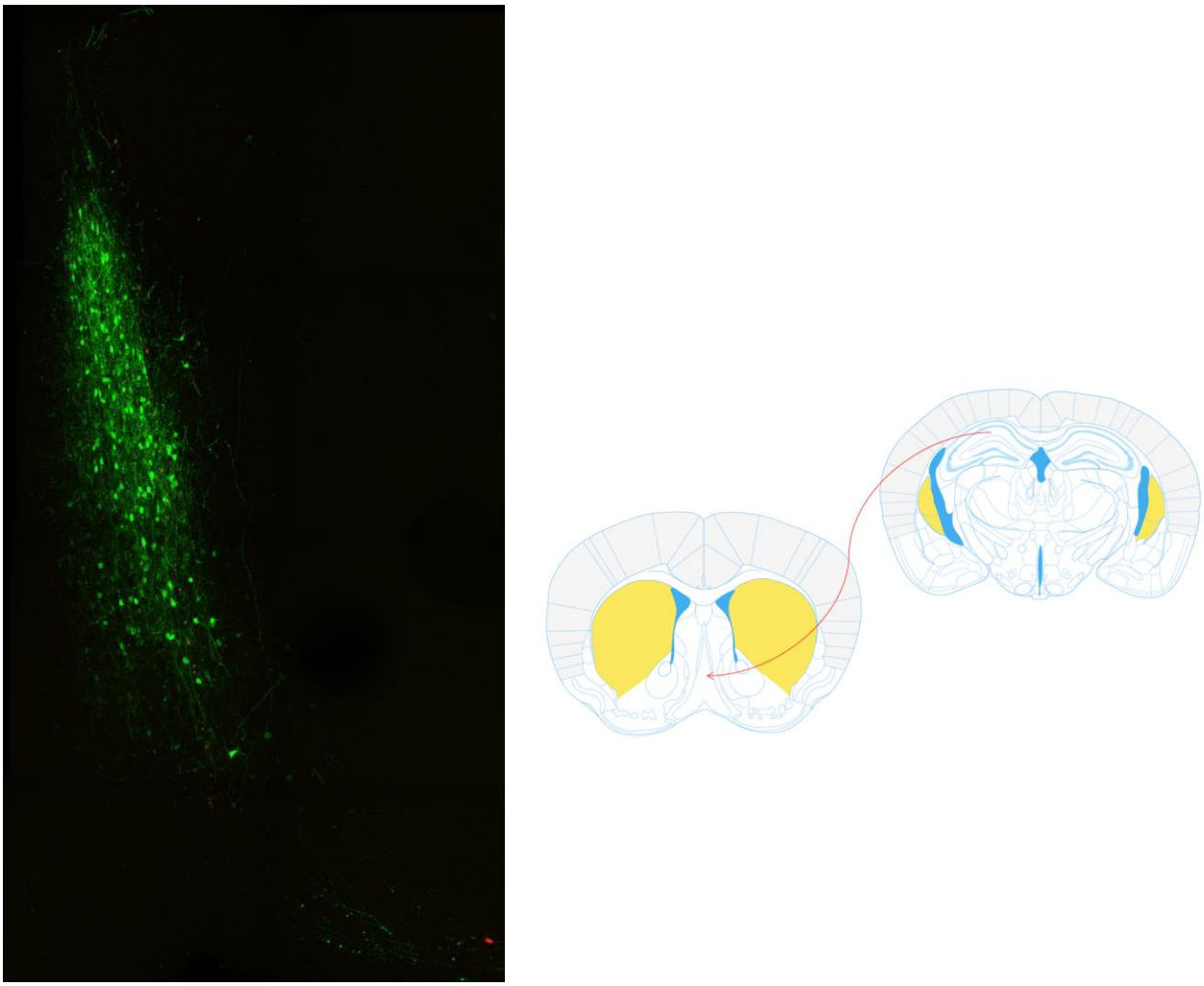

Figure 6.2: example of double-labeling results in medial septum after blocking synaptic activity. Left: In a PV-Cre+ mouse, septal neurons were infected with AAV-FLEX-TeLC-GFP, which blocks synaptic release. Right: schematic of SAD-B19 infection, starting in hippocampus and spreading retrograde to septal projection neurons.

In the first experiment, we created a SAD-B19 mono-synaptic priming infection in dorsal hippocampus of animals expressing Cre in parvalbumin-positive neurons. As the medial septum is known to send a strong parvalbumin-positive projection to the hippocampus, we then 'silenced' the activity of those septal neurons by injecting an AAV conditionally expressing tetanus light-chain fused to EGFP (AAV-FLEX-TeLC-GFP) (Figure 6.2). Those neurons which would normally receive SAD-B19 via their axonal projection into the hippocampus sustained no infection. Conversely, in controls, robust spread of RABV SAD-B19 was sustained (Figure 6.1).

For five animals in the first synaptically-blocked condition, we observed zero RABV+ neurons. In another five animals with only EGFP sham expression, we observed 219 RABV+ neurons.

In a separate experiment, we explored whether natural activity could influence viral spread. We hypothesized that long-term reductions in neural activity, as would occur in barrel cortex and barreloids of the thalamus following whisker-trimming, would reduce spread of RABV. Thus we created a bilateral priming infection in the barrel cortex of mice which were unilaterally whisker-trimmed and examined the retrograde spread of virus from barrel cortex to the barrel-projecting thalamus (figure not shown). Since this experiment compared two conditions within the same animal, it seemed ideal for exploring the activity dependence of RABV.

In a cohort of four animals, we examined the spread of SAD-B19 five days following RABV infection. We found a striking increase in spread in the non-whisker-trimmed hemisphere (figure not shown; animal 1: 50% reduction, 21 vs. 10; animal 2: 75% reduction, 44 vs. 11; animal 3: 85% reduction, 13 vs. 2; animal 4: 35% reduction, 29 vs. 19).

While this evidence is not conclusive, it is highly suggestive of a link between neural activity and the kinetics of RABV trans-synaptic transfer.

Future improvements: Wickersham et al.

The inventor of the deletion-mutant rabies virus tracing system has continued to improve the underlying technology. Most recently, he has proposed a breakthrough approach to the problem of cytotoxicity but removing the L-transcriptase gene from the virus and reintroducing *in trans*, much like the system of complementation *in trans* use for G-glycoprotein. This holds the promise of completely nullifying any cytotoxic effects of the parent RABV strain. Because

the L gene of RABV is too large for including within an AAV genome, this system relies on alternate expression mechanisms, in particular lentiviruses (Wickersham, et al. 2015). By allowing for very low expression levels of Cre from the RABV vector, stronger expressing vectors can be driven to increase RABV packaging and expression. Techniques like this which directly target to pathogenicity of rabies, namely its ability to amplify itself in an immune-avoidant manner, promise to have the greatest effect in improving RABV as both an experimental research vector as well as a clinical therapeutic vector.

Bibliography: Parts 3-6

Bergami, M., Masserdotti, G., Temprana, S.G., Motori, E., Eriksson, T.M., Göbel, J., Yang, S.M., Conzelmann, K.-K., Schinder, A.F., Götz, M., et al. (2015). A Critical Period for Experience-Dependent Remodeling of Adult-Born Neuron Connectivity. Neuron *85*, 710–717.

Bostan, A.C., Dum, R.P., and Strick, P.L. (2010). The basal ganglia communicate with the cerebellum. Proc. Nat. Acad.Sci. USA *107*, 8452–8456.

Callaway, E.M., and Luo, L. (2015). Monosynaptic Circuit Tracing with Glycoprotein-Deleted Rabies Viruses. J. Neurosci. *35*, 8979–8985.

Cetin, A. and Callaway, E.M. (2014) Optical control of retrogradely infected neurons using drug-regulated "TLoop" lentiviral vectors. J. Neurophys. *111*, 2150-2159.

Chen, T.-W., Wardill, T.J., Sun, Y., Pulver, S.R., Renninger, S.L., Baohan, A., Schreiter, E.R., Kerr, R.A., Orger, M.B., Jayaraman, V., et al. (2013). Ultrasensitive fluorescent proteins for imaging neuronal activity. Nature *499*, 295–300.

Conzelmann, K., and Hagendorf (2011). Recombinant Fluorescent Rabies Virus Vectors for Tracing Neurons and Synaptic Connections. In Imaging in Neuroscience, (CSH Press),

Coulon, P., Derbin, C., Kucera, P., Lafay, F., Prehaud, C., and Flamand, A. (1989). Invasion of the peripheral nervous systems of adult mice by the CVS strain of rabies virus and its avirulent derivative AvO1. J. Virol. *63*, 3550–3554.

DeNardo, L.A., Berns, D.S., DeLoach, K and Luo L. (2015) Connectivity of mouse somatosensory and prefrontal cortex examined with trans-synaptic tracing. Nat. Neurosci. *18*, 1687-1697.

Dietzschold B, Li J, Faber M, Schnell M. (2008) Concepts in the pathogenesis of rabies. Future Virol. 3(5):481-90

Eccles, J.C., Eccles, R.M. and Lundberg, A. (1957) The convergence of monosynaptic excitatory afferents on to many different species of alpha motoneurones. J. Physiol.*137*, 22-50.

Finke, S., and Conzelmann, K.-K. (2005). Replication strategies of rabies virus. Virus Res. *111*, 120–131.

Finke, S., Mueller-Waldeck, R., and Conzelmann, K.-K. (2003). Rabies virus matrix protein regulates the balance of virus transcription and replication. J. Gen. Virol. *84*, 1613–1621.

Frank, E. and Westerfield, M. (1983) Development of sensory-motor synapses in the spinal cord of the frog. J. Physiol. *343*, 593-610.

Franklin, K.B.J., and Paxinos, G. (2013). Paxinos and Franklin's The mouse brain in stereotaxic coordinates (Amsterdam: Academic Press, an imprint of Elsevier).

Gerfen, C.R., and Bolam, J.P. (2010). The Neuroanatomical Organization of the Basal Ganglia. In Handbook of Behavioral Neuroscience, (Elsevier), pp. 3–28.

Geue, L., Schares, S., Schnick, C., Kliemt, J., Beckert, A., Freuling, C., Conraths, F.J., Hoffmann, B., Zanoni, R., Marston, D., et al. (2008). Genetic characterisation of attenuated SAD rabies virus strains used for oral vaccination of wildlife. Vaccine *26*, 3227–3235.

Ghanem, A., and Conzelmann, K.-K. (2015). G gene-deficient single-round rabies viruses for neuronal circuit analysis. Virus Res.. *In Press.*

Ghanem, A., Kern, A., and Conzelmann, K.-K. (2012). Significantly improved rescue of rabies virus from cDNA plasmids. Eur. J. Cell Bio. *91*, 10–16.

Gong, S., Doughty, M., Harbaugh, C.R., Cummins, A., Hatten, M.E., Heintz, N., and Gerfen, C.R. (2007). Targeting Cre recombinase to specific neuron populations with bacterial artificial chromosome constructs. J. Neurosci. *27*, 9817–9823.

Hongo, T., Lundberg, A., Phillips, C.G., Thompson, R.F. (1984) The pattern of monosynaptic Ia-connections to hindlimb motor nuclei in the baboon: a comparison with the cat. Proc. R. Soc. Lond. B Biol. Sci. *221*, 261-289.

Hoshi, E., Tremblay, L., Féger, J., Carras, P.L., and Strick, P.L. (2005). The cerebellum communicates with the basal ganglia. Nat. Neurosci. *8*, 1491–1493.

Jackson, A.C. (2013) Rabies: scientific basis of the disease and its management. Amsterdam; Boston: Elsevier/Academic Press.

Jinno, S., Klausberger, T., Marton, L.F., Dalezios, Y., Roberts, J.D.B., Fuentealba, P., Bushong, E.A., Henze, D., Buzsaki, G., and Somogyi, P. (2007). Neuronal Diversity in GABAergic Long-Range Projections from the Hippocampus. J. Neurosci. *27*, 8790–8804.

Kaifosh, P., Lovett-Barron, M., Turi, G.F., Reardon, T.R., and Losonczy, A. (2013). Septo-hippocampal GABAergic signaling across multiple modalities in awake mice. Nat. Neurosci. *16*, 1182–1184.

Kanda, T., Sullivan, K.F., and Wahl, G.M. (1998). Histone-GFP fusion protein enables sensitive analysis of chromosome dynamics in living mammalian cells. Curr. Biol. *8*, 377–385.

Kelly, R.M. and Strick, P.L. (2000) Rabies as a transneuronal tracer of circuits in the central nervous system. J. Neurosci. Methods *103,* 63-71.

Kiritani, T., Wickersham, I.R., Seung, H.S., and Shepherd, G.M.G. (2012). Hierarchical Connectivity and Connection-Specific Dynamics in the Corticospinal-Cortico-striatal Microcircuit in Mouse Motor Cortex. J. Neurosci. *32*, 4992–5001.

Klausberger, T., and Somogyi, P. (2008). Neuronal Diversity and Temporal Dynamics: The Unity of Hippocampal Circuit Operations. Science *321*, 53–57.

Lafon, M. (2005). Rabies virus receptors. Journal of NeuroVirology *11*, 82–87.
Lin, J.Y. (2011) A user's guide to channelrhodopsin variants: features, limitations and future developments. Exp. Physiol. *96*, 19-25.

Lovett-Barron, M., Turi, G.F., Kaifosh, P., Lee, P.H., Bolze, F., Sun, X.-H., Nicoud, J.-F., Zemelman, B.V., Sternson, S.M., and Losonczy, A. (2012). Regulation of neuronal input transformations by tunable dendritic inhibition. Nat. Neurosci. *15*, 423–430.

Lovett-Barron, M., Kaifosh, P., Kheirbek, M.A., Danielson, N., Zaremba, J.D., Reardon, T.R., Turi, G.F., Hen, R., Zemelman, B.V., and Losonczy, A. (2014). Dendritic Inhibition in the Hippocampus Supports Fear Learning. Science *343*, 857–863.

McClure, C., Cole, K.L.H., Wulff, P., Klugmann, M., and Murray, A.J. (2011). Production and Titering of Recombinant Adeno-associated Viral Vectors. J. Vis. Exp. *27*, e3348.

Mebatsion, T., König, M., and Conzelmann, K.-K. (1996). Budding of Rabies Virus Particles in the Absence of the Spike Glycoprotein. Cell *84*, 941–951.

Mendelsohn, A.I., Simon, C.M., Abbott, L.F., Mentis, G.Z. and Jessell, T.M. Activity Regulates the Incidence of Heteronymous Sensory-Motor Connections. Neuron *87*, 111-123.

Mori, T., and Morimoto, K. (2014). Rabies virus glycoprotein variants display different patterns in rabies monosynaptic tracing. Front. Neuroanat. *7*. 47.

Morimoto, K., Hooper, D.C., Carbaugh, H., Fu, Z.F., Koprowski, H., and Dietzschold, B. (1998). Rabies virus quasispecies: Implications for pathogenesis. Proc. Nat. Acad. Sci. USA *95*, 3152–3156.

Morimoto, K., Hooper, D.C., Spitsin, S., Koprowski, H., and Dietzschold, B. (1999). Pathogenicity of different rabies virus variants inversely correlates with apoptosis and rabies virus glycoprotein expression in infected primary neuron cultures. J. Virol. *73*, 510–518.

Morimoto, K., Foley, H.D., McGettigan, J.P., Schnell, M.J., and Dietzschold, B. (2000). Reinvestigation of the role of the rabies virus glycoprotein in viral pathogenesis using a reverse genetics approach. J. Neurovirol. *6*, 373–381.

Namburi, P., Beyeler, A., Yorozu, S., Calhoon, G.G., Halbert, S.A., Wichmann, R., Holden, S.S., Mertens, K.L., Anahtar, M., Felix-Ortiz, A.C., et al. (2015). A circuit mechanism for differentiating positive and negative associations. Nature *520*, 675–678.

Nassi, J.J., Cepko, C.L., Born, R.T., Beier, K.T. (2015) Neuroanatomy goes viral! Front Neuroanat. *9*, 80.

Ogawa, S.K., Cohen, J.Y., Hwang, D., Uchida, N. and Watabe-Uchida, M. (2014) Organization of monosynaptic inputs to the serotonin and dopamine neuromodulatory systems. Cell Rep. *8,* 1105-1118.

Osakada, F., Mori, T., Cetin, A.H., Marshel, J.H., Virgen, B., and Callaway, E.M. (2011). New Rabies Virus Variants for Monitoring and Manipulating Activity and Gene Expression in Defined Neural Circuits. Neuron *71,* 617–631.

Palusa, S., Ndaluka, C., Bowen, R.A., Wilusz, C.J., and Wilusz, J. (2012). The 3' untranslated region of the rabies virus glycoprotein mRNA specifically interacts with cellular PCBP2 protein and promotes transcript stability. PLoS ONE *7,* e33561.

Pollak Dorocic, I., Fürth, D., Xuan, Y., Johansson, Y., Pozzi, L., Silberberg, G., Carlén, M. and Meletis, K. (2014) A whole-brain atlas of inputs to seretonergic neurons of the dorsal and median raphe nuclei. Neuron *83,* 663-678.

Rancz, E.A., Franks, K.M., Schwarz, M.K., Pichler, B., Schaefer, A.T. and Margrie, T.W. (2011) Transfection via whole-cell recording in vivo: bridging single-cell physiology, genetics and connectomics. Nat. Neurosci. *14,* 527-532.

Roy, A., and Hooper, D.C. (2008). Immune evasion by rabies viruses through the maintenance of blood-brain barrier integrity. J. Neurovirol. *14*, 401–411.

Schnell, M.J., Mebatsion, T., and Conzelmann, K.K. (1994). Infectious rabies viruses from cloned cDNA. EMBO J. *13*, 4195–4203.

Schnell, M.J., McGettigan, J.P., Wirblich, C., and Papaneri, A. (2009). The cell biology of rabies virus: using stealth to reach the brain. Nat. Rev. Microbiol. *8,* 51-61.

Scott, C.A., Rossiter, J.P., Andrew, R.D., and Jackson, A.C. (2008). Structural abnormalities in neurons are sufficient to explain the clinical disease and fatal outcome of experimental rabies in yellow fluorescent protein-expressing transgenic mice. J. Virol. *82,* 513-521.

Sousa, V.H., Miyoshi, G., Hjerling-Leffler, J., Karayannis, T., and Fishell, G. (2009). Characterization of Nkx6-2-Derived Neocortical Interneuron Lineages. Cereb. Cortex *19*, i1–i10.

Sun, Y., Nquyen A.Q., Nquyen, J.P., Le, L., Saur, D., Choi, J., Callaway, E.M. and Xu, X (2014) Cell-Type-Specific Circuit Connectivity of Hippocampal CA1 Revealed through Cre-Dependent Rabies Tracing. Cell Rep. *7,* 269-280.

Turi, G.F., Wittmann, G., Lechan, R.M., and Losonczy, A. (2015). Ambient GABA modulates septo-hippocampal inhibitory terminals via presynaptic GABAb receptors. Neuropharmacol. *88*, 55–62.

Ugolini, G. (1995). Specificity of rabies virus as a transneuronal tracer of motor networks: Transfer from hypoglossal motoneurons to connected second-order and higher order central nervous system cell groups. J. Comp. Neurol. *356*, 457–480.

Ugolini, G. (2010). Advances in viral transneuronal tracing. J. Neurosci. Meth. *194*, 2–20.

Vélez-Fort, M., Rousseau, C.V., Niedworok, C.J., Wickersham, I.R., Rancz, E.A., Brown, A.P.Y., Strom, M., and Margrie, T.W. (2014). The Stimulus Selectivity and Connectivity of Layer Six Principal Cells Reveals Cortical Microcircuits Underlying Visual Processing. Neuron *83*, 1431–1443.

Watabe-Uchida, M., Zhu, L., Ogawa, S.K., Vamanrao, A., and Uchida, N. (2012). Whole-Brain Mapping of Direct Inputs to Midbrain Dopamine Neurons. Neuron *74*, 858–873.

Wertz, A., Trenholm, S., Yonehara, K., Hillier, D., Raics, Z., Leinweber, M., Szalay, G., Ghanem, A., Keller, G., Rózsa, B., Conzelmann, K.K. and Roska, B. (2015) Single-cell-initiated monosynaptic tracing reveals layer-specific cortical network modules. Science. *349*, 70-74.

Wickersham, I.R., Finke, S., Conzelmann, K.-K., and Callaway, E.M. (2007a). Retrograde neuronal tracing with a deletion-mutant rabies virus. Nat. Meth. *4*, 47–49.

Wickersham, I.R., Lyon, D.C., Barnard, R.J.O., Mori, T., Finke, S., Conzelmann, K.-K., Young, J.A.T., and Callaway, E.M. (2007b). Monosynaptic Restriction of Transsynaptic Tracing from Single, Genetically Targeted Neurons. Neuron *53*, 639–647.

Wickersham, I.R., Sullivan, H.A., and Seung, H.S. (2010). Production of glycoprotein-deleted rabies viruses for monosynaptic tracing and high-level gene expression in neurons. Nat. Protoc. *5*, 595–606.

Wickersham, I.R., Sullivan, H.A., Pao, G.M., Hamanaka, H., Goosens, K.A., Verma, I.M., and Seung, H.S. (2015). Lentiviral Vectors for Retrograde Delivery of Recombinases and Transactivators. Cold Spring Harbor Protocols *2015*, pdb.prot075879.

Wirblich, C., and Schnell, M.J. (2011). Rabies Virus (RV) Glycoprotein Expression Levels Are Not Critical for Pathogenicity of RV. J. Virol. *85*, 697–704.

Zampieri, N., Jessell, T.M., and Murray, A.J. (2014). Mapping Sensory Circuits by Anterograde Transsynaptic Transfer of Recombinant Rabies Virus. Neuron *81*, 766–778.

Zhang, F., Wang, L.-P., Boyden, E.S., and Deisseroth, K. (2006). Channelrhodopsin-2 and optical control of excitable cells. Nat. Meth. *3*, 785–792.

Experimental Procedures

Rescue of CVS-N2c$^{\Delta G}$ variants

DNA rescue plasmids for CVS-N2c were created previously (Wirblich and Schnell, 2011). Four sequence differences were noted for CVS-N2c$^{\Delta G}$ relative to previously published sequences (GenBank HM535790), though we have not explored whether these changes are new mutations or represent historical sequencing errors. Rescue plasmids for deletion mutant CVS-N2c$^{\Delta G}$-insert variants were created by removing the G-gene sequence and introducing 5' XmaI and 3' NheI restriction sites and subsequent ligation with expression inserts, while maintaining the entire ~500bp G-L intergenic sequence, with the goal of preserving native viral expression levels and tropism. Removal of the G-L intergenic sequence in a mCherry-expressing variant did not noticeably change the level or pattern of fluorescent protein expression in culture (data not shown). Two fluorescent protein expression inserts were initially constructed, expressing either GFP or dsRed. Rescue was performed in Neuro2A cells (ATCC CCL-131) by co-transfection (Lipofectamine 2000) of CVS-N2c$^{\Delta G}$ genomic plasmid, pCAGGS-T7, pTIT-L, pTIT-N-, pTIT-P (Finke et al., 2003), pCAGGS-N2c(G). Although pTIT helper plasmids correspond to SAD-B19 sequences, their use in only the very first round of rescue minimized genetic drift of CVS-N2c$^{\Delta G}$. pCAGGS-N2c(G) was created by insertion of the N2c glycoprotein gene into the pCAGGS expression plasmid. Rescue took up to 10 days, significantly longer than SAD-B19$^{\Delta G}$. Supernatants from rescue cultures were collected for up to 10 days following the first appearance of virus. It is possible that more efficient RABV backbone plasmids could avoid the use of T7 (Ghanem et al., 2012), but here we found that T7 polymerase was causal to the rescue. All culture of Neuro2A cells and derived lines took place in EMEM with 10% FBS without

antibiotics. Cells were grown at 37C and 5% CO_2 until confluent, then held in extended harvesting conditions at 34C and 3% CO_2. Harvested supernatant was filtered at 0.45um and stored at -80 °C until used.

Packaging of CVS-N2c$^{\Delta G}$

We considered that maintenance of the virus exclusively in murine neural tissue is likely important to the thousand-fold improvement in neurotropism of the CVS-N2c strain compared to SAD-B19. Neuro2A cells stably expressing either N2c(G) or EnvA_cytG were created for viral amplification and pseudotyping (Figure 1B,C). The resulting cell lines are called N2A-N2c(G) and N2A-EnvA_cytG. For each variant, the glycoprotein gene was cloned into the MLV expression vector pCMMP-IRES-GFP, transfected into Gryphon retroviral packaging cells (Allele Biotech), and MLV-N2c(G)-IRES-GFP after filtering was used to infect Neuro2A cells. We found that Neuro2A cells are significantly less vital in culture than the traditional viral production cell line, BHK-21. Due to their limited vitality, we continued selection of these cells via FACS for more than 6 months. While titers produced are now useful for experimental purposes, they are still at least 2 orders of magnitude lower than titers produced from BHK-21 cells. However, the N2A-N2c(G) packaging line makes up much of the difference in viral counts by increasing effective titer, possibly due to improved neurotropism. Neuro2A cells expressing EnvA_cytG were created similarly, from a chimeric protein made from EnvA and the tail of N2c(G). Cross-pseudotyping (using EnvA_B19 to pseudotype CVS-N2c$^{\Delta G}$) yielded very low titer, suggesting that the interaction of C-terminal glycoprotein and RABV M protein is critical for proper packaging.

Amplification was performed by adding rescue supernatant to N2A-N2c(G) cells. Due to the relatively slow metabolism of cells in these conditions, we found it necessary to collect subsequent viral supernatants for up to 28 days in modified culture conditions of 34C and 3% CO_2. Virus for injection was spin-purified by ultracentrifugation (2 hour, 20000 RPM) and resuspension of viral pellets in phosphate buffered saline. Pseudotyping was performed by adding amplified supernatant to N2A-EnvA-cytG cells. This was done at the highest possible multiplicity-of-infection (MOI), but typically only 0.20. As noted above, our CVS-N2c$^{\Delta G}$ titers (approximately 10^8 per ml) are orders-of-magnitude lower than what we obtained for SAD-B19$^{\Delta G}$. The resultant virus only infects cells which express the avian TVA receptor, as tested using HEK293-TVA cells (Osakada et al., 2011) and, as designed, does not infect Neuro2A or HEK-293 cells (Figure 1C).

All SAD-B19$^{\Delta G}$ variants were rescued and amplified per standard protocol (Wickersham et al., 2010). Rescue plasmids were constructed from the "Supercut" rescue plasmid (Ghanem et al., 2012). Titers assayed by fluorescent foci were 10^9 - 10^{10} for native-enveloped and 10^8 – 10^9 for EnvA-pseudotyped.

Testing specificity of viral infection and expression

To test the selectivity of our AAV construct we injected AAV driving the Cre-dependent expression of N2c glycoprotein into the spinal cord of wild-type animals. 1 µl of the AAV-FLEX-nGFP-2A-RABV[G] was injected into the ventral horn at spinal segments L3-L6.

Animals were sacrificed after two weeks and the spinal cords assayed for GFP expression. To test for contaminating wild-coat virions in our EnvA-pseudotyped CVS-N2c$^{\Delta G}$ preparations we injected 1.2 μl of these viruses into the ventral horn of spinal segments L3-L6. After 10 days animals were sacrificed and examined for expression of fluorescent protein.

Analysis of Spread

Mice expressing *Adora2a*-Cre (RRID: MMRRC_031168-UCD; Aged 12 to 16 weeks) were used for cortico-striatal tracing. Mice expressing *ChAT*-Cre (RRID: IMSR_JAX:006410) were used for spino-motor neuron tracing. For all injections, animals were anesthetized using isoflurane and given analgesics. For cortico-striatal injections, a craniotomy was created above dorsal striatum and injection pipette was lowered to target (0.75 mm AP, 2.2 mm ML, 3.3 mm DV). For AAV, we injected 39 nl of a 1:2 cocktail of AAV-FLEX-TVA_mCherry with AAV-FLEX-nGFP-2A-RABV[G]. Following two weeks of recovery and AAV expression, a secondary surgery was performed by the same technique and 300 nl of RABV$^{\Delta G}$(EnvA) was injected. All AAVs were serotyped 2+1, using established procedures (McClure et al., 2011). Pairs of animals were sacrificed at 5, 10, and 15 days following RABV$^{\Delta G}$ infection, brains harvested and sliced at 100 μm by microtome for visualization. There was no significant difference in viral spread over the three differing infection periods. Imaging was done by confocal microscopy (Leica SP5 for cortico-striatal, Zeiss 710 for spinal cord). All sections containing priming infection were imaged and double-labeled cells counted. Additionally, the locus and extent of priming infection was verified as the same, ±100μm, for all six animals. For secondary labeling, slices at 5 AP coordinates (Bregma +2.8, +2.1, +0.5, +0.1, -0.2) were viewed and dsRed+ cells in cortex manually counted.

For analysis of viral spread within the spinal cord, procedures were followed as above, but instead of craniotomy, injections were made into the ventral horn of the cord between L3 and L4 of 12-week old *ChAT*-Cre mice. All secondary labeling was counted within lumbar, thoracic and cervical spinal cord as well as the hindbrain (defined as caudal to Bregma -5.4) (Franklin and Paxinos, 2013).

Gene expression analysis and cytotoxicity

Neuro2A cells were infected with either SAD-B19 or CVS-N2c strains of RABV$^{\Delta G}$-GFP. For immunocytochemical analysis, Neuro2As were cultured in poly-l-lysine coated Labtek chamber slides and fixed with 4% paraformaldehyde in phosphate buffer after 2 or 4 days. Cultures were counterstained with neurotrace-647 (Invitrogen) and mounted in Mowiol. Images of infected and uninfected cells were taken using a Zeiss 510 confocal microscope with identical settings for each culture. In each field of view the mean grey scale value for infected and uninfected cells was calculated, with uninfected cell values subtracted from infected as background values. Each culture was repeated 3 times with >50 cells analyzed per condition. Culture conditions were identical for analysis of propidium iodide incorporation. After fixation, cells were treated with 100 μg/ml RNAse for 20 minutes at 37°C before addition of 500 nM propidium iodide for 3 minutes at room temperature.

Tissue preparation for *in vitro* electrophysiological recordings.

Following surgical procedures above, C57 wild-type mice were infected with SAD-B19 or CVS-N2c strains of RABV$^{\Delta G}$-hChR2-YFP. Six – 10 and 14 days after virus injection we

prepared coronal slices (350 µm) from the forebrain containing the injection sites, as described previously (Turi et al., 2015). During recording slices were maintained at room temperature and perfused at 1-2 ml per minute with artificial cerebrospinal fluid (ACSF) containing (in mM) 125 NaCl, 25 $NaHCO_3$, 3 KCl, 1.25 NaH_2PO_4, 1 $MgCl_2$, 2 $CaCl_2$, 22.5 glucose, 3 sodium pyruvate and 1 ascorbate, and saturated with 95% O_2 and 5% CO_2. Slices were visualized with Dodt contrast optics using a Zeiss Examiner Z1 upright microscope equipped with a 63× objective (1.0 NA; Zeiss) and two-photon scanning apparatus (Bruker Technologies).

***In vitro* electrophysiological recordings and hChR2 photostimulation.**

For whole-cell current-clamp recordings we patched hChR2 expressing neurons in the secondary motor and cingulate cortices. The intracellular signals were amplified by a Dagan BVC-700A amplifier. Recording pipettes were pulled from borosilicate glass to tip resistances of ~4–7 MΩ and filled with intracellular solution containing low Cl^- (in mM): 140 potassium gluconate, 4 NaCl, 10 HEPES, 4 Mg_2ATP, 0.3 $Tris_2GTP$, 14 phosphocreatine and 0.1 Alexa 594. Pipette capacitance was compensated, and the signals were filtered at 1–10 kHz and digitized at 50 kHz. hChR2 photostimulation was performed with a blue DPSS laser (473 nm, CrystaLaser) coupled to the microscope's two-photon scan-head (Lovett-Barron et al., 2012). For testing the efficacy of the hChR2 expression we run a 5 Hz photostimulation protocol on the cells held at their resting membrane potential. After recording of 5-8 traces the number of photostimulation evoked spikes was divided by the number of the light stimuli.

Hippocampal window implant

Following surgical procedures above, C57 wild-type mice were infected in the medial septum with SAD-B19 or CVS-N2c strains of RABV$^{\Delta G}$-GCaMP6f. Hippocampal window implant surgeries were performed as described previously (Kaifosh et al., 2013, Lovett-Barron et al., 2014). Briefly, we anesthetized mice with isoflurane and treated them with buprenorphine (0.1 mg/kg, subcutaneous) to minimize postoperative discomfort. We exposed the skull and drilled a 3-mm diameter circle centered over left dorsal CA1, matching the size of the cannula window to be implanted. We removed the bone and dura, and then slowly aspirated cortex covering the hippocampus while constantly irrigating with chilled cortex buffer until the external capsule was exposed. Then we implanted the sterilized window implant by wedging it into place, and secured the top of the cannula to the skull and stainless steel head-post with grip cement, leaving it to dry for 15–20 min before returning mice to the home cage (awake and mobile in 5–20 min). We monitored mice every 12 hours for three days after surgery, administering buprenorphine to minimize any signs of discomfort. Three days after the surgery the animals were habituated to handling and head-fixation then we started to image the GCaMP6f expressing cells.

In vivo cytotoxicity and blebbing analysis

Following injection of SAD-B19 or CVS-N2c strains of RABV$^{\Delta G}$-GCaMP6f into the medial septum, or RABV$^{\Delta G}$-hChR2-YFP into striatum to retrogradely infect cortico-striatal neurons, we selected regions with similar numbers of infected neurons for analysis (n = 3 animals per condition; 10-15 neurons analyzed per region for hChR2; 2-10 neurons for GCaMP6f). Identical magnification was used for each sample and the number of blebs were counted for each infected neuron.

Two-photon imaging

We used an *in vivo* resonant galvo-based imaging system (Bruker) and an ultra-fast pulsed laser beam (Coherent; 920-nm wavelength) controlled with an electro-optical modulator to excite GCaMP6f through a 40X objective. Distilled water served to connect the water immersion objective with the cannula. Fluorescent light was detected with photomultiplier tube (green GCaMP6f fluorescence, GaAsP PMT) operated with PrairieView software. *In vivo* imaging was performed in head-fixed mice running on a linear treadmill (Kaifosh et al., 2013). We tracked locomotor behavior by measuring treadmill wheel rotation, recorded as changes in voltage across an infrared photo-transistor as wheel spokes blocked light from an infrared LED. Time series were collected in green (GCaMP6f signal) channel at 512 × 512 at ~30 Hz then underwent motion-correction as described in (Kaifosh et al., 2013). Regions of interest (ROIs) were manually drawn over corrected time-series in Image J (NIH), to isolate the somata of cells of interest and the extracted ΔF/F signals were aligned with the running signal.

Conditional Recombination

To analyze germline recombination by CVS-N2c$^{\Delta G}$-FLPo-mCherry we injected 50 nl of virus into the ventral spinal at L3 of RCE-FRT mice (Sousa et al., 2009). These animals contain a Frt-flanked STOP cassette prior to the GFP coding sequence, and so report expression of Flp-recombinase. 10 days after CVS-N2c$^{\Delta G}$-FLPo-mCherry injection neurons in the thoracic spinal cord were imaged using a Zeiss 510 confocal microscope and expression of mCherry, GFP or both was noted.

Activity Dependence of RABV spread

Priming viruses described previously for SAD-B19 with complementation via B19*CVS(G) glycoprotein were injected into Nr5a1-Cre animals. Saturating amounts (>200nl) were injected into barrel cortex of 12-week-old mice. At the end of injection surgery, animals were unilaterally whisker-trimmed on the right-side whisker pad and then left to recover per standard recovery protocol above. At 5 days post RABV infection, animals were euthanized, brains extracted, and slices prepared at 100um. Cells counts of RABV+ neurons were based on confocal images and were done blind to left-right orientation of slices.

Viral Reagents

CVS-N2c$^{\Delta G}$ RABV and AAV complementation vectors are available from Addgene as Jessell Lab plasmids. Packaging cells (N2A-N2cG, N2A-EnvA_cytG) are available from the authors.

Animal Controls

Figure: D1rda-Cre [D1R] expression analysis illustrating striatal localization of Cre expression (GENSAT)

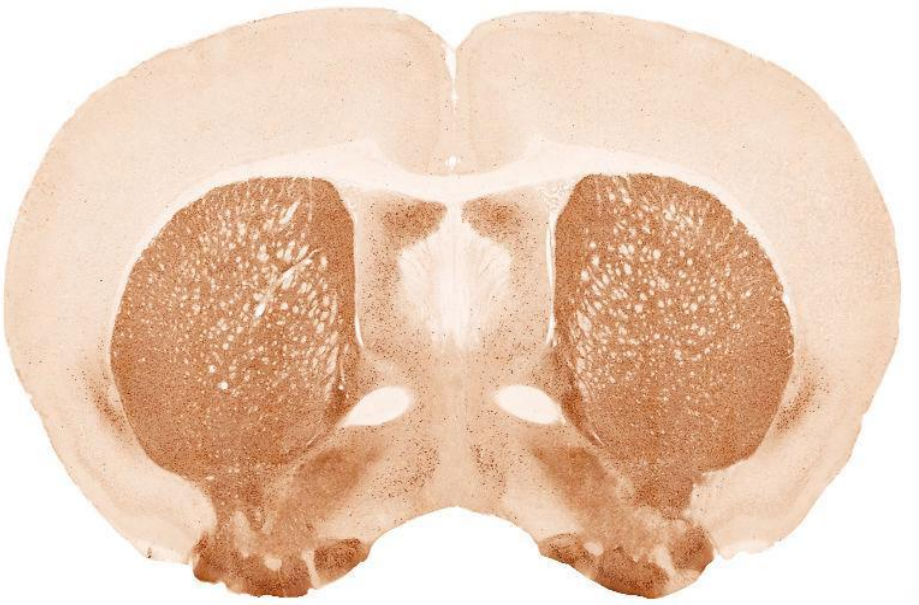

Figure: Drd2-Cre [D2R] expression (GENSAT)

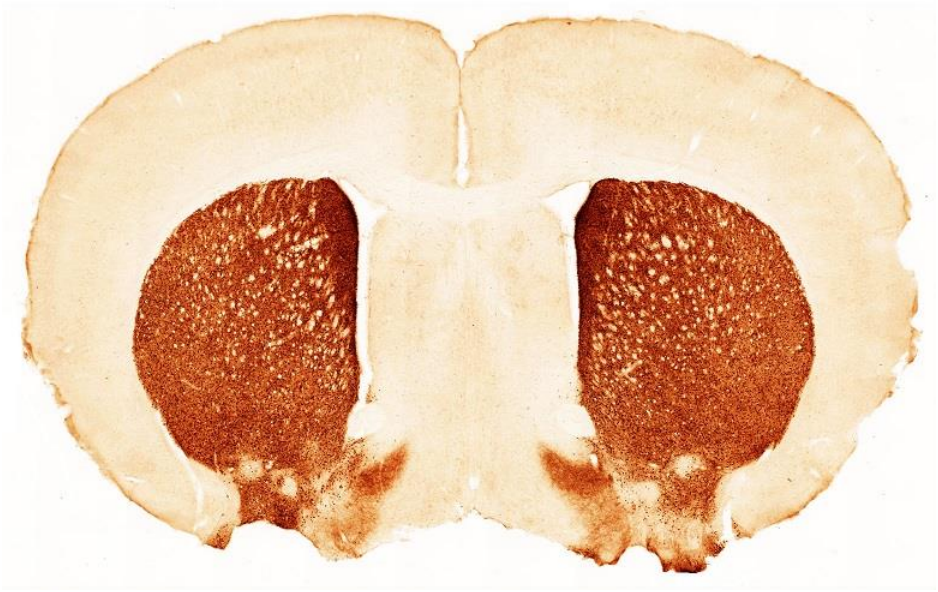

Figure: Adora2A-Cre [A2AR] expression (GENSAT)